UiT The Arctic University of Norway

Faculty of Science and Technology, Department of Geoscience

Rockfall and snow avalanche impact dynamics for road protection design at Svarthola, Senja

A hazard evaluation aided by numerical models and physical formulas

Linn Asplin

Master's thesis in Geology (GEO-3900), May 2021

Abstract

Rockfalls and snow avalanches are a major natural hazard and common phenomenon in mountainous areas in Norway, endangering people and infrastructure. Svarthola, on Fv 862, Senja, is a 100 m long unprotected stretch of road that experiences a high frequency of mass movements. The road is situated at a tunnel portal, between a 100 m high cliff and the fjord. As such, it is the only short access route between the northern and western parts of the island, and frequent road closures have created safety and access issues. It is therefore classified by Troms and Finnmark County as one of the most dangerous roads in the region, and the installation of a protection structure is considered necessary.

This study focuses on the impact dynamics from rockfalls (kinetic energy, velocity, jump height) and snow avalanches (snow pressure, velocity, flow height) at Svarthola for protection design. An analysis of the hazard at the site was performed through fieldwork and desktop mapping in order to estimate the size of the mass movements relevant for the design. This data were used in numerical modelling to obtain the impact dynamics.

The road experiences frequent rock fall inundation, with boulders up to 2 m^3 causing damage and road closures. Rockfall analysis shows variable impact dynamics for the different event scenarios, ranging from 1,700 kJ for annual events up to 7,100 kJ for a 100-year event. The analysis showed impact velocities between 22 and 50 m/s. The median jump heights were 0.9-1.2 m, where some rock blocks can jump >20 m if they hit the lower cliff part above the road. The fall height of a block can be up to 100 m.

The road experiences a lower frequency of snow avalanches but they are often leading to road closures. Impact dynamics were obtained through numerical modelling and physical formulas. The impact dynamics for a 100-year dry-slab avalanche event with a volume of 16,900 m^3 is estimated as follows: snow pressure of 130-270 kPa, impact velocity between 20 and 37 m/s and flow height of 2-3.7 m in the northern part of the road and up to 1.2 m in the southern part.

Finally, an analysis of the relationship between the rockfall and avalanche history and climate factors were done with the aim to propose the implications of climate change. Svarthola will most likely experience more rockfall events in the future due to the projected increase in rainfall intensity and frequency. The dry-snow avalanche hazard may disappear completely due to the rarity of snow cover in these low coastal areas, but the likelihood of wet-snow avalanches and slushflows may increase in a wetter climate.

Acknowledgements

These past nine months have been special in many ways and I think most of have been affected by the pandemic in one or another way. It has been a lot of work writing this thesis but it has also been a lot of fun and I have learned a lot. I want to thank several people who have made this possible:

My supervisor Louise M. Vick for the time you have put into guiding me through this process. Thank you for providing this topic to me. I hope I can do this for a living soon.

Thanks to my co-supervisor Håvard L. Haukenes for all Team-meetings and discussions during the course of this thesis. You have made this journey easier. I also want to thank TFFK for your cooperation and for letting me stay in your office when it was possible. It was great to be part of your team. Thanks to Knut Pedersen in RoadCap.

Thanks to fellow student and friends in the ‘red barrack’ for all support and encouragement.

I want to give a special thanks to my friends, you know who you are, and to my family in Sweden, for motivating and supporting me and being there for me through this year. You are the best. I miss you who are across the border. Special thanks to Eli for all the company.

To the last, I want to thank you Simon. For dealing with my roller-coaster year of emotions.

Now awaits new adventures.

Linn

Table of Contents

1 Introduction

1.1 Background and motivation statement

In the field of geohazards, there is an increasing need to improve the understanding of mass movement dynamics in complex terrain (Bartelt et al., 2017). The most common geohazards in Norway consist of avalanches (snow, rock, clay and debris), landslides and floods. More than 2000 fatalities and considerable damage to infrastructure have been caused by geohazards over the last 150 years (Jaedicke et al., 2008). Recent climate trends and climate projections indicate an increase in the frequency of geohazards in some areas (Hanssen-Bauer et al., 2017). Their impact is expected to rise due to population growth and development of infrastructure close to slope instabilities (Solheim et al., 2005).

Norway's topography, particularly near the coast, is characterized by deep fjords and steep mountainous terrain that was mainly formed by the occurrence of several glacial cycles over the last 2.7 million years (Fredin et al., 2013). Due to a complex geological history, many of Norway's mountainsides have become unstable (Ballantyne, 2002), making infrastructure, including high- and county roads, along the Norwegian coast vulnerable to various geohazards.

The Norwegian Public Roads Administration, Statens vegvesen (SVV) have the overall responsibility of the protection of roads that are threatened by geohazards. The County Council overtook the authority for the county roads by 1st of January 2020 and is responsible for i.e. planning, building and maintaining these roads. Every fourth year Norway's highways and county roads are investigated for avalanche danger and this plan is delivered to the National Transport Plan who identifies investment priorities. In the plan, all stretches of roads of at least 1 km with frequent avalanche events are identified as an avalanche zone (skredpunkt) and are given a risk ranking. The ranking is based on six factors that describe the avalanche danger and the consequences for road users and accessibility, i.e. annual traffic numbers and the frequency of events. It ranges from 0–9, where 3.5 and higher is classified as high risk. A mitigation measure is suggested for most of the endangered roads with a risk ranking over 2.5 (middle and high risk) (Kvalvågens et al., 2019).

Troms and Finnmark County Council (TFFK) adopted a new type of avalanche protection program for all these roads in October 2020, where 25 out of 246 are in priority to be protected until 2026 (Troms og Finnmark fylkeskommune, 2020).

Svarthola, the subject of this study, is part of the county road (Fv) 862 on Senja in southern Troms and is prone to rockfalls, ice and snow avalanches. SVV has registered Svarthola as

an avalanche zone with a factor of 4.22 (high risk). It is included in the new avalanche protection program.

Svarthola is a 100 m exposed stretch of road at risk of different avalanches throughout the year with no protection solution other than closing the road. This has dramatic consequences for people and commercial traffic who need to use the road. As a consequence, it has become essential to do a hazard evaluation at Svarthola in order to investigate the possibility of installing a protection structure in the near future. A temporary tunnel system (RoadCap) was considered in the plan phase due to the short construction time, but under the course of the thesis TFFK decided that it will take form as a rock/snow shed. They started the project in the autumn 2020 and plan to build the shed by 2022. In order to dimension and build the shed, numerical modelling is needed to predict the dynamic impacts of the avalanches endangering the road.

1.2 Objectives of the study

The main objective of this master thesis is to provide a technical overview of the avalanche dynamics affecting the unprotected section of Fv 862, Svarthola. The thesis will focus specifically on the dynamics of rockfalls and snow avalanches as the main processes threatening the road, however ice falls will also be referenced in parts. The thesis is in collaboration with TFFK, who has ultimate responsibility for development at the site. The main aims of the thesis are to:

i. Determine the impact dynamics from rockfall and snow avalanches at Svarthola in order to specify what the protection structure needs to withstand, which the supplier can use as a design criteria. This is aided by fieldwork, desktop mapping and numerical models.
ii. For the rockfall analysis the impact energies, velocities and the jump heights will be calculated through the modelling. This allows presenting the impact dynamics by different scenarios that provides an overview of the potential magnitudes of the impacts relevant for the design.
iii. For the snow avalanche analysis the impact pressures, velocities and flow heights will be the calculated. The numerical model will be aided by alternative methods due to steep terrain at the site and the limitations within the model to replicate this process. This allows presenting a design scenario and the possible variety the different approaches can produce. This framework will achieve higher confidence in the results.

iv. Present the rockfall and snow avalanche impact history at the site in relationship with weather patterns and to put it in context to climate change.

The results of this master thesis can be used as a reference for the protection design at Svarthola. For example, model results may inform the decision process when specifying the design of the cushion layer and backfill material. However, it is important to note that this thesis is an academic work only, and not meant to provide direct technical specifications for the designer.

2 Study area

Svarthola (69.27°N, 17.35°E) (Figure 1) is situated in the inner part of Mefjorden on the northwestern part of the island of Senja in Troms and Finnmark County. The site is part of Fv 862 that stretches from Botnhamn in the north to Straumsbotn in the southwest. The road is an important passage for the export of fish from the small fishing villages, and for the increasing volumes of tourist traffic moving between the north and south of the island.

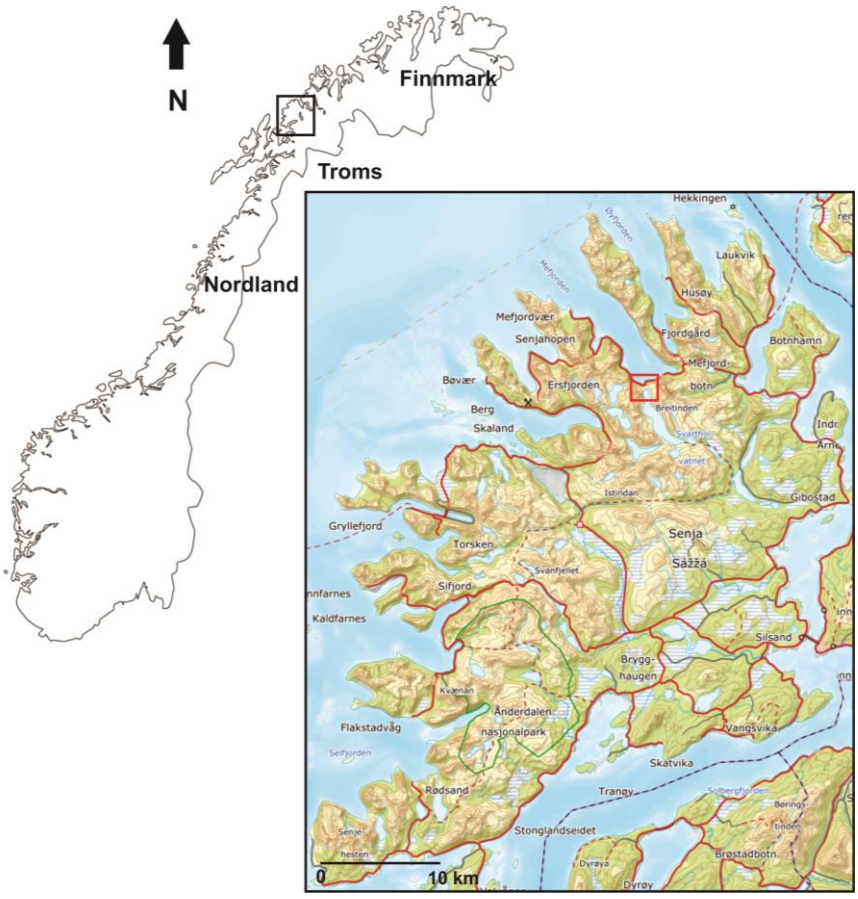

Figure 1. Topographic overview map of Senja, showing the location of Svarthola (red box). Inset is an overview map of Norway, showing the location of the topographic map (NMA 2020).

Svarthola is approximately a one-hour drive from Finnsnes, and 2.5 hours by ferry and car from Tromsø. The road is situated at 30 m a.s.l between a steep northwest-facing slope and the coast. It is a 100 m long unprotected stretch of road that sits between the portal to the Svartholla tunnel at the north end, and a rock shed at the south (Figure 2-3). The tunnel was built in 1978 and the rock shed in the mid-90s, but unfortunately the rock shed is too short and does not quite cover the most hazardous parts of the road.

Svarthola is, along with other roads on the west side of Senja, exposed to rockfall and snow avalanches. SVV classifies the road as one of the most dangerous in the county, with an estimated cost of 55 million NOK (uncertainty of 40%) to build a structure to protect the road from rock, snow and ice hitting the road (Kvalvågens et al., 2019).

Figure 2. Ortho perspective image of Svarthola, displaying the 100 m long exposed stretch of road (red box) between the tunnel and rock shed. Photo: Linn Asplin, 2020.

2.1 Terrain

The topography has a great impact on the mass movement potential of a slope, including steepness and form. Rockfalls are often released from the source area at slope angles between 45-90°, and snow avalanches from 30-55° (Langeland et al., 2019). Snow has the tendency to accumulate at concave formations (McClung Schaerer, 2006).

The mapped area of Svarthola stretches from sea level up to relatively flat terrain at about 300 m a.s.l (Figure 3-4). The terrain between the road and the sea consists of a steep slope made up of scree material and trees. In between the road and the slope, there is a 6–12 m

wide ditch. The slope aspect ranges from SW–NW, and is characterized by vertical to subvertical cliffs and steep terrain covered with vegetation.

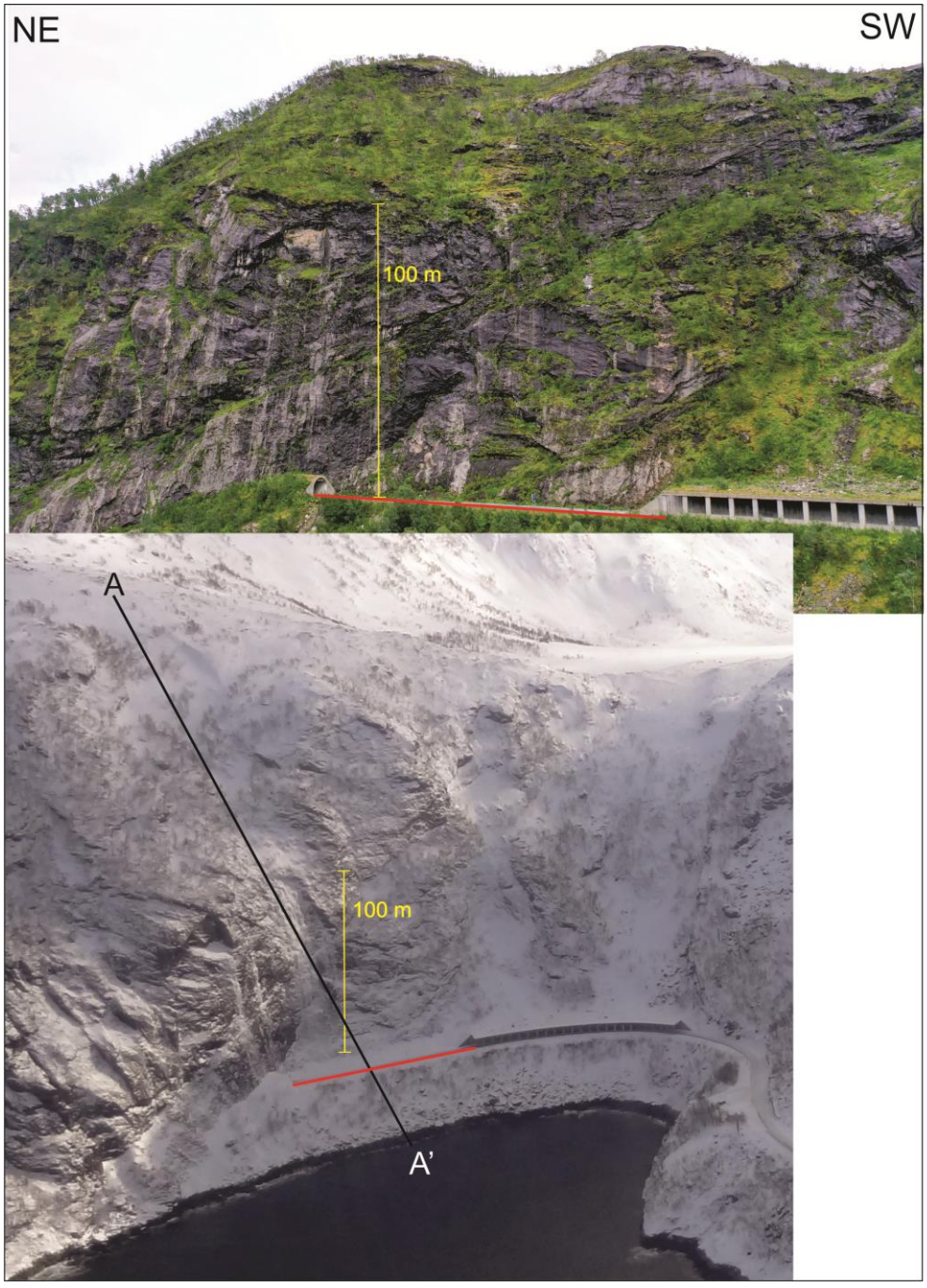

Figure 3. Drone photo and photo taken from helicopter of Svarthola during summer and winter, showing the research extent. The 100 meters stretch of road (red line) that is being investigated is situated between the Svartholla tunnel to the left and the rock shed to the right. Note the steep terrain that characterizes Svarthola, especially the 100 m high cliff above the road. Also note that the profile line (A-A') used for the slope profile shown in the next figure is marked. Photo 1: Linn Asplin, 2020. Photo 2: Andreas Persson, 2018.

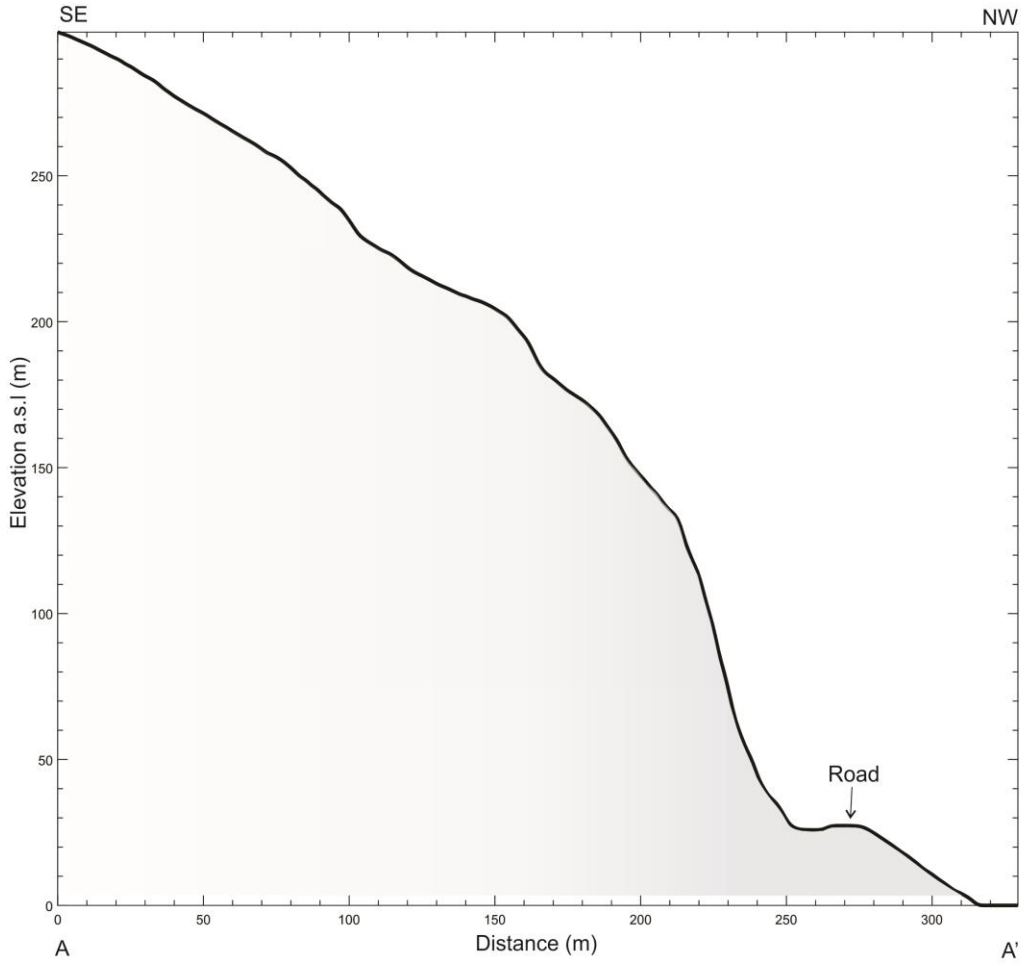

Figure 4. Slope profile (A-A') across the study area, Svarthola, showing the steep terrain that is situated above the road (black arrow). The profile line is marked in figure 3.

2.2 Geology

The regional and bedrock geology are essential for the assessment of the hazard mapping because the rock mass behavior is controlled by rock mechanical properties as well as the structural features such as joint sets and their orientation (Wylie Mah, 2004).

Senja Island is part of the West Troms Basement Complex (WTBC) that stretches from Senja in the south up along the coast to Vanna in the north (Zwaan, 1995). The rocks of the WTBC comprises Neoarchean to Paleoproterozoic (2.89-1.76 Ga) tonalitic gneisses and igneous and meta-supracrustal rocks (Bergh et al., 2010). Senja consists mainly of granite, gabbro, diorite and gneisses (Ramberg et al., 2013). Svarthola is composed of granite and granodiorite. The quaternary deposits consist of avalanches deposits. Areas close to the site is composed of moraine and glacial till (Figure 5) (NGU, 2020).

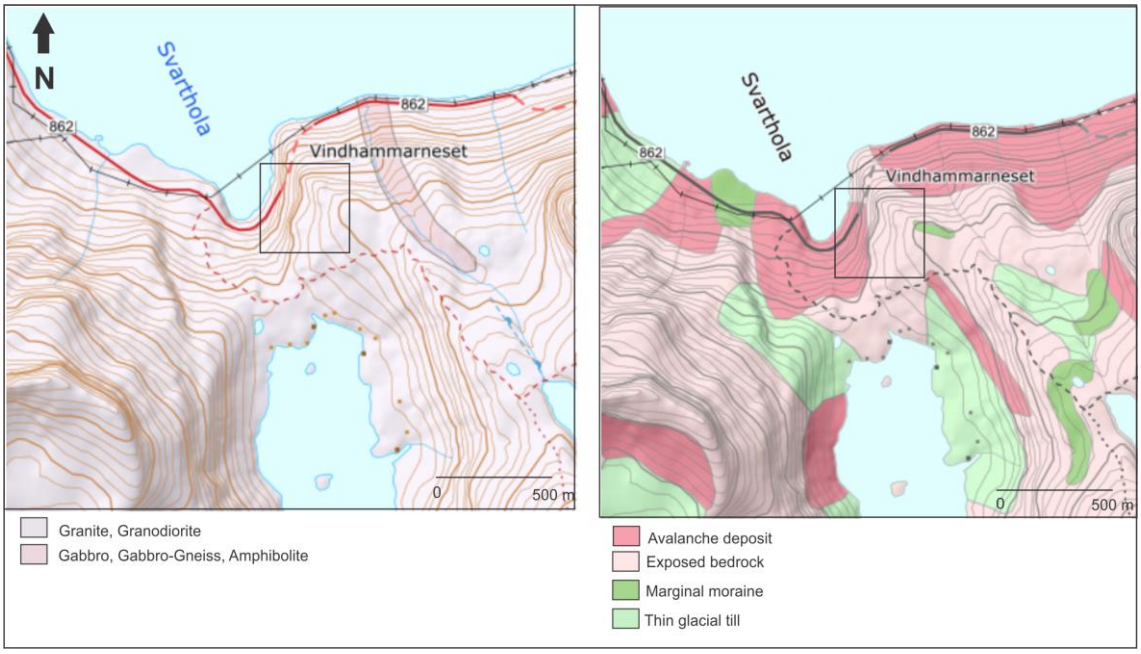

Figure 5. Main rock types of Svarthola (left) consist of granite and granodiorite. Quaternary deposits (right) is comprised of avalanche deposits. Modified after NGU (2021).

2.3 Climate

Meteorological conditions such as precipitation, wind and air temperature have a strong control on the timing of avalanche release. However the triggering mechanisms are complicated by local variations in the i.e. snow cover and geology (Jaedicke et al., 2008).

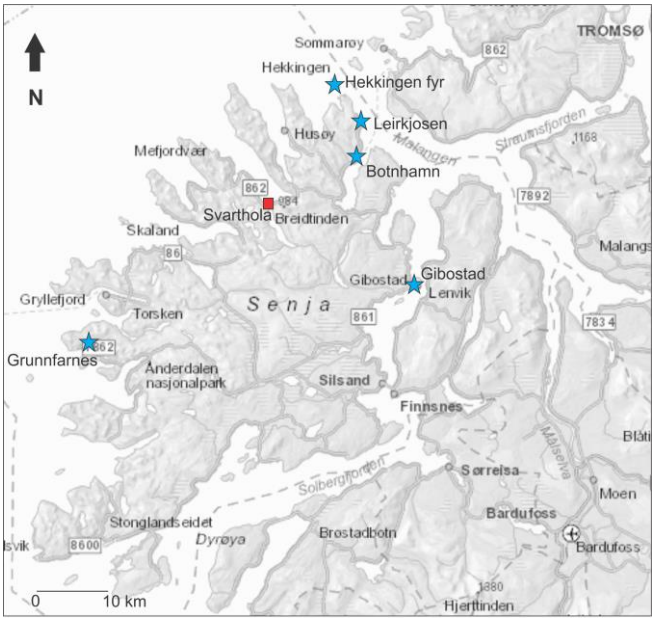

Five weather stations; Hekkingen fyr, Leirkjosen, Botnhamn, Gibostad and Grunnfarnes (Figure 6) are chosen to represent the weather conditions at Svarthola. These weather stations are located between 13-31 km distance from Svarthola and at 3-33 m a.s.l.

Figure 6. Weather stations (blue star) that are used to analyze the weather conditions. They are situated between 13-31 km distance from Svarthola and at 3-33 m a.s.l.

Svarthola is at a latitude of 69°, meaning it experiences short cool summers and long winters with many months of snow cover. The mean annual temperature of northern Senja varies between 3.0°C and 3.7°C (depending on the station), where January is the coldest month (-4.4°C to -3.0°C), and July is the warmest month (12.3°C to 11.5°C) (Table 1, Figure 7) (NMI, 2020).

Table 1. Month normal 1961–1990 for mean temperature (°C) from weather stations on Senja (NMI 2020).

Station	Altitude (m)	Jan	Feb	Mar	Apr	May	Jun	Jul	Aug	Sep	Oct	Nov	Dec	Year (°C)
Leirkjosen (88680)	9	-3.0	-2.8	-1.4	1.3	5.3	9.0	11.5	11.2	7.8	3.9	0.2	-1.9	**3.4**
Hekkingen fyr (88690)	33	-2.2	-2.1	-1.1	1.6	5.3	8.7	11.1	11.0	8.0	4.4	1.0	-1.1	**3.7**
Gibostad (88900)	12	-4.4	-4.2	-2.3	1.0	5.5	9.7	12.3	11.6	7.5	3.3	-0.8	-3.0	**3.0**

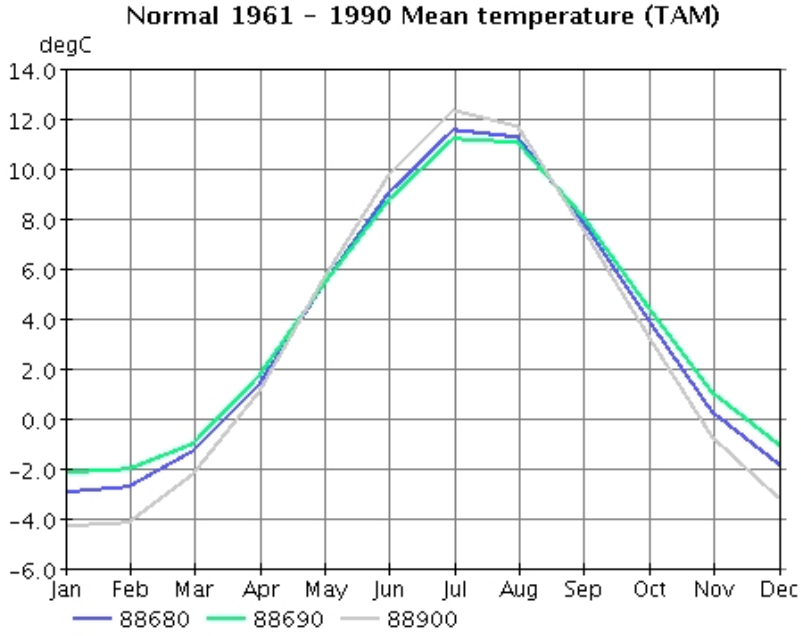

Figure 7. Month normal 1961–1990 for mean temperature (°C) from weather stations on Senja (NMI 2020).

The mean annual precipitation (normalized by month) on Senja ranges from 900–1000 mm, whereas 279-417 mm comes during the winter months (December-May). The data indicates that the precipitation is greatest from September to February (Table 2, Figure 8). The daily extreme ranging between 54.0-73.1 mm and 3-days precipitation between 80.7-137.0 mm (Table 3) and they are recorded during the winter months (December-May) (NMI, 2020).

Table 2. Month normal 1961–1990 for precipitation (mm), from weather stations on Senja (NMI 2020).

Station	Altitude (m)	Jan	Feb	Mar	Apr	May	Jun	Jul	Aug	Sep	Oct	Nov	Dec	Year (mm)
Leirkjosen (88680)	9	95	88	72	56	44	54	67	78	104	128	108	106	**1000**
Hekkingen fyr (88690)	33	79	74	65	57	61	52	63	69	87	117	91	95	**910**
Gibostad (88900)	12	85	80	60	54	39	47	63	71	91	119	94	98	**900**
Grunnfarnes (88460)	3	104	91	85	74	54	67	78	91	114	148	127	127	**1160**
Botnhamn (88660)	6	113	97	90	79	56	66	76	90	115	154	120	135	**1200**

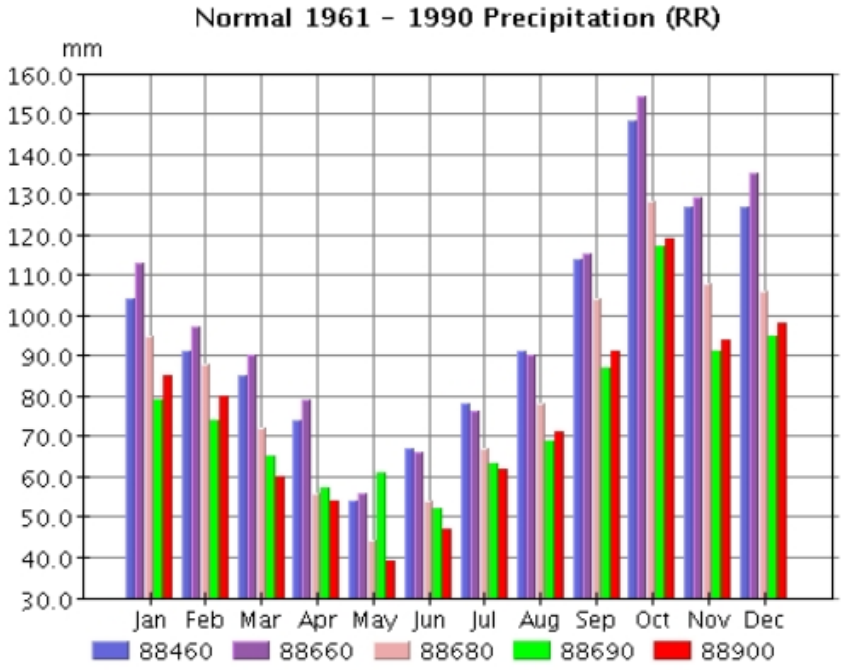

Figure 8. Month normal 1961–1990 for precipitation (mm) from weather stations on Senja (NMI 2020).

Table 3. Daily- and 3-day extreme precipitation (mm) on Senja for the period 1961-1990. Note that all records are during the winter months (NMI 2020).

			Max precipitation Dec-May (mm)	
Station	Altitude (m)	Distance	1-day	3-day
Gibostad (88900)	12	22 km SE	65.0 (02.1961)	92.5 (02.1961)
Grunnfarnes (88460)	3	31 km SW	73.1 (05.2019)	84.6 (02.2013)
Hekkingen Fyr (88690)	33	18 km NNE	57.6 (03.2000)	82.0 (01.2001)
Leirkjosen (88680)	9	16 km NE	54.0 (12.1982)	80.7 (12.1987)
Botnhamn (88660)	6	13 km NE	73.0 (12.1989)	137.0 (12.1989)

The distribution of precipitation on Senja is displayed in Figure 9A. The map shows a higher amount of precipitation on western Senja and at the highest elevations. Western Senja gets most of the snow throughout the year, but the inland parts of Senja and the highest altitudes have more days per year with snow cover. In these areas it takes longer for the snow to melt compared to the western coastal places. The mountainous areas get the greatest snow depths (Figure 9B). The maximum snow depth for three weather stations are displayed in Table 4, ranging between 108–179 cm (NMI, 2020).

Table 4. Maximum snow depth (cm) displayed for three weather stations at Senja, ranging between 108–179 cm (NMI 2020).

Station	Altitude (m)	Distance	Max snow depth (cm)
Gibostad (88900)	12	22 km SE	166 (01.1976)
Grunnfarnes (88460)	3	31 km SW	108 (03.2000)
Hekkingen Fyr (88690)	33	18 km NNE	-
Leirkjosen (88680)	9	16 km NE	179 (03.1981)
Botnhamn (88660)	6	13 km NE	-

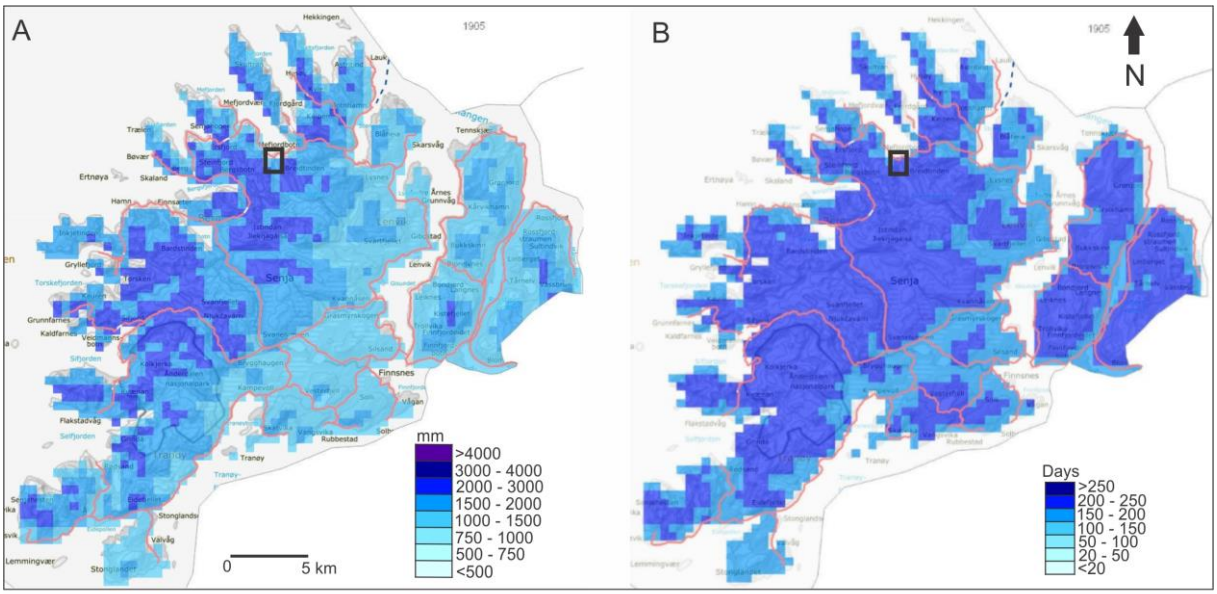

Figure 9. A) Month normal precipitation (mm) for years 1971-2000 on Senja. The precipitation is highest on the western part of the Island, along the coast, and at the highest altitudes. B) Amount of days per year with snow cover above 5 cm for years 1971–2000 on Senja. The inland and highest altitudes have more days/year with snow cover above 5 cm. Note the inset of Svarthola (black box). Modified after SVV (2019).

The main wind direction on northern Senja is SE to S based on the wind rose from Hekkingen Fyr located in the open sea (Figure 10). The wind direction will most likely vary a lot locally at Senja depending on the terrain surrounding the area. SW winds normally bring a mild climate with a lot of precipitation. NW winds normally bring colder weather together with

snow during the winter, including at low altitudes. S and E wind directions normally bring low precipitation and stable weather (Rasmussen, 2019). The weather station at Kistefjell (28 km SE) indicates that the strongest wind direction between December–May comes from W (Figure 10).

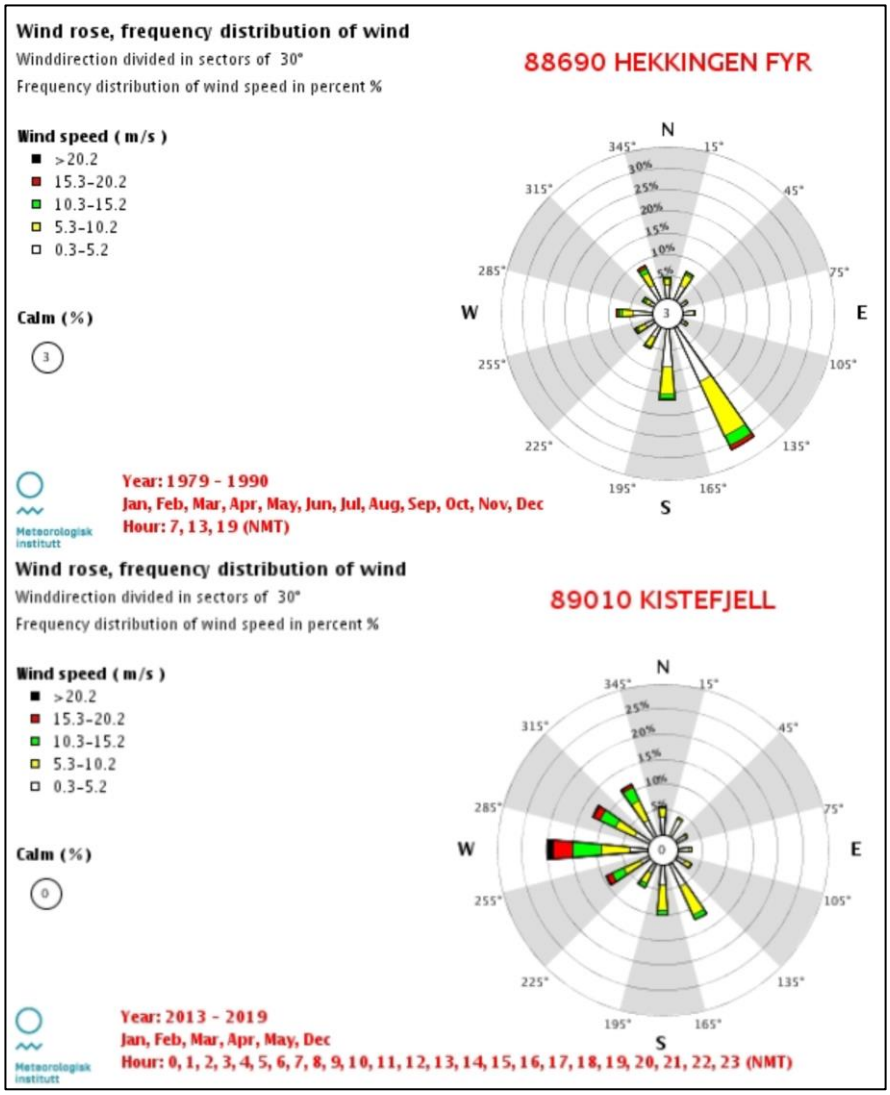

Figure 10. Wind data from the weather station, Hekkingen Fyr, from years 1979-1990, situated outside the northern part of Senja. The wind rose indicate a SE to S wind direction to be the main wind direction on Senja. Wind data from Kistefjell (28 km SE) indicates W winds to be dominated during the winter months (NMI 2020).

2.4 Rockfall and avalanche history

Historical records give an indication of the rockfall and avalanche frequency at the site. It is also possible to investigate the relationship between meteorological conditions and historical events. Historical events and future climate predictions can also help to investigate the change and risk of mass movements that one can face in the next, i.e. 50 years. A more thorough climatic analysis will be presented in the results and discussion chapter.

To obtain an overview of historical rockfall and avalanche events at Svarthola a database distributed by SVV was used (SVV, 2020). Unfortunately, the historical coverage of events is limited. Systematic registration of impact events by road authorities began in the 1970s, with the majority of registrations in the last 30 years. The database is dependent on that the contractors log the events and many events never end up being registered. It should therefore be noted that these registrations do not present a complete picture, however it can give an indication of what the mass movement trends.

There are 33 events registered at Svarthola between 1981 and 2020 (Table 5, Figure 11) (Kvalvågens et al., 2019). The road is closed on average six times a year due to rocks, snow or ice hitting the unprotected stretch of road, or because the avalanche danger is too high to keep the road open for traffic. The rockfalls and snow avalanches are recorded to hit the section of road closer to the tunnel portal most frequently (SVV, 2020).

Table 5. Registered rockfall and avalanche events at Svarthola between 1981 and 2020 (SVV 2020).

Year	Event	Number of events
2020-2007	Rockfall	13
2020-1981	Snow avalanche (dry)	7
2020-2008	Ice	8
2020	Snow avalanche (wet)	1
1998-1997	Unknown/event not specified	4

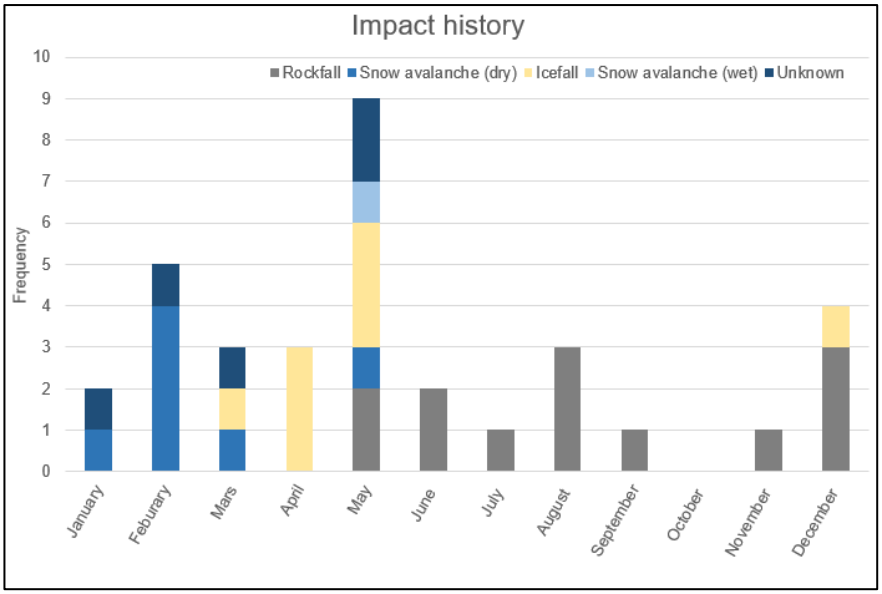

Figure 11. Rockfall and avalanche events registered between 1981 and 2020 at Svarthola, distributed per month. Note that 'unknown' are events that has not been specified in the registration database (SVV 2020).

2.4.1 Rockfall

Rockfalls are the most frequent mass movement type at Svarthola with 13 registered events, where five of these occurred recently (2020). They occur from May-December with the highest frequency in August and December (Table 5, Figure 11). The highest volume of collective blocks in an event are 5 m^3 (SVV, 2020).

On the 22nd of August 2020 a rockfall was released from the steep slope during heavy rainfall (Figure 12) (SVV, 2020). The estimated volume of the event is less than 1 m^3 (B. A. Reilertsen, personal communication, August 21, 2020). The event closed the road for 13 days due to the work of removing loose rocks at the slope (scaling).

Figure 12. Rockfall event on the 22.08.20. Note the release area (red circle) with fresh exposed bedrock. The estimated volume of the event was less than 1 m^3, together with loose material. The event closed the road for 13 days due to the work of scaling loose rocks from the slope to prevent further failures (SVV 2020).

On the 1st of June 2020, a boulder was released from the slope, and stopped at the road (Figure 13).

Figure 13. Rockfall event on the 01.06.2020. Note the boulder (red circle) in front of the truck (SVV 2020).

2.4.2 Snow avalanche

Snow avalanches are the second most common mass movement, where there is a registration of eight events and one of them is as a wet snow avalanche. The latest event was registered in 2016 and the largest known event happened 35 years ago. They typically occur from January-May with the highest frequency in February (Table 5, Figure 11). The avalanche danger is considered to increase with heavy snowfall and strong winds from SE (A. Persson, personal communication, October 29, 2020). The consequences of an event is critical since the road is located in the avalanche path, which means that the snow hits the road if it is released and endangers the road users and the snow has to be removed. A second problem related to snow at Svarthola is cornices that break and hit the road (B. A. Reilertsen, personal communication, August 21, 2020). This problem is not further evaluated since a potential protection structure for the mass movement types is assumed to withstand these impacts.

The largest known event, which occurred on the 6th of February 1986, buried a plow truck that drove pass the area (Figure 14).

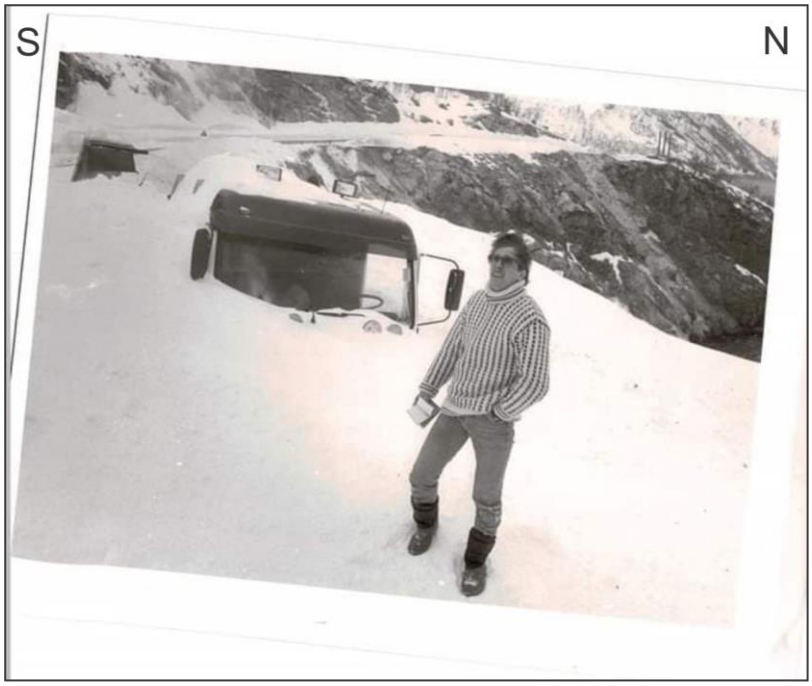

Figure 14. A photo taken on the 6th of February 1986 after a snow avalanche had been released and buried the plow truck. Note that today's existing snow shed may protect against parts of the snow masses of a similar event. Photo: RMT Senja A/S, Facebook.

2.4.3 Ice

Eight icefall events are registered. They occur from Mars-May and in December with highest frequency in April and May (Table 5, Figure 11).

On the 28th of April 2020 a large ice event occurred where the debris covered most of the road corridor (Figure 15). Ice events are not further evaluated in this thesis, since the impact dynamics are difficult to calculate and they are most likely higher during a snow and/or a rockfall event (due to longer fall heights and higher densities). It is assumed that a snow shed will also protect the road from ice events.

Figure 15. Ice event on the 28.04.2020. Note that the debris covers most of the road corridor (SVV 2020).

3 Theory

The following describes the mechanical rock and snow mass movement processes. This mechanical understanding forms the basis for the numerical simulation models employed in this project.

3.1 Rockfall

The term rockfall refers to the mass movement of rock fragments down a slope, through the air, by free fall, bouncing, rolling or sliding (Bozzolo Pamini, 1986; Varnes, 1978). In Norway, the term commonly denotes volumes below 100 m^3 (Hestnes Lied, 1980).

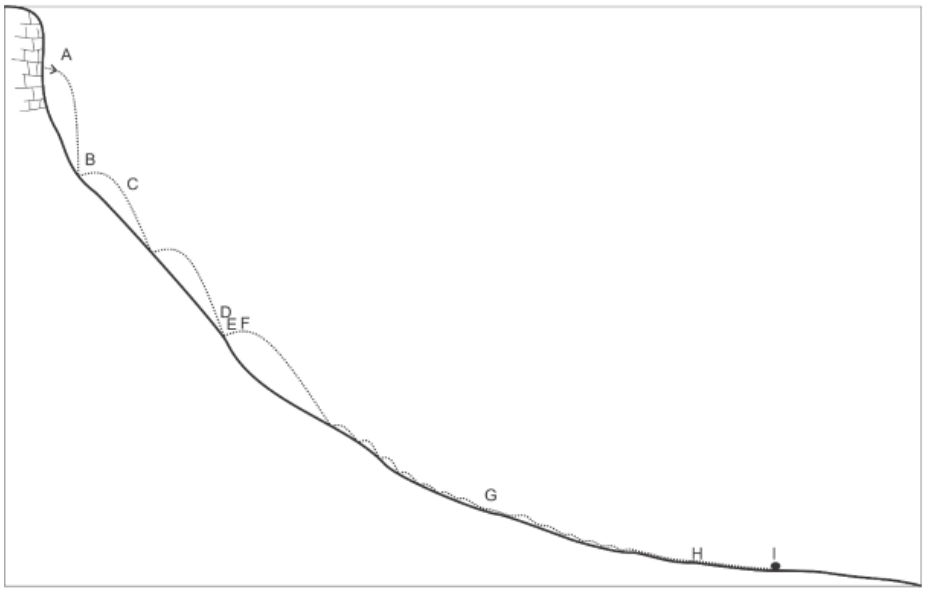

Figure 16. Schematic slope profile outlining the rockfall dynamics as various phases of movement: A) Detachment B) Initial Impact C) Ballistic trajectory D) Impact E) Ground contact and interaction F) Launching G) Rolling I) Stopping. From Vick (2015).

3.1.1 Rockfall dynamics

Rockfall dynamics are complex, driven by gravity, material properties and laws of motion (Scheck, 2010). The following outlines the current understanding of rockfall dynamics.

- **Detachment**

Rockfalls initiate when a rock block detaches from the source area (Figure 16a). The initiation is dependent on the source materials susceptibility and the triggering mechanism (Dorren, 2003). The susceptibility is dependent on the slope angle and the structural properties, such as, the type, roughness, joint orientation, spacing, aperture, filling and weathering. These properties control the potential size and mode of the detached block (Palma et al., 2012).

- **Rock mass susceptibility**

Discontinuities (i.e. bedding planes, joints, fractures, faults) and their orientation mainly control if it is feasible for the rock mass to fail and in what manner (Wylie Mah, 2004). The discontinuity orientation often generates one of three different failures: sliding, toppling or planar (Figure 17). The orientation also determines the size and shape of the detached block (Vick, 2015).

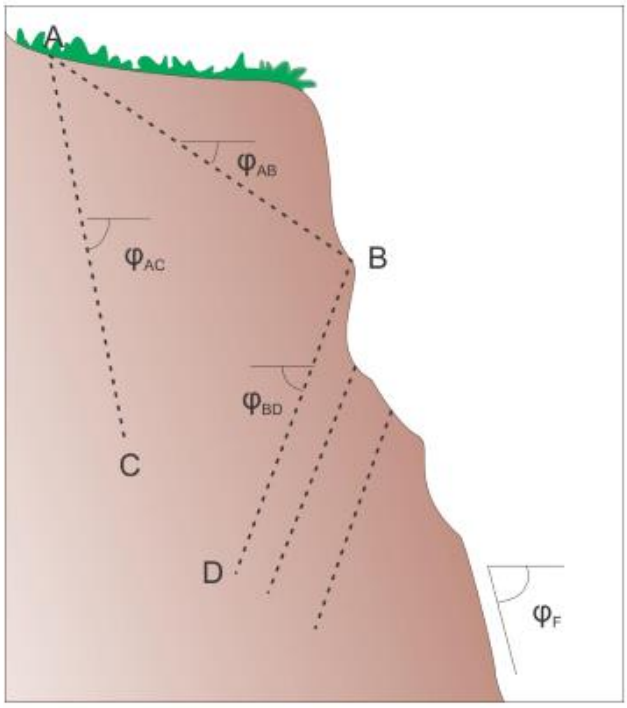

Figure 17. Schematic of a source area, showing three different failure types: sliding, toppling and planar. From Vick (2015).

- **Initial impact (kinetic energy) and ground conditions**

The initial impact, the rock block's first ground contact, is a crucial moment of the rockfall dynamics (Figure 16b). If the slope angle is more than 70° the detached rock enters a period of free-fall (Dorren, 2003). If the source area is less than 70° it is likely that the rock will travel down the slope by a bouncing, rolling and/or sliding motion (or in a ballistic trajectory). If the rock hits the initial impact from a source high above the high potential energy is converted to high kinetic energy and makes the rock run out from the slope. However, if the initial impact happens close to the source area, less kinetic energy is generated and allows the rock to stop on impact or shortly after. The overall angular momentum of a rock increases after its first initial impact and increases until it has reached its maximum rotational velocity (Wylie Mah, 2004).

The ground conditions will affect how much the kinetic energy is reduced on the initial impact and the following impacts with the slope surface. A rock can lose between 75-86% of the energy generated in free-fall on the first ground contact (Dorren, 2003; Evans Hungr, 1993). Hard surface impacts allows the rock to keep most of the energy due to the stiffness of the surface. Soft surfaces (i.e. soil) absorbs some of the energy as it deforms (forming impact scars). This slows the rock down and reduces the runout length (Bozzolo Pamini, 1986).

The kinetic energy of the rock, together with the slope angle and characteristics, angular momentum, velocity, will determine whether the rock is bouncing, rolling, sliding or moving at all, after the initial impact with the slope (Bozzolo Pamini, 1986).

- **Rockfall runout**

The shape and size of the rock are the main factors affecting the distance it will travel from the source area (Azzoni De Freitas, 1995).

Spherical rocks travel further and faster than other shapes, such as flat or long blocks, as they have fewer angular edges and therefore generate less friction with the surface. Spherical rocks are also able to maintain angular momentum easier than i.e. flat shaped rocks (Glover, 2015). However, if an irregular rock travels along its short axis, it may travel faster than an spherical rock of equal mass (Wylie Mah, 2004).

Larger rocks are known to travel further and have greater velocity at a given travel distance than smaller rocks made up of the same material (Crosta Agliardi, 2004). This is due to the kinetic energy, being a function of mass, it is greater for bigger rocks, and they are also less affected by slope irregularities (Vick, 2015).

Even if the source area is kept constant, the rock will be deposited at various locations. As the trajectory of the rock, especially the outgoing direction at an impact is influenced by variable factors on the slope. However, generally, larger rocks travel the furthest and slopes that are longer with little gradient variations will allow rocks to travel greater distances from its source (Azzoni De Freitas, 1995).

3.1.2 Triggering factors

Rockfalls can be triggered by natural or human-induced processes. The focus on this thesis is on the naturally occurring processes. These include (Wylie Mah, 2004):

- Rainfall
- Snow melt

- Freeze-thaw
- Weathering
- Root penetration and wedging

The most common triggering factors are intense rainfall episodes and freeze-thaw processes in water-filled discontinuities (Delonca et al., 2014). High water input (from rainfall or snowmelt) may lead to the breakdown of minerals and can create weakness planes (joints) in the rock mass. It may also increase the pore water pressure in joints, resulting in the reduction of the shear strength (Braathen et al., 2004). As the temperature falls below 0°C the water within the joints freeze to ice and may lead to freeze-thaw activity (Dorren, 2003; Walder Hallet, 1985). All exposed bedrock slopes are affected by physical and chemical weathering, in various degrees and rates, which can promote block instability (Dorren, 2003). Roots can penetrate into the discontinuities and lead to thrust wedging which decreases the stability and promotes rockfalls (Fernandez-Hernández et al., 2012).

3.2 Snow avalanches

Snow avalanches are rapid flows of snow sliding, flowing or tumbling down a slope. The avalanche masses can in addition to snow (consisting of varying amount of air, ice and water) contain rock debris, soil and vegetation (Schweizer et al., 2003). Snow avalanches are generally divided into two types: slab- and loose-snow avalanches. (McClung Schaerer, 2006). In this thesis, the focus will be on slab avalanches, as these are the typical type occurring at Svarthola, and are generally more dangerous.

A slab avalanche involves the release of a cohesive slab that is initiated by the failure of a weak snow layer (i.e. depth hoar, faceted crystals) within the snow pack and moves down on a sliding plane (Figure 18-19) (Schweizer et al., 2003). A tension fracture occurs in the weak layer that propagates along the layer and perpendicular to the ground, called the crown (defining the height of the avalanche). The fractures delineate the area of the slab, the length can vary from 10 m to 10 km and the thickness can range from few centimeters to several meters (Lied Kristensen, 2003). The crown height varies normally between 0.5-2 m (Figure 18-19). The volume of an avalanche can differ a lot due to these variations. They are generally between 100-100 000 m^3, but there are records of volumes up to 1 million m^3 (Norem, 2014).

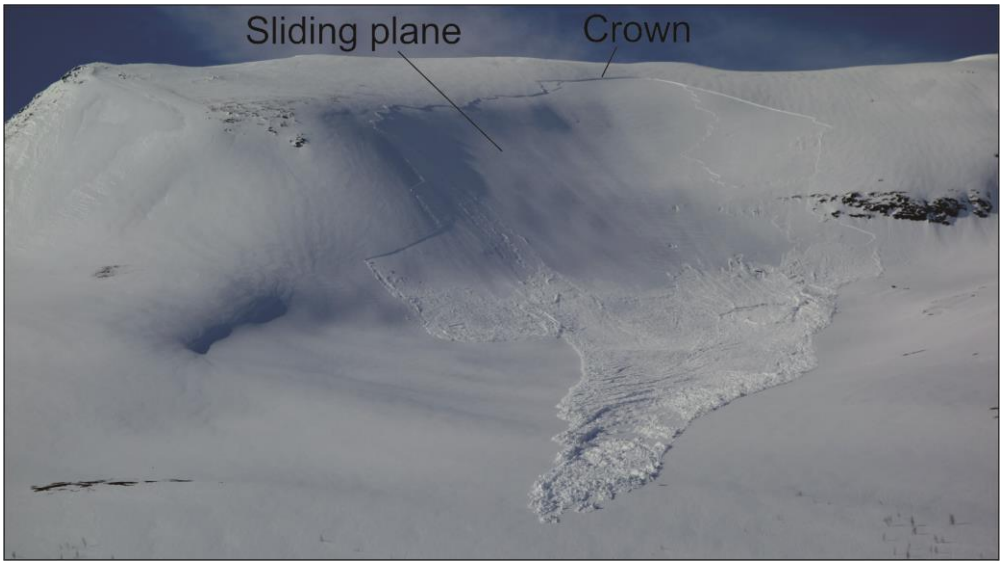

Figure 18. **Slab avalanche that has moved down a sliding plane. Note that the crown is clearly visible. Photo: Linn Asplin, 2021.**

3.2.1 Avalanche dynamics

- **Avalanche paths**

The slab avalanche is generally divided into three parts; the starting zone, the track (or path) and the runout zone (Figure 19). The starting zone is characterized by a crown, and comprises the release area. The formation of a starting zone is mainly influenced by the slope gradient, where 30–60° slope inclination is required to generate a slab fracture (McClung Schaerer, 2006; Pudasaini Hutter, 2007). Other factors that influence the formation of a starting zone includes slope aspect in relation to wind and solar radiation, terrain form, vegetation and roughness (Norem, 2014).

After the initial fracture in a weak layer and if the fracture propagates and the forces exceed the shear strength the slab is released. As the slab accelerates, it leaves the starting zone and entrains more snow as it moves downwards and into the track. The track is generally at slope angles of 20-30° (Figure 19) (Pudasaini Hutter, 2007). The shape, relief, inclination, vegetation and roughness of the track influences the characteristics of an avalanche. For example, a steep track leads to high avalanche velocities (McClung Schaerer, 2006). The avalanche, generally, flows down the steepest path of the slope while being channeled by terrain features, which direct the flow to the bottom (Pudasaini Hutter, 2007).

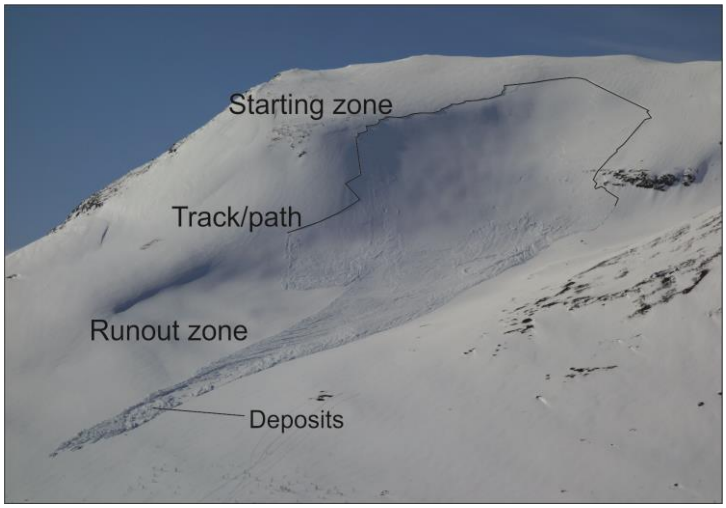

Figure 19. Photo outlining the three parts of an avalanche path: starting zone, track/path and runout zone. A black line marks the crown. Note that this is a small avalanche and the three parts can be much bigger. Photo: Linn Asplin, 2021.

Finally, the moving avalanche reaches the runout zone (or deposition zone), this is where the motion ends. The slope inclinations are commonly less than 10° here. The transition of the avalanche path to the runout zone is abrupt when the path leading to the ground is steep. The greater the volume of an avalanche, the further the runout distance and hence the greater the potential distance to deposition (McClung Schaerer, 2006; Pudasaini Hutter, 2007).

- **Motion**

After failure, when the avalanche starts to move down the slope, the internal structure is broken down. It is said that the avalanche flows like a granular material (Norem, 2014; Pudasaini Hutter, 2007). However, the avalanche movement is a complex process and it does not yet exist a complete physically and mathematically description of this phenomena (Rudolf-Miklau et al., 2015). The movement of dry-slab avalanches can be divided into powder snow (airborne-powder) and mixed-motion (Perla Martinelli, 1976; Rudolf-Miklau et al., 2015). In powder motion most of the snow swirls through the air, seen as a snow cloud (suspension layer). Pure powder motion is rare but it can occur when an avalanche goes over a cliff (Figure 20A) (Perla Martinelli, 1976). In mixed-motion avalanches, observations suggest that there is a dense flow component along the surface, with a transition layer, called saltation layer over, and a powder component on top if the velocity is high enough (Figure 20B) (Barbolini et al., 2009; Rudolf-Miklau et al., 2015). The dense masses, where the particles have close contact with each other, have relatively high densities (100–300 kg/m^3). This component dictates the frontal velocity and is the most destructive (Rudolf-Miklau et al., 2015). Dry (slab) avalanches may reach velocities of 60–70 m/s. The powder component

often has a longer runout distance than the dense mass but is less destructive (Norem, 2014).

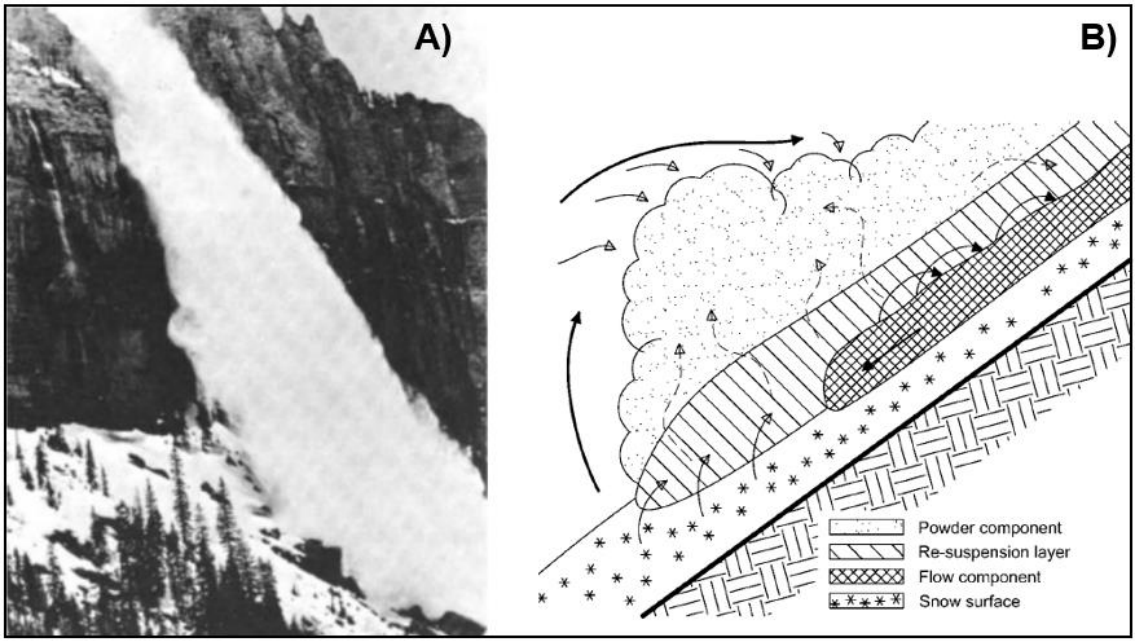

Figure 20. A) A seldom pure powder-motion avalanche that goes over a cliff in Colorado, USA (Perla Martinelli, 1976). B) Illustrations of the movement of a mixed avalanche with a dense flow component, saltation and powder layer (Rudolf-Miklau et al., 2015).

3.2.2 Contributory and triggering factors

Terrain, precipitation (especially new snow), wind, temperature and snowpack stratigraphy are essential contributory factors for slab avalanche formation (Schweizer et al., 2003). The state of the snowpack is greatly affected by the weather and the main meteorological factors that increase the natural release of an avalanche are (Norem, 2014; Schweizer et al., 2003):

- Snowfall
- Wind
- Temperature

New snow and rapid accumulation of snow increases the load (stress) on a snow pack. Under the rapid loading, the snow has less time to absorb the weight and it becomes a balance between the new applied stress and the strength of the old snow pack (Pudasaini Hutter, 2007). The likelihood of an avalanche to initiate is greater under these conditions. A new snow depth of about 90-100 mm within 3 days is considered critical for the release of extreme avalanches, about 30-50 mm within a storm in general, and 2-3 mm/h is observed to increase the avalanche danger (Norem, 2014; Schweizer et al., 2003).

Wind can transport large quantities of snow and can increase the load on the snowpack significantly. Snow will mainly be deposited in lee areas as cornices, or filling in hollows and gullies where the wind typically decelerates. The threshold wind speed for the transport of loose, cold snow is between 5-10 m/s (McClung Schaerer, 2006). Wind loading can trigger an avalanche if the load of the wind slab gets larger than the strength of the weak layer (Eckerstorfer, 2013).

Temperature is a complex factor that affects the snowpack properties in various ways. It affects mainly the surface layers and again, the rate of change is important. Rising temperature during a storm and rapid increase shortly after contributes to instability. Rapid warming contributes to increased deformation of the surface layers, which leads to increased strain and strain rates at the slab/weak layer interface. Solar radiation can decrease the snow stability similar to rapid warming (Schweizer et al., 2003). It is often a contributing factor for wet loose-snow avalanches in the spring. Weak layer formation at the snow surface can be influenced by radiation. It is considered to affect the upper 10–20 cm of the snowpack (Norem, 2014).

3.3 Avalanche mitigation and remediation

There are various structural methods to protect roads from mass movements. In general, the mitigation measures that cost the most give the best protection and can be used for all types of mass movements (Norem, 2014). In this thesis the focus is on galleries, a form of rockfall and snow avalanche protection also termed a shed. A shed consists of reinforced concrete slabs normally covered by a cushion layer that can reduce the impact energy transmitted to the shed. The structure is within the runout path and therefore the structures must be dimensioned based on various criteria, such as impact energy and velocity at the point of shed placement (Rudolf-Miklau et al., 2015). It is an advantage to divert the mass movements over the critical infrastructure (road) instead of stopping the mass movement because this reduces the overall load on the structure. The earth loads on the rock shed from backfill and the shear stresses, should also be accounted for (Norem, 2014). As the shed is open on the downhill side, the possibility of backflow from an avalanche should be considered (suction pressure) (Rudolf-Miklau et al., 2015).

The action of falling rocks on a rock shed, the impact force, is influenced by the block (mass, shape) and its kinematics (velocity, impact angle) and on the cushion layer on the shed roof (thickness, compaction degree) (Volkwein et al., 2011). Engineers commonly use so-called design blocks for the protection structure, a specified rock block that is selected for the

design that the structure intend to withstand. The impacts are usually estimated by using rockfall modelling software or testing (Green, 2016; Vagnon et al., 2020).

The snow avalanche actions against a construction causes dynamic pressure to develop, both stationary- and short-term impact pressures (Rudolf-Miklau et al., 2015). Figure 21 shows a schematic diagram of the impact pressure distribution for a snow avalanche that hits a wall consisting of a dense mass flowing along the ground, a saltation layer and a powder part. The impact pressure on an object can be calculated by the dynamic pressure equations for fluids (described in method chapter, 4.4.2). The avalanche impact dynamics (impact pressure, velocity and flow height) are usually estimated by the use of an avalanche modelling software (Rudolf-Miklau et al., 2015).

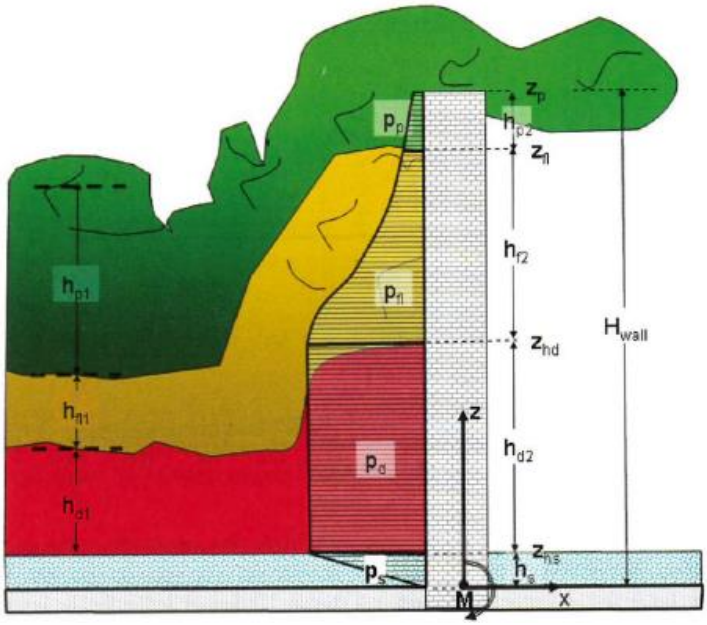

Figure 21. Illustration diagram of the impact pressure distribution when a snow avalanche hits an obstacle that consist of a dense flow component (red), a saltation layer (yellow) and a powder part (green) (Rudolf-Miklau et al., 2015).

The impact pressure can be regarded as a measure of destructiveness and the damage potential (Table 6). It is very rare that snow sheds are damaged, however there are cases where they have been destroyed by unforeseen vertical avalanche impacts (Figure 22).

Table 6. Avalanche (impact) pressure as a measure of damage potential (Rudolf-Miklau et al., 2015).

Avalanche pressure	Damage potential
up to 1 kPa	Windows are smashed in
up to 5 kPa	Doors are pushed in
up to 30 kPa	Wooden or brick structures are damaged or destroyed
up to 100 kPa	Trees will be uprooted
up to 1000 kPa	Concrete structures are damaged or destroyed

Figure 22. A snow shed that was damaged by a wet-snow avalanche that fell almost vertically on the roof in Switzerland. Photo: Stefan Margreth, 2009.

There is no verified method yet to calculate vertical avalanche impact and our understanding of the dynamics of the airborne snow motion is poorly understood. Experiments on snow hitting a dam (mound) has shown that the snow is launched over it following a projectile motion/parabolic trajectory (described in the methods chapter, 4.4) (Barbolini et al., 2009; Hákonardóttir et al., 2003).

4 Data and methods

This chapter presents the methods used for data collection and analysis, as well as software used for data analysis and presentation. First is a short description of the fieldwork, followed by a description of digital data and software used. Thereafter methods applied to get the impact dynamics of rockfalls and snow avalanches are presented.

4.1 Fieldwork, digital data and software

Fieldwork was conducted on the 21st of August 2020 together with the supervisor Louise M. Vick, and 29th August and 18th October alone. A rockfall event occurred during this period on the 22nd of September 2020, after which additional data was immediately collected on our behalf by the TFFK. The main tasks of the fieldwork were:

- Produce mapped data as inputs to the numerical modelling, including mapping the dimensions of 40 boulders with a measuring stick and their locations with a Garmin GPS (Etrex 30x), and delineate the terrain characteristics.
- Collect rock samples for geological characterization and for boulder density assessment.
- Collection of drone video and image data with a DJI Mavic 2 Pro.
- Recording of geological and structural measurements using FieldMove Clino, an Ipad mapping application.
- On-site meeting with the local contractor with responsibility for reporting and clearing avalanche events that have stopped at the road, in order to gain insight into historical avalanche events and other problems at Svarthola.
- Collection of additional field data (video and image data) after the rockfall event and rockfalls induced by the scaling team for use in numerical model calibration.

The following desktop datasets were obtained for use or analysis in this thesis:

- A WMS server topographic map in grayscale (NMA, 2020c).
- Orthophotos from 2016 (resolution 0.2 m and 0.5 m) (NMA, 2020b).
- LiDAR-derived DTM of 1 m resolution and resampled to 5 m within the snow module (NMA, 2020a).
- Bedrock and quaternary geological maps in 1:50,000 (NGU, 2020).

All spatial data was projected in WGS 1984 UTM Zone 33N (local grid) and analyzed in Esri ArcGIS Pro 2.6.3. Functions such as slope angle and hillshade (315°) were used in GIS to analyze and present the data. Statistical data was analyzed in Microsoft Excel 2016. Figures

were constructed in CorelDRAW Graphics 2017. The numerical modelling software RAMMS (RApid Mass Movement Simulation) was used to get impact dynamics from rockfalls and snow avalanches. Two of the modules of the RAMMS series will be used in this thesis, ROCKFALL and AVALANCHE. The methods applied for the modelling will be explained in the following subchapters. Thorough manual description refer to Bartelt et al. (2016; 2017).

4.2 Numerical modelling

When calculating impact it is helpful to use a simulation model which replicates the complex dynamics of the mass movements. The software RAMMS is today commonly used by engineers worldwide, including in Norway, to simulate rockfalls and snow avalanches. However, any numerical model is an approximation of a complex natural process. As we do not yet fully understand the mass movement dynamics, there are simplifications and limitations within the model algorithms. For the user it is important to know the sensitivity of the input parameters because these have a great impact on the results, such as the delineation of the release areas and terrain materials, the dimension of rock shapes and volumes and the snow release depth. To calibrate the model by, e.g. a known event can minimize the uncertainties to some extent, but the lack of information from historical events can make this difficult.

In order to reach reliable and realistic results, the information derived from the models are put into context and compared with the avalanche history, field observations, experience from experts and earlier studies done at similar areas. In addition, the avalanche model is combined with physical formulas.

4.3 Rockfall

The rockfall simulations were run for four different scenarios (1-4). The DTM, rock density and terrain materials assigned for these simulations were those obtained in the calibration. A greater release area was delineated based on rockfall susceptibility, steepness, outcropping rock and height in the terrain to maximize kinetic energy. Scenarios are based on annual probabilities, increasing in hazard. Engineers in Norway should design a rock shed accordingly to an event with a 100-year return (Statens vegvesen, 2015). Scenarios 1-3 were run with the same number of rocks and rock shapes, but with different rock sizes/volumes (so-called design blocks) depending on the hazard level (larger volumes represent a greater return period). These scenarios are based on registered rockfall events in the database and mapped boulders.

The following scenarios were selected:

1. Annual events
2. 50-year return period
3. 100-year return period
4. Worst-case

The different scenarios aim to give a technical overview of the impact dynamics of rockfall events with different frequencies. Scenario 3 is sub-divided into 3a and 3b, where scenarios 1-3a are relevant for the rock shed design and the other scenarios are for academic purpose.

4.3.1 RAMMS::ROCKFALL model description and setup

RAMMS::ROCKFALL employs a rigid body motion to replicate rock trajectories in 3D terrain. The simulation ends when the rocks reaches a threshold minimum velocity or when the computing time is met. The following is descriptions of the input parameters that are needed for running a simulation, including the input data that were used in this study.

Calibration of RAMMS was performed taking advantage of the rockfalls induced by the scaling team where several important parameters could be identified, such as the release area, the boulder variation and distribution. The delineation was done from information and photos distributed by the scaling team and from field observations gathered before and after the event (Figure 23). This process ensured confidence in the input parameters for the wider-scale deterministic modelling.

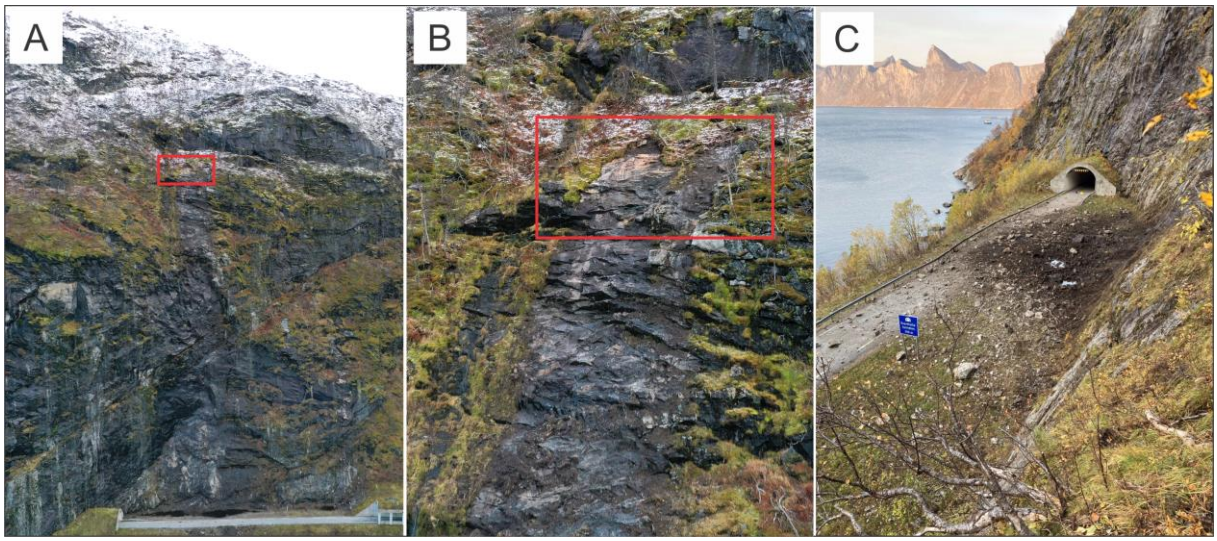

Figure 23. Images taken after the scaling in September 2020 which were used for the calibration of RAMMS A) Overview of the release area (red box) B) Close-up of release area (red box) C) Overview of the rockfall distribution.

Digital terrain model (DTM)

A high-resolution (0.5-10 m) rasterized DTM for the study area is required. The DTM is a georeferenced raster that describes the topography in 3D. The preferred resolution is 5 m or higher in order to get an accurate simulation. For this study, a 1 m resolution was used for all simulations.

Release area

The rockfall release areas can be specified as a point, line (made up of many points) or as an area (made of one or several cells). The user can decide to define the area by draw it directly in the model or by importing an ESRI shapefile. A shapefile was created made up of five points covering the release area for the calibration.

Rock

Rocks are modelled as rigid polyhedral (rigid body). Boulders can be imported as point clouds or created using the rock builder tool (recommended) with pre-defined realistic rock shapes. The model library include three typical shapes: equant (three equal axes), flat (one short, two long axes) and long (two short axes, one long). These rock shapes were modelled from real rocks by laser scans, so natural irregularities and angularities are accounted for (Vick, 2015). The rock volume and rock density can be adjusted to match the release rock from an historical rockfall event. Upon release, the rocks are subjected to a user-defined number of random orientation, which adds probabilistic elements to the simulation. The rocks mass center position are mapped at all times during a simulation, described in three translational and rotational degrees of freedom.

Mapped boulders were recreated in the RAMMS rock builder tool by defining the axes lengths, volumes and shapes as close to the real rocks as possible. A density of 2700 kg/m^3 was assigned for these boulders corresponding to the mean density of a metamorphosed granite (Smithson, 1971). Input parameters for the calibration are summarized in the result section 5.4 and full description are displayed in Appendix A.

Terrain material

The terrain material can be categorized by drawing or importing polygon shapefiles, with terrain ranging from extra soft to extra hard (with several steps between). Every category controls the rock's interaction with the slope. The interaction is described by the sliding of a block through the material as a function of Coulomb friction and drag force. Additional drag

force can be applied by the user in the form of a forest and/or a water body. Additional mathematical explanations of the algorithm are available in the manual.

The slope was divided into three different material domains based on field observations and by analyzing drone photos. They were divided by outcropping rock (orange), rock close to surface (no color) and softer vegetated areas (yellow), an open-dense forest (green) below the road, and water (blue) for the fjord. All terrain shapefiles were loaded into RAMMS and different material descriptions were applied for the simulations using the guidelines in Bartelt et al. (2016). The materials were varied until the result replicated the block distribution that was caused by the scaling team and dynamic results were realistic. Other parameters such as rock block size and release area were kept constant.

4.4 Snow avalanche

The snow avalanche analysis follows a somewhat different approach than the rockfall analysis due the limitations within the model to replicate the process of airborne flow. Svarthola has a steep avalanche path, where the end of the track consists of a 100 m high cliff and parts of the snow masses may get airborne. The impacts from one design scenario, a dry-slab avalanche with a 100-year period, were obtained through three different methods;

1. RAMMS – the numerical model is used to the get the impacts dynamics at the road.
2. Physical formulas – the numerical model is used to the cliff point (‘takeoff’) where parts of the snow masses may become airborne. The ‘takeoff’ velocity from the model is used as input to manual physical formulas. The physical formulas consist of the projectile motion and the dynamic pressure formula.
3. RAMMS and physical formulas – the numerical model is used to the ‘takeoff’ point and the average impact velocity from the model and physical formulas is used in the dynamic pressure formula.

The thesis focus on dry-slab avalanches and further investigations should be done to establish the wet-snow avalanche impacts. This study does not include calculations on the static loads or backflow pressure or considers the impact angle, but aim to give a technical overview of the impact dynamics at the road.

4.4.1 RAMMS::AVALANCHE model description and setup

In RAMMS::AVALANCHE, the motion of the movement from initiation to runout is calculated and the slope-parallel velocities and flow heights are calculated. The model was developed from observations of dry-slab avalanches flowing along the terrain.

Digital terrain model (DTM)

The resolution of the DTM should not be too high or too low because that could include details in terrain that is covered with snow during the winter and/or give inaccurate calculations of the friction parameters and the movement of the avalanche (Bühler et al., 2013; Christen et al., 2010). The DTM was resample to a resolution of 5 m RAMMS. This should represent the snow cover that evens out the terrain during winter. Engineers often use this resolution in numerical models to predict the avalanche dynamics (Christen et al., 2012).

Release area

Information concerning the release areas is sparse and for this reason the release areas were first identified using GIS terrain analysis of the slope angle. Terrain between 30-55° was identified as potential release areas (McClung Schaerer, 2006; NVE, 2020b; Pudasaini Hutter, 2007). Drone images were also used to verify the areas by studying the terrain form and slope aspect.

Release depth

The release depth for each release area is specified by the user within the model and from this the volume is calculated automatically. Information concerning the release depths are very sparse. For this reason, a procedure that is described by the Norwegian Water Resources and Energy Directorate (NVE) is used. This method was first introduced by Salm et al (1990) and it is adapted by Swiss guidelines. It is based on climate data, where the release depth is decided by the greatest precipitation amount over three days as a function of the return period, i.e. the greatest 3-day snow depth in a 100-year return period. These data are based on statistical projections from nearby weather stations. The snow data are obtained for the winter months (December-May) where the precipitation is assumed to come as snow (1 mm rain = 1 cm snow) (NMI, 2020; Winiger et al., 2005). The 3-day snow depth was then adjusted for:

- altitude difference of the weather station and release area (+/- 5 cm snow for every 100 m);
- mean slope angle;
- snowdrift (in Switzerland +/- 30-50 cm).

The mean slope angle adjustment refers to the theory that more snow is able to accumulate at less steep areas (27-40°) than steeper terrain (40-55°). There are no standard values for this adjustment (NVE, 2020b).

Friction parameters

RAMMS replicates the flow by employing the Voellmy friction law. This physical model divides the frictional resistance into two parts: a dry-Coulomb friction (μ) and a viscous-turbulent friction (ξ). μ controls when the flow is close to stopping, ξ controls when the flows is running quickly. These two friction coefficients can be adjusted by the user to fit the site specific case. RAMMS recommends to automatically generate a μ and ξ file (= variable calculation mode) in the software that is based on topographic data analysis (slope angle, altitude and curvature), forest information and global parameters. The global parameters consist of the volume category (tiny-large) and the return period (10-, 30-, 100-, and 300-years). The default altitude limits are 1500 m. a.s.l. and 1000 m a.s.l in accordance to release areas in Switzerland. Additional physical theories and models of the friction parameters are available in the manual.

The friction parameters (μ & ξ) were set automatically within RAMMS. No forest was specified because it was assumed that the sparsely spread bushes were easily destroyed and did not slow down the avalanches. In order to adjust for the Norwegian conditions where the climate is generally colder at lower altitudes than in Switzerland the altitude limits were changed. According to Håland et al. (2015) the results get more accurate if this parameter is changed in accordance to the tree line at the study area. The avalanche path is above the tree line and therefore the altitude limits were changed to 500 m a.s.l and 0 m a.s.l.

Snow density and cohesion

The default value for the avalanche density is 300 kg/m^3 and is recommended to be kept if no further information is available. Cohesion is not affecting the avalanche dynamics of a dry slab avalanche in the same extent as wet-snow avalanches. There is not sufficient studies in Norway of its affects and therefore suggested to be neglected (Håland et al., 2015). The default density was used and the cohesion was neglected for the simulation.

4.4.2 Physical formulas: projectile motion and dynamic pressure

There is no verified method to calculate impact pressures from airborne granular flows which is possible at the steep cliff at Svarthola (S. Margreth and P. Gauer, personal communication, January 18-23, 2021). Improved understanding achieved over the last 5-10 years of the flow of snow avalanches against dams have shown that they follow parabolic

paths during ballistic trajectory (Barbolini et al., 2009; Hákonardóttir et al., 2003). The avalanche impact pressure after a free-fall can be determined by the physical principle of the parabolic trajectory/projectile motion. This method was introduced by Stefan Margreth, snow and avalanche expert and senior consultant in WSL Institute for Snow and Avalanche Research SLF (Davos, Switzerland) and by Peter Gauer, senior engineer in Norwegian Geotechnical Institute, NGI (Oslo, Norway). There are several simplifications in this method. It is a 2D point-mass model and therefore does not consider the dimensions or mass of avalanche. It also does not consider the interaction of the particles within the avalanche, as well as the frictional forces from the air resistance and topography on the way down. The kinematic equations are based on the assumption of energy conservation of the flow through the air.

The first step is to determine velocity of the avalanche as it leaves the terrain. The velocity can be divided into horizontal and vertical components along the x- and y-axes given by:

$$V_{0x} = V_x = V_0 cos(\alpha)$$

$$V_{0y} = V_0 sin(\alpha),$$

where V_0 is the RAMMS-velocity at takeoff and α is the slope angle from the horizontal. Since all forces except gravity are negligible the horizontal velocity is constant. The impact velocity in the vertical is then calculated from the following:

$$V_y^2 = V_{0y}^2 + 2gH,$$

where g is the gravitational acceleration ($-9.80\ m/s$) and it is negative in this case, assuming that the positive direction is up. H (m) is the height difference of the vertical fall from the top of the cliff and down to the impact point.

The final (impact) velocity (V_i) can then be found by:

$$V_i = \sqrt{v_x^2 + v_y^2},$$

The impact velocity can be used to find the impact pressure at the impact point. A widely used expression for the impact pressure on large obstacles is:

$$p = p_{av} u^2$$

This corresponds to the snow density, p_{av}, and flow velocity, u^2, of the undisturbed flow. It is derived from the dynamic pressure for fluids:

$$p_{dyn} = p_{av}\frac{u^2}{2}$$

$$p = C_D p_{dyn},$$

where p_{av} is the avalanche density and u is the velocity of the avalanche. The snow density is assumed to be reduced to 200 kg/m^3 through the fall (S. Margreth, personal communication, January 18, 2021). This density is used for method 2 and 3. C_D is the drag factor and commonly set to 2 for dry snow avalanches (Barbolini et al., 2009).

The projectile motion may overestimate the impact velocity because friction along fall is missing so reality might be in-between this and the RAMMS velocity (S. Margreth, personal communication, January 23, 2021). The average velocity is given by:

$$\mathrm{V_{ai}} = \frac{(\mathrm{Vpm} + \mathrm{Vramms})}{2},$$

where Vpm is the velocity calculated from the projectile motion and Vramms is the velocity on top of the cliff calculated by RAMMS. This velocity is used for method 3.

The projectile motion method is illustrated in Figure 24:

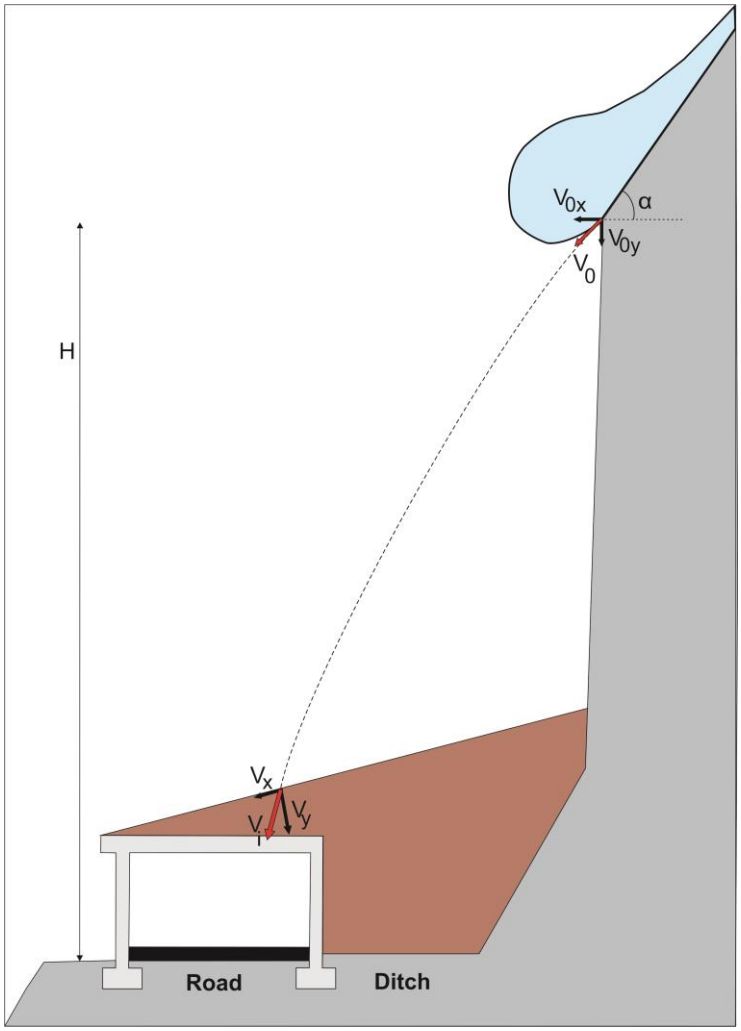

Figure 24. Illustration of how the projectile motion can be used to calculate the impact velocity on a snow shed from an airborne snow avalanche in order to get the impact pressure. Note that the snow shed and backfilling are added for an illustration purpose and to replicate the future situation at best, impact dynamics are calculated at the road.

5 Results

This chapter begins with a presentation of the observations made in field, such as evidence of mass movements, boulder and slope characteristics. The next section provides a description of the input parameters used for the rockfall modelling, followed by the model outputs. These results include the kinetic energy, velocity and jump height. In the next part the snow avalanche analysis is presented, including the input parameters for the modelling and the model outputs used to calculate the snow pressure and velocity at impact. The chapter ends with a brief investigation of the avalanche activity and meteorological factors.

5.1 Fieldwork observations

5.1.1 Evidence of mass movements

Mapping of the area around the problem stretch of road and down to the waterline revealed loose rocks and talus of varying age. Many of the boulders observed were freshly fractured or had left recent damage to the vegetation. Evidence of ongoing rockfall activity could be seen by freshly exposed outcrop, scars on the road and the fence lining the outer shoulder of the road. A recent rockfall was observed (21st of August 2020) at the southern end of the site, where small boulders, fresh soil and torn vegetation formed a small cone in the inner shoulder of the road (Figure 25).

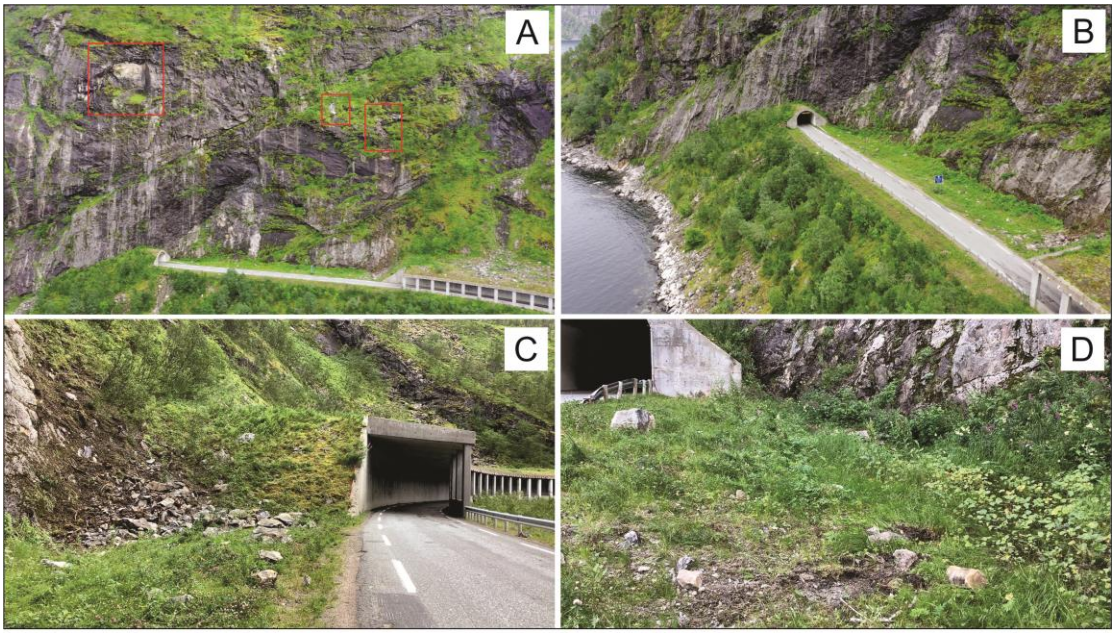

Figure 25. Images taken during the fieldwork that show evidence of mass movements: A) Examples of freshly exposed outcrop (red box). Note rockfalls that have stopped on the existing rock shed B) Overview of recent rockfalls that have stopped in the ditch C) Recent rockfall in the southern end of the site D) Close-up of recent rockfalls and scars left in the ditch.

The mapping of the area did not reveal any clear evidence of past snow avalanche activity because any deposits had melt and it was difficult to identify any avalanche paths in the steep open terrain by i.e. indirect evidence from avalanche damage to the vegetation.

5.1.2 Boulder characteristics

The 40 representative boulders that were mapped (Figure 26) had a volume range from 0.1-12.5 m^3. The rock volume distribution (Figure 27) shows 77.5% were from 0.1–0.5 m^3, 7.5% were from 0.5–1.0 m^3 and 15% were from 1.0-12.5 m^3.

Figure 26. Drone image of the area (black polygon) where the boulders were mapped, 30 were mapped below- and ten above the road. Below drone image are examples of boulders that were mapped. These boulders were used in the numerical modelling.

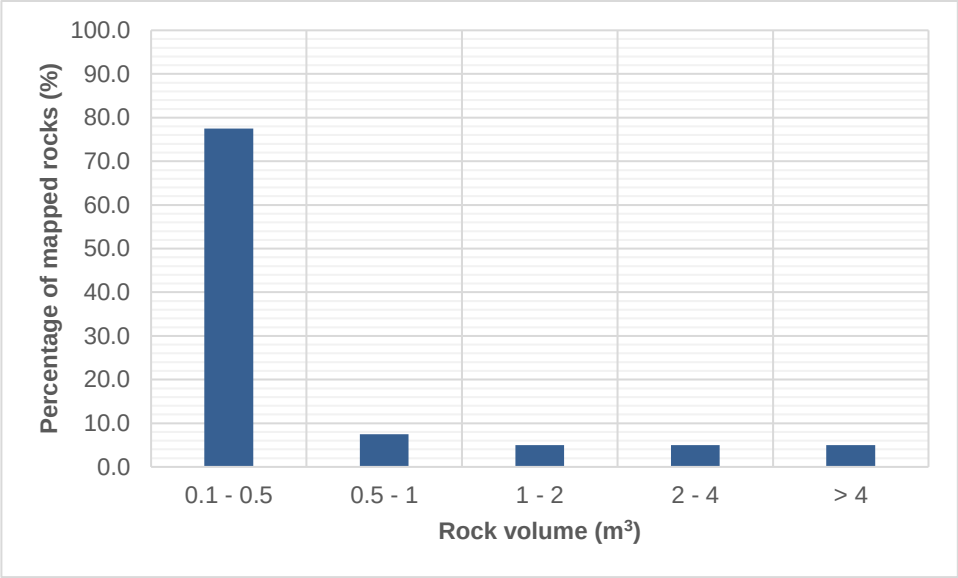

Figure 27. Frequency distribution histogram of mapped rocks of the site.

5.1.3 Bedrock and structural geology

The collected rock samples from the field were identified by Jiri Konopasek, professor in petrology, as tonalitic gneiss, tonalitic pegmatite, amphibolitic gneiss and banded tonalitic dioritic gneiss (Figure 28). These metamorphic rocks have similar rock density as a granite, equal to around 2700 kg/m^3 (Smithson, 1971). A sensitivity analysis was made and determined density has little to no effect on the dynamic simulation results.

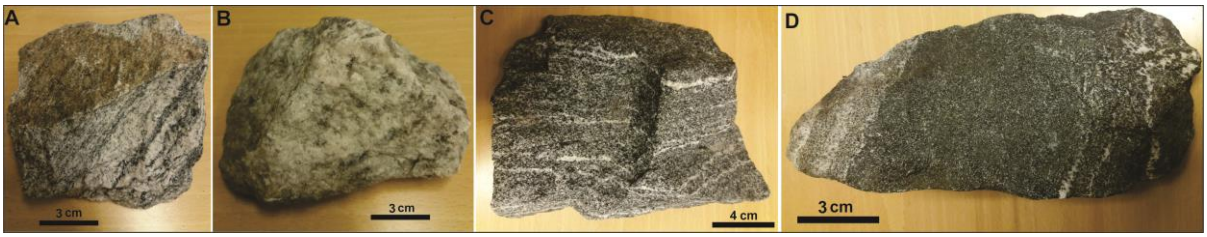

Figure 28. Rock samples from Svarthola a) tonalitic gneiss b) tonalitic pegmatite c) amphibolitic gneiss d) banded tonalitic dioritic gneiss (J. Konopasek, personal communication, October 15, 2020).

The rock mass is characterized by a shear zone and four main joint sets (J1-4). The shear zone (SZ) strikes NE-SW and is clearly visible, J1 has a moderately dip (61°) while striking NE-SE, (61°), J2 has a vertical to subvertical dip (78°) while striking N-S and appears to have the highest persistence (length), J3 has a moderately dip (47°) while striking NW-SE and J4 has a moderately dip (60°) while striking NE-SW (Table 7, Figure 29).

Table 7. Summary of the main joint sets of the site. Orientation values are given as dip direction/dip angle in degrees.

Joint set	Mean orientation (dip direction/dip angle with variance)
1	292/61 ± 15°
2	177/78 ± 4°
3	135/47 ± 4°
4	049/60 ± 20°

Figure 29. Drone image with illustrations of the main joints sets (J1-4) and the SZ that strikes through the cliff.

5.1.4 Slope and terrain characteristics

The first 100 m above the road consists of a cliff (45-90°). Above the cliff the terrain is flatter (35-60°). This area is covered by vegetation with loose material beneath, few smaller cliffs and a gully with avalanche deposits. The vegetated areas are eroded by rainwater. A 16 m^3 boulder was observed within the slope (Figure 30-31).

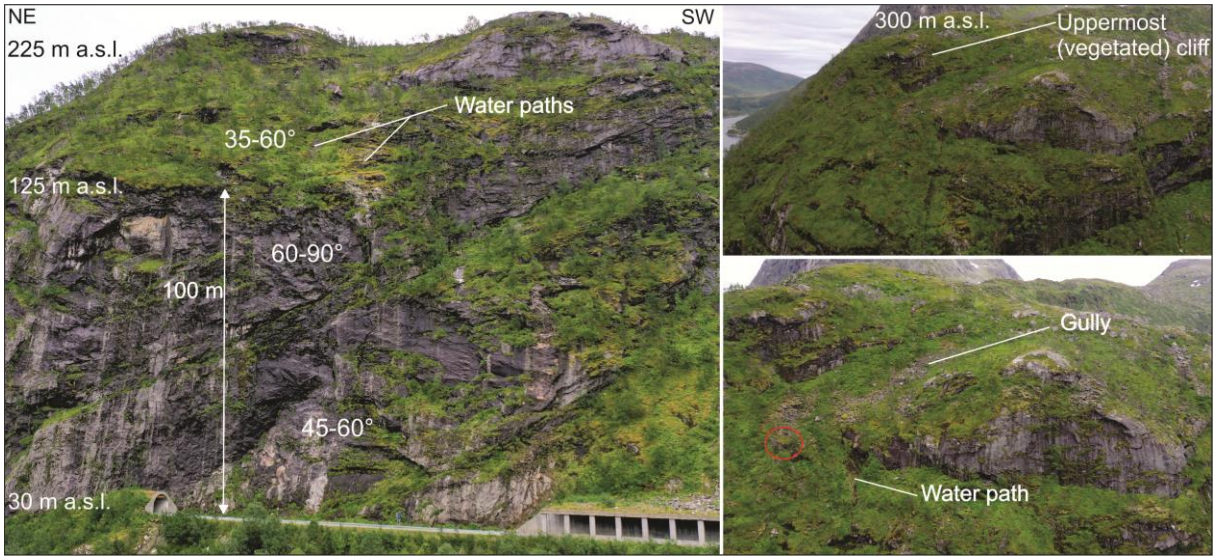

Figure 30. Slope and terrain characteristics that show the 100 m high steep cliff above the road. The terrain above is characterize by a steep slope covered with vegetation and several smaller cliffs. There are several water paths in the terrain. A large boulder (16 m^3) was observed within the slope (red circle) (also shown in Figure 31A).

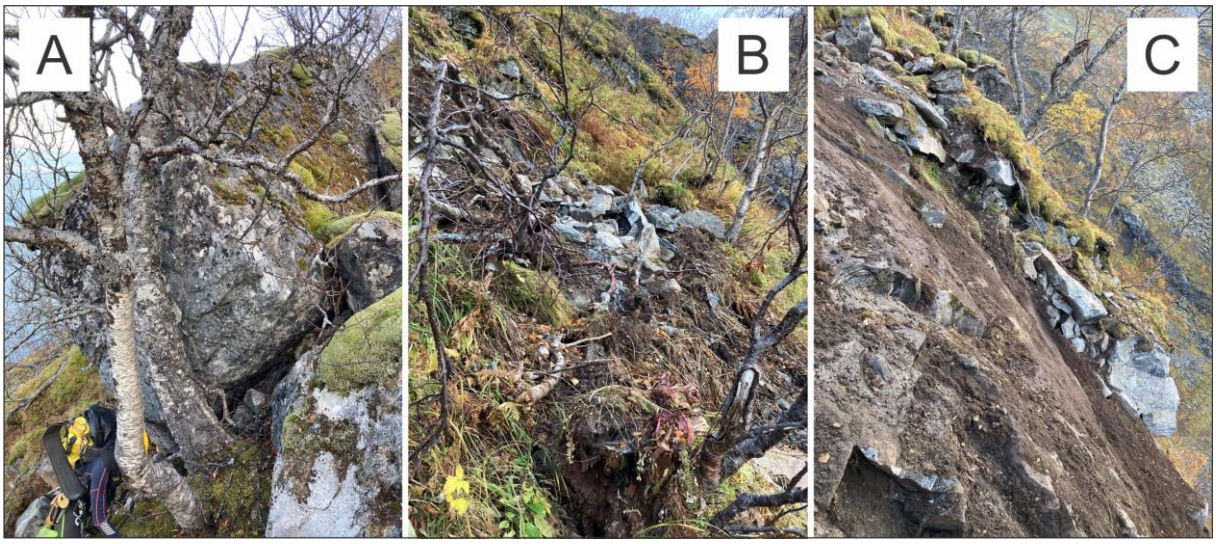

Figure 31. Images obtained from the scaling team A) A large boulder, estimated to be 16 m^3 B) Rockfalls that has stopped within the slope C) Loose rocks under the vegetation.

5.2 RAMMS::ROCKFALL input data

The input parameters for the modelling were obtained from the field observations and includes the following sets:

- Rock size (volume) and rock shape
- Release areas
- Terrain type

Rock size (volume) and rock shape

Based on the frequency distribution of the mapped rocks (Figure 27) and the registered rockfall events the numerical modelling was done with rock volumes of 0.1 m^3, 0.5 m^3, 2 m^3 and 4 m^3 (depending on the scenario). The worst-case scenario was computed with rocks up to 12.5 m^3, which was the biggest boulder that was mapped. Experiences from the scaling show that the rocks released from the upper terrain will bounce against the slope and are fragmented.

The dimensions of the boulders according to the RAMMS shapes belonged to flat (45%), equant (35%) and long (20%) (Figure 32-33). The scenarios were run with flat and equant rocks and with all rock shapes in the worst-case scenario.

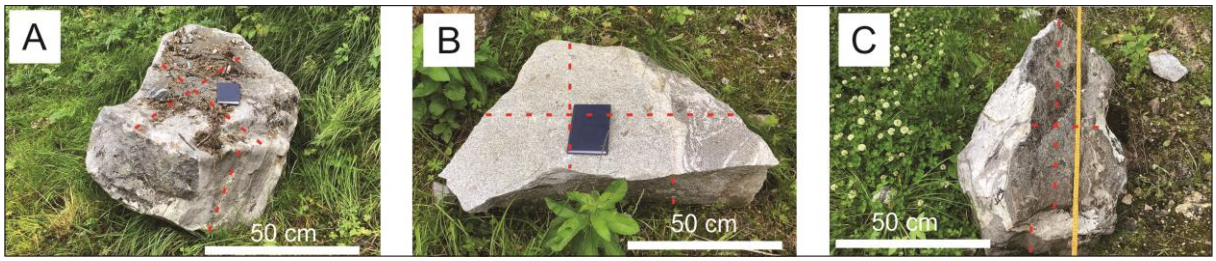

Figure 32. Rock shapes observed during the fieldwork that were used for the numerical modelling: A) Equant B) Flat C) Long. The red dashed lines illustrates the axes.

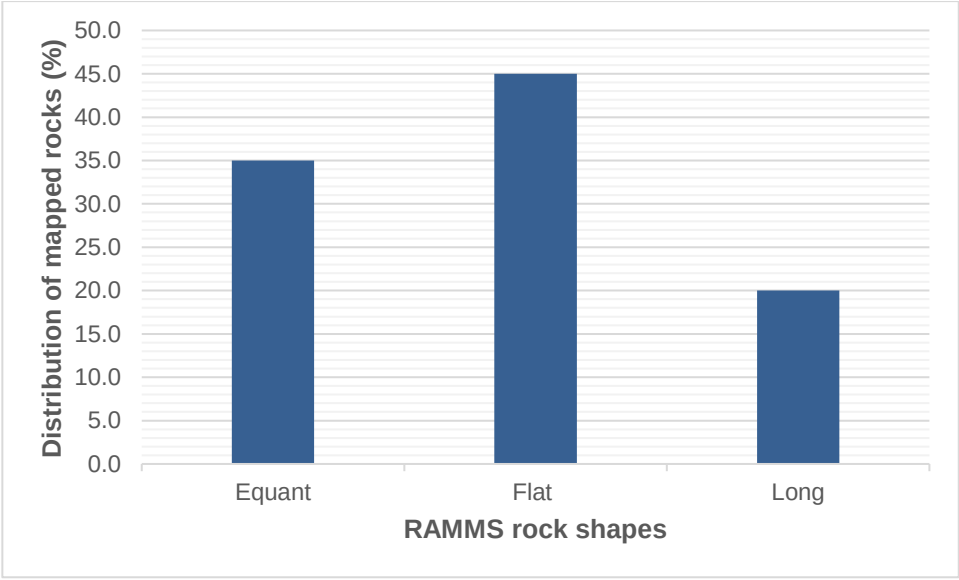

Figure 33. Frequency distribution histogram of mapped rocks defined according to RAMMS shapes.

Release areas

Terrain above 45° was selected as release areas (NVE, 2020c) and the uppermost parts of the rock cliffs were used to give the highest possible impact energies on the road (Figure 34-35). The areas were specified as lines made up of 51 points (with five possible release orientations). From each source location the selected boulder library was released 5 times.

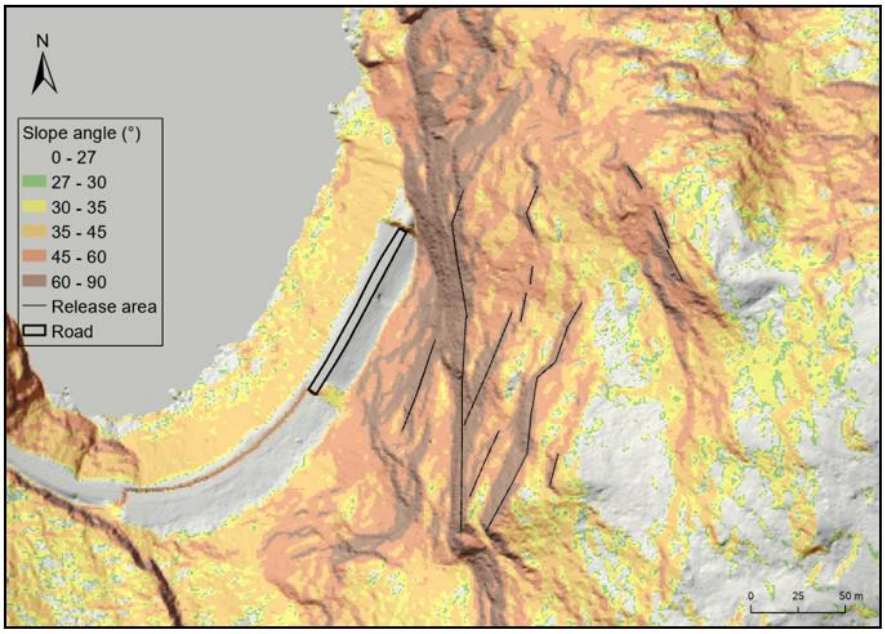

Figure 34. Hillshade map with slope angle where the release areas (black lines) used in the modelling are shown.

Figure 35. Drone image with the release areas (red lines) used in the modelling are shown.

Terrain types

The terrain characteristics of the slope were delineated into three different RAMMS categories of hard (grey) for the outcropping rock, medium hard (orange) for the rock close to surface and soft (yellow) for the softer vegetated area (Figure 36), in addition to forest and water for the fjord below the road for better visualization of the simulation results. These terrain types were selected as they gave the best fit of the rock distribution in the calibration exercise.

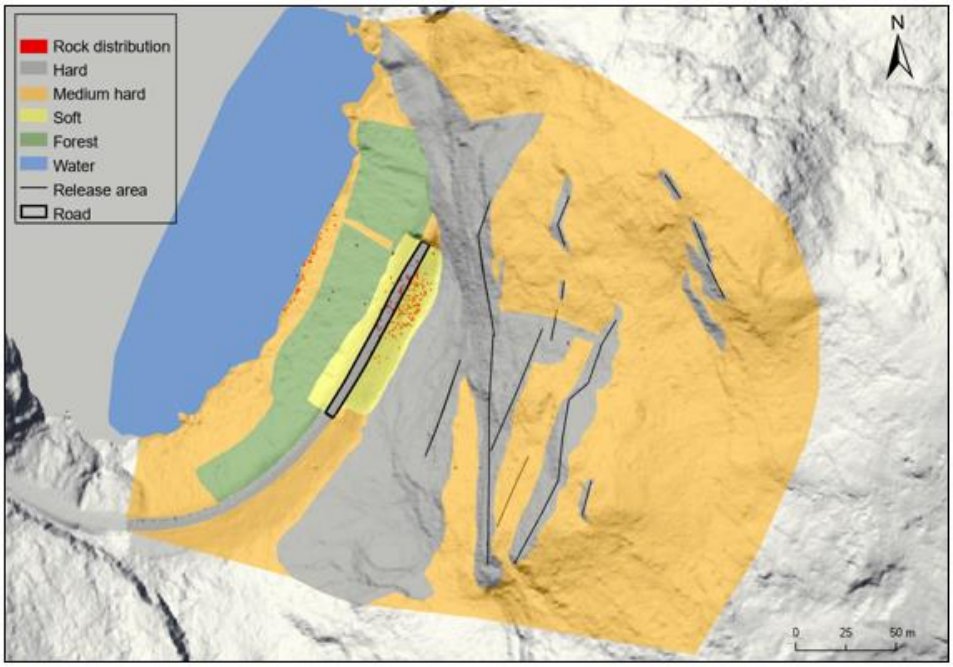

Figure 36. Hillshade map with the terrain types used in RAMMS: hard (grey), medium hard (orange), soft (yellow), forest (green) and water (blue). The rock distribution after scaling (red dots) are shown, which were used for this calibration.

A summary of the general settings and input parameters used in RAMMS::ROCKFALL can be displayed in Table 8-9 respectively (see Appendix A for all input settings):

Table 8. Summary of the general settings used for all simulations in RAMMS.

DTM resolution	2 m
Terrain material	Hard, medium hard, medium soft + forest and water (only for visualization)
Rock density	2,700 kg/m^3
Number of random orientation	5
Release area	Lines above 45° made up of 51 points

Table 9. Summary of the input parameters for the different scenarios simulated in RAMMS. Block dimensions can be seen in Appendix A.

Scenario	Calibration	1. Annual	2. 50-year	3a-b.100-year	4. Worst-case
Rock number	9	2	2	2	40
Rock shape	Equant Flat Long	Equant Flat	Equant Flat	Equant Flat	Equant Flat Long
Rock volume (m^3)	0.1 0.3 0.5	0.5	1	2 4	0.1 – 0.8 1.5, 3.5, 4.0 5.0, 12.5
Number of trajectories	225	510	510	510	10,200

5.3 RAMMS::ROCKFALL model results

Results for kinetic rock energy, velocity and jump heights for simulations of the four different scenarios are presented in the following section.

Model results for kinetic energy and velocity specifically are presented and discussed in terms of the 95th percentile values. The 99th percentile values are included in brackets for comparison. Results for these are also divided into two domains and presented separately for the northern (60 m) and southern parts (40 m) of the road to reduce the spatial bias. Statistics are presented for each domain across lines representing the ditch and the road location (to remove data outside of the area of interest).

Jump height results are presented slightly differently. Due to the height of the cliff (c. 100 m high) the maximum jump heights of the 95th percentile are skewed to this value (> 30 m). In order to obtain realistic jump heights the CDF curve (Cumulative Distribution Function) and the median value from the barrier plot are used instead. They are presented across the whole road stretch rather than in domains, because they have little impact on the construction of the rock shed, but help to validate the results.

Results across all scenarios show a similar pattern: the impact energies and velocities increase from the source area and accelerate at 100 m above the road where the boulder motion changes to free-falling (Figure 37-51). At this point jump heights increase until they hit the ground at the base of the cliff. At this point most of the boulders stop in the ditch before they reach the road, however some continue to the water line with low energies and velocities. Energies and velocities are markedly lower in the southern portion of the map The model results do not capture the blocks that bounce out from the lower part of the cliff that is

less steep, and reach down to the fjord (>20 m). This observation was made by the scaling team who induced rockfalls after the event in September 2020.

5.3.1 Scenario 1: Annual events

Simulation results are presented in Figures 37-39. In the northern domain the maximum kinetic rock energy reaches values of 1,734 kJ (Q99 = 1,773 kJ) at the road (corresponding to a 0.5 m^3 rock). In the southern domain, the same block hits the road with up to 964 kJ (Q99 = 1,342 kJ) on impact. The frequency distribution and box plots show that the ditch experiences more high energy impacts with impact frequencies greatest between 400 and 1,000 kJ, reduced to 300 kJ at the road.

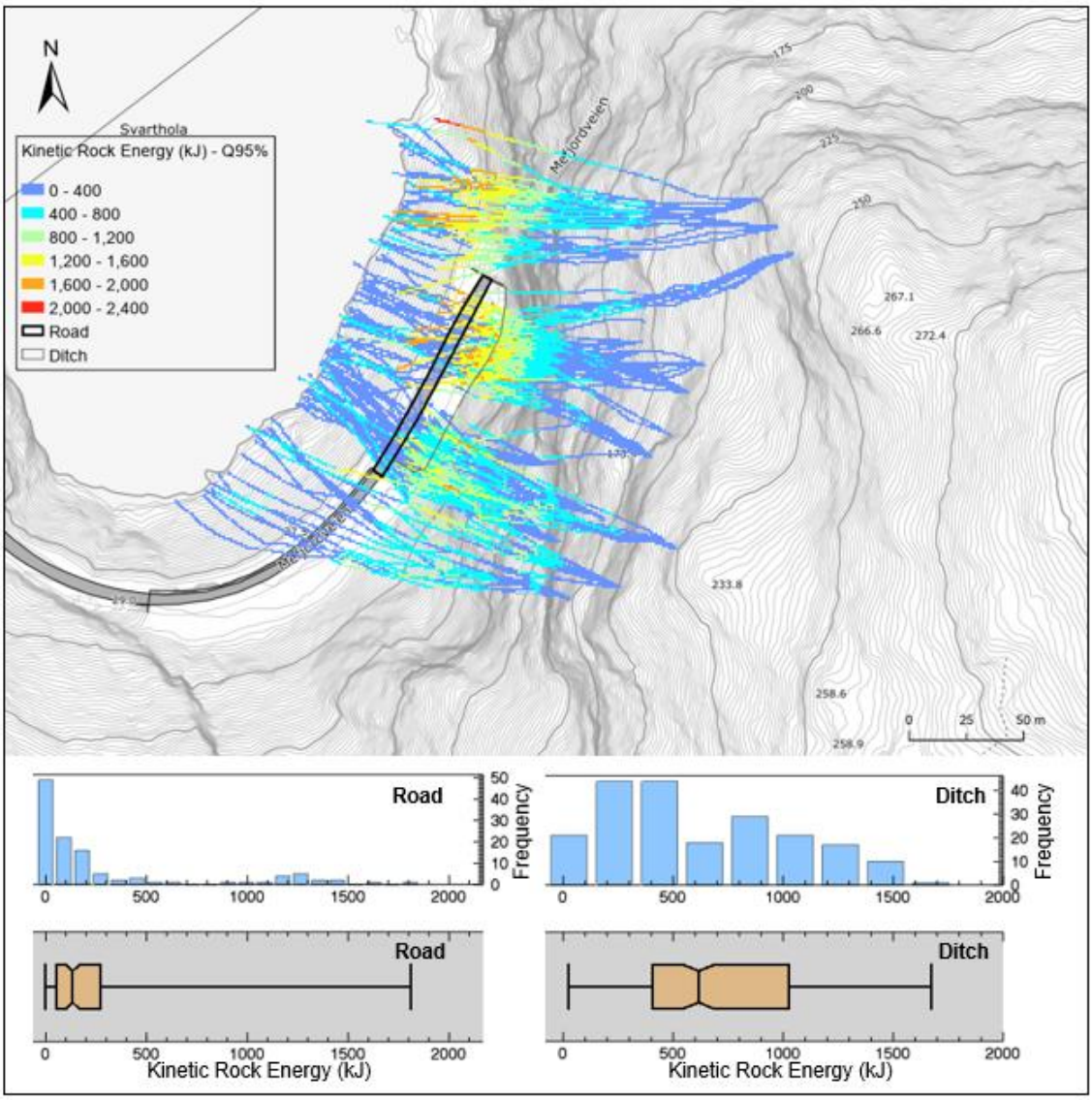

Figure 37. The 95th percentile kinetic energies of rockfalls for an annual scenario are displayed. Note higher energies in the northern part of the road (black polygon). The maximum values range from 964 to 1,734 kJ. The frequency distribution and the box plots show that the ditch experiences more high energy impacts with impact frequencies greatest between 400 and 1,000 kJ, reduced to 300 kJ at the road.

Figure 38 shows the velocity of the simulated rocks. In the northern domain the maximum velocity reaches values of 50 m/s. In the southern domain, the same rocks hit the road with velocities of 37 m/s (Q99 = 44 m/s). The frequency distribution and box plots show that the ditch experiences more high velocity impacts with impact frequencies greatest between 20 and 40 m/s, reduced to 18 m/s at the road.

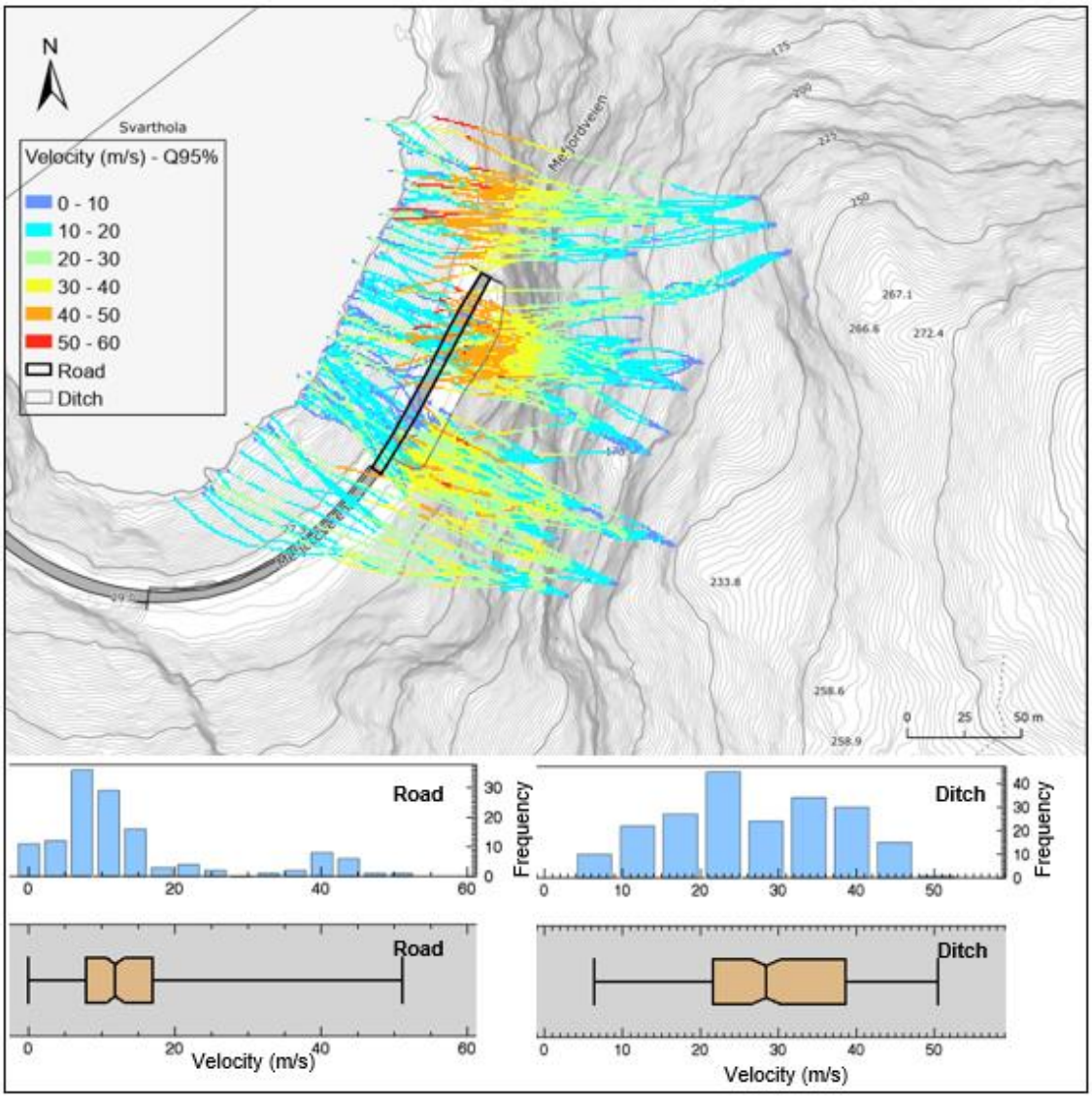

Figure 38. The 95th percentile velocities of rockfalls for an annual scenario are displayed. Note greater velocities in the northern part of the road (black polygon). The maximum values range from 37 to 50 m/s. The frequency distribution and the box plots show that the ditch experiences more high velocity impacts with impact frequencies greatest between 20 and 40 m/s, reduced to 18 m/s at the road.

Figure 39 shows the jump height of the simulated rocks. The CDF curve indicates that 80% of the boulders had a jump height of less than 3 m and the median jump height is estimated to be 0.9 m at the road. The box plots show that the ditch experiences higher frequency of greater jump heights than at the road.

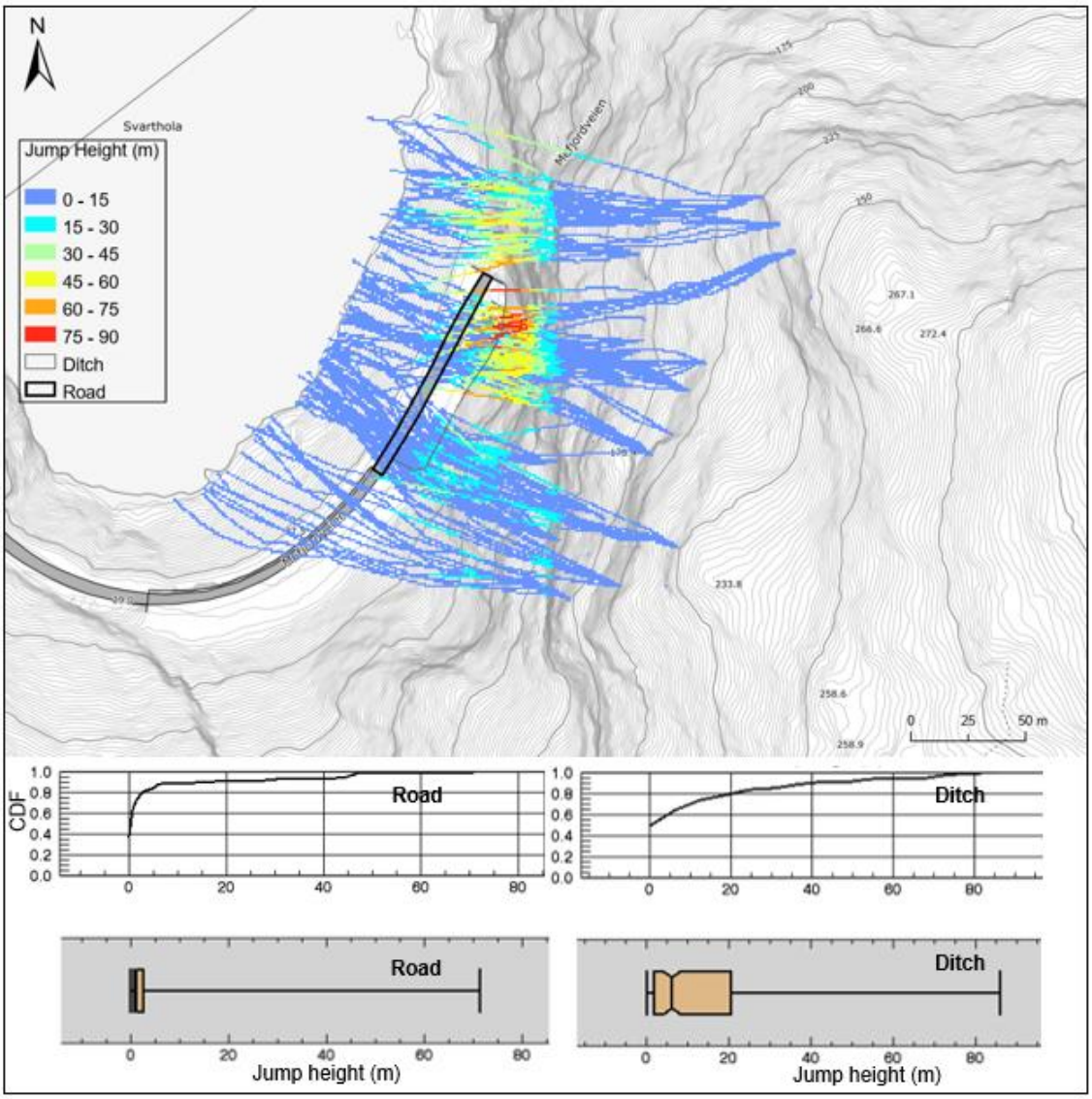

Figure 39. The 95th percentile jump heights of rockfalls for an annual scenario are displayed. Note higher jump heights in the northern part of the road (black polygon). The maximum values range from 0.9 to 3 m (Note that the CDF curve and median value are used, see explanation 5.3). The box plots show that the ditch experiences higher frequency of greater jump heights than at the road.

5.3.2 Scenario 2: 50-year return period

Simulation results are presented in Figures 40-42. In the northern domain the maximum kinetic rock energy reaches values of 3,560 kJ (Q99 = 4,166) at the road (corresponding to a 1.0 m^3 rock). In the southern domain, the same block hits the road with up to 2,108 kJ (Q99 = 2,508 kJ). The frequency distribution and box plots show that the ditch experiences more high energy impacts with impact frequencies greatest between 800 and 2,500 kJ, reduced to 600 kJ at the road.

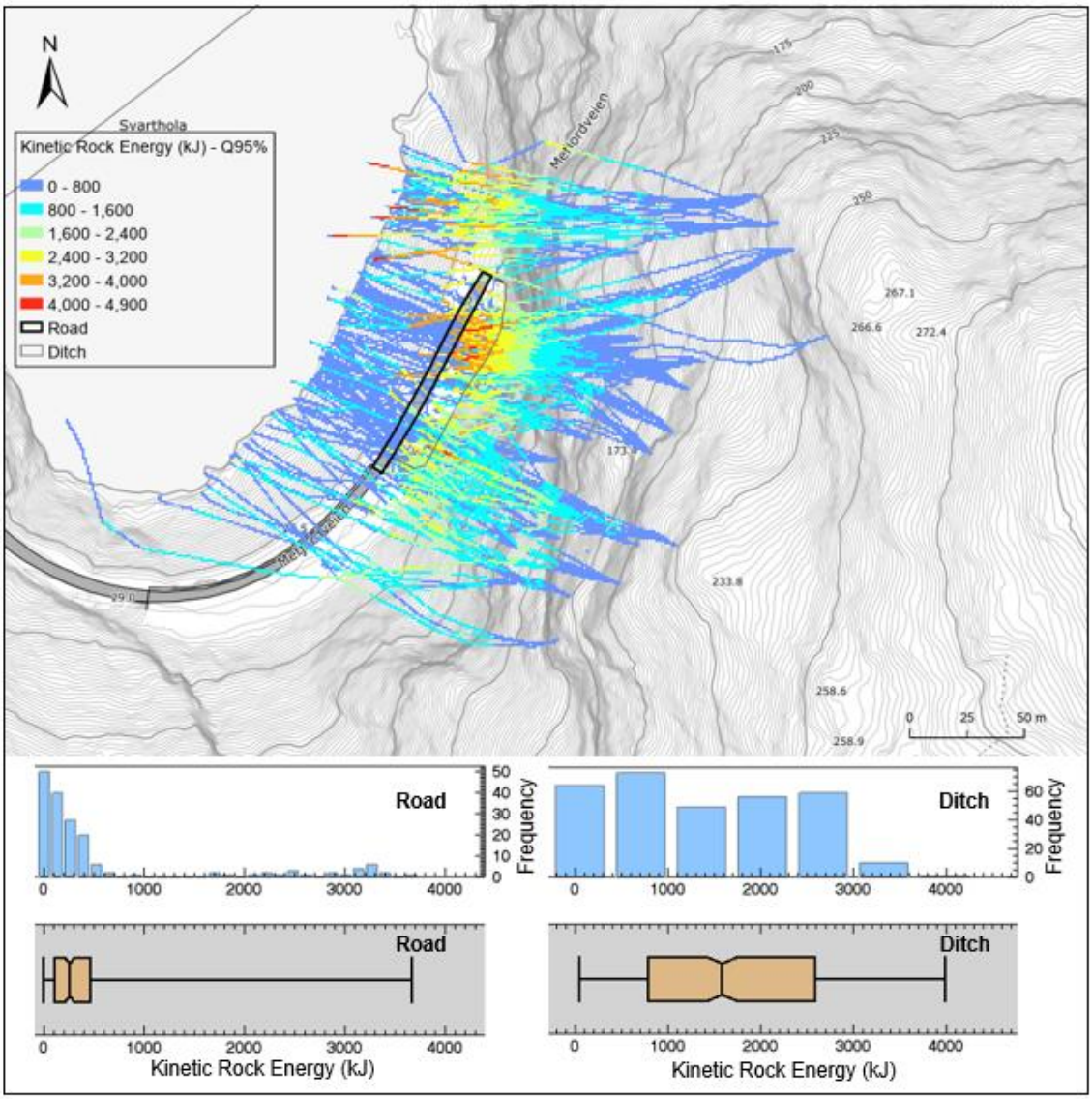

Figure 40. The 95th percentile kinetic energies of rockfalls for a 50-year return period are displayed. Note higher energies in the northern part of the road (black polygon). The maximum values range from 2,108 to 3,560 kJ. The frequency distribution and the box plots show that the ditch experiences more high energy impacts with impact frequencies greatest between 800 and 2,500 kJ, reduced to 600 kJ at the road.

Figure 41 shows the velocity of the simulated rocks. In the northern domain the maximum velocity reaches values of 49 m/s (Q99 = 54 m/s). In the southern domain, the same rocks hit the road with velocities of 40 m/s (Q99 = 43 m/s). The frequency distribution and box plots show that the ditch experiences more high velocity impacts with impact frequencies greatest between 20 and 40 m/s, reduced to 15 m/s at the road.

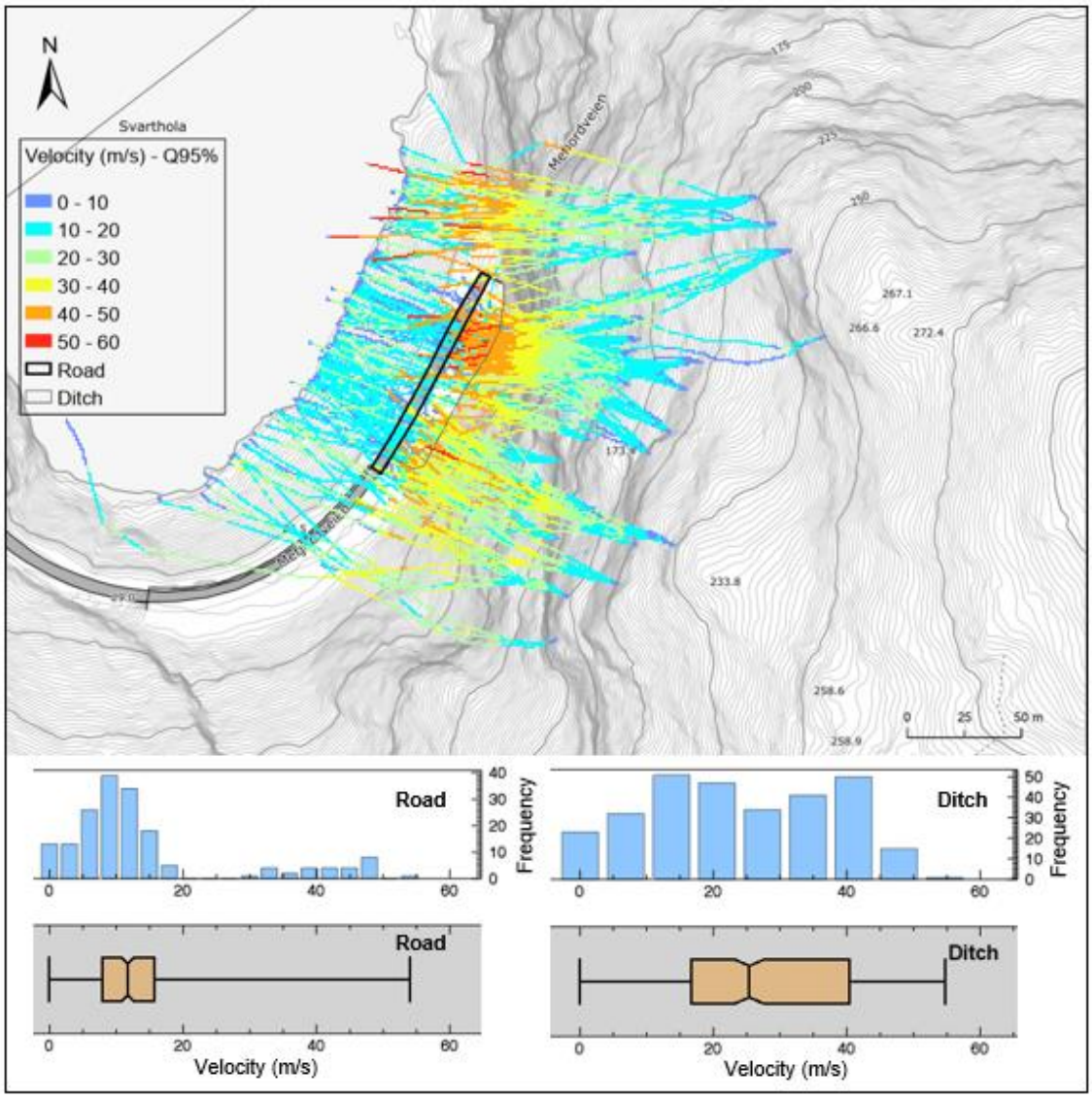

Figure 41. The 95th percentile velocities of rockfalls for a 50-year return period are displayed. Note greater velocities in the northern part of the road (black rectangle). The maximum values range from 40 to 49 m/s. The frequency distribution and the box plots show that the ditch experiences more high velocity impacts with impact frequencies greatest between 20 and 40 m/s, reduced to 15 m/s at the road.

Figure 42 shows the jump height of the simulated rocks. The CDF curve indicates that 80% of the boulders had a jump height of less than 2 m and the median jump height is estimated to be 1 m at the road. The box plots show that the ditch experiences higher frequency of greater jump heights than at the road.

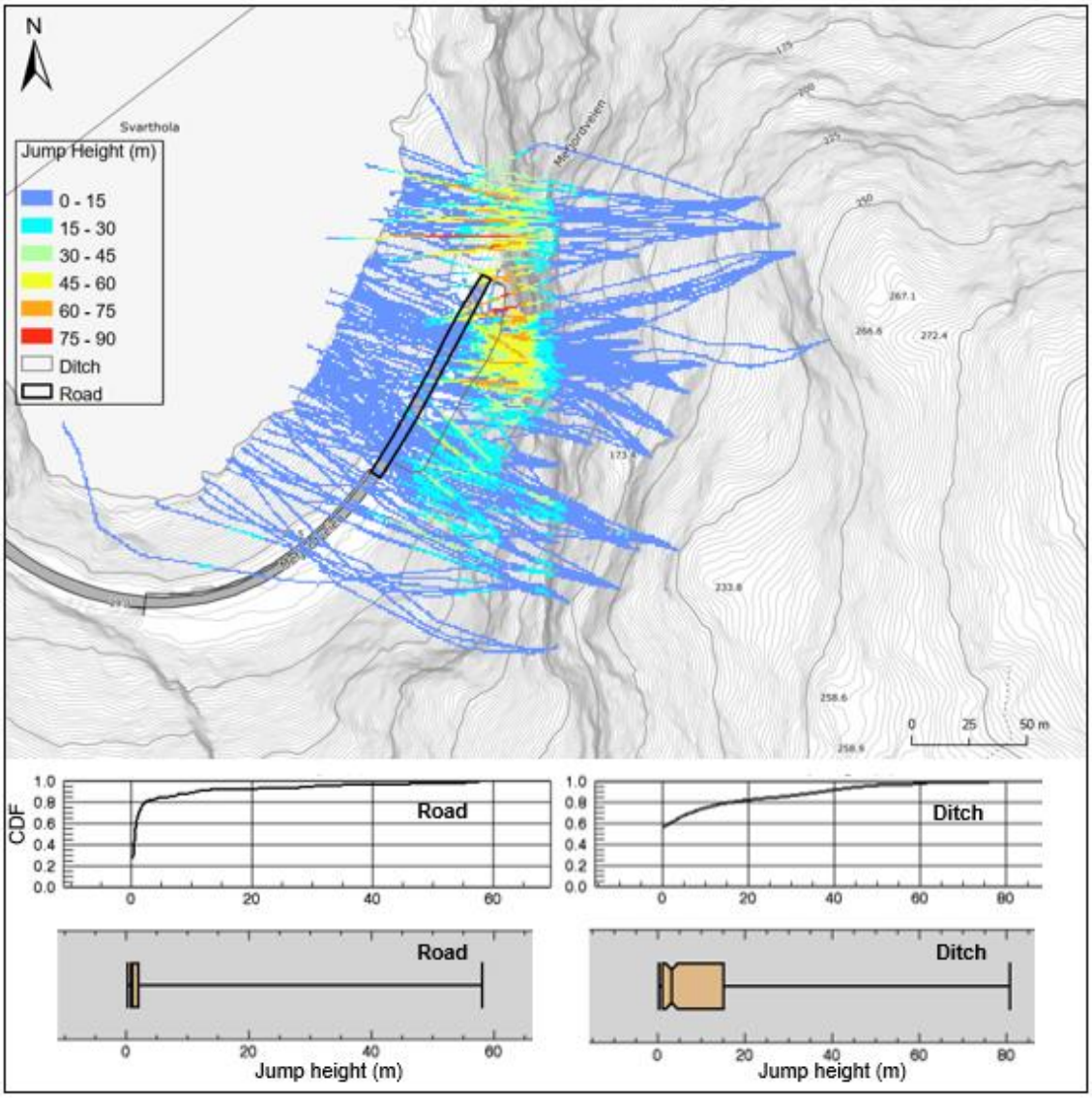

Figure 42. The 95th percentile jump heights of rockfalls for a 50-year scenario are displayed. Note higher jump heights in the northern part of the road (black polygon). The maximum values range from 1 to 2 m (CDF curve and median value). The box plots show that the ditch experiences higher frequency of greater jump heights than at the road.

5.3.3 Scenario 3: 100-year return period

Scenario 3 has been simulated twice, with the addition of both a 2 m^3 and 4 m^3 block respectively. While a 4 m^3 block was mapped in the field, the conservative nature of the rockfall model means results applying this boulder are so extreme that a protection structure cannot be designed to withstand it (H. L. Haukenes, personal communication, November 30, 2020). I have therefore simulated rockfall using this boulder for academic purposes only.

Scenario 3a: 2 m^3 rock

Simulation results are presented in Figures 43-45. In northern domain the maximum kinetic rock energy reach values of 7,085 kJ (Q99 = 8,949 kJ) at the road (corresponding to a 2 m3 rock). In the southern domain, the same block hits the road with up to 1,783 kJ (Q99 = 5,852). The frequency distribution and box plots show that the ditch experiences more high energy impacts with impact frequencies greatest between 1,500 and 4,500 kJ, reduced to 1,000 kJ at the road.

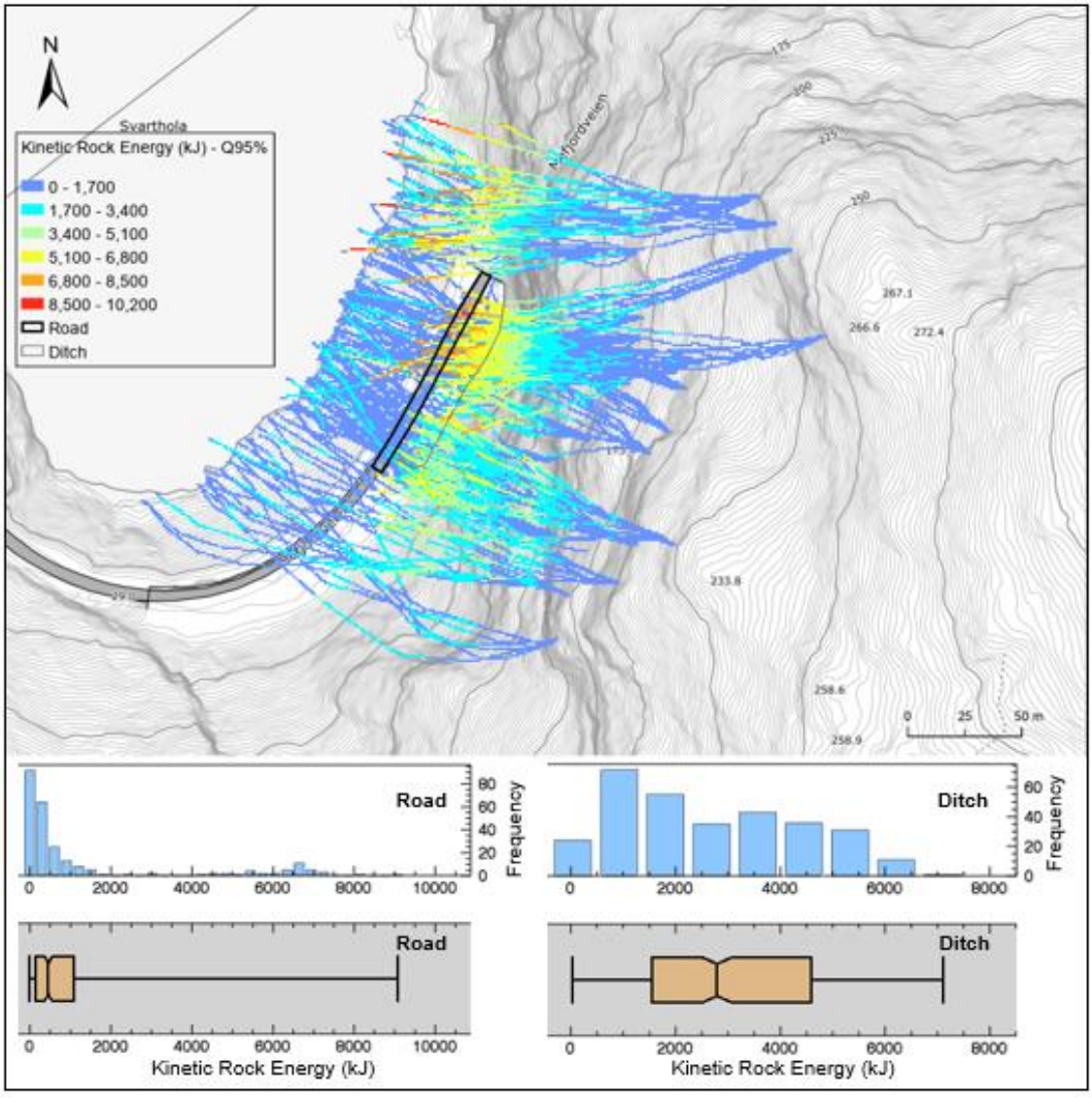

Figure 43. The 95th percentile kinetic energies of a 2 m^3 large rock for a 100-year return period are displayed. Note higher energies in the northern part of the road (black polygon). The maximum values range from 1,783 to 7,085 kJ. The frequency distribution and the box plots show that the ditch experiences more high energy impacts with impact frequencies greatest between 1,500 and 4,500 kJ, reduced to 1,000 kJ at the road.

Figure 44 shows the velocity of the simulated rocks. At the northern domain the maximal velocity reach values of 50 m/s (Q99 = 56 m/s). At the southern domain, the same blocks hits the road with velocities of 22 m/s (Q99 = 44 m/s). The frequency distribution and box plots show that the ditch experiences more high velocity impacts with impact frequencies greatest between 20 and 40 m/s, reduced to 15 m/s at the road.

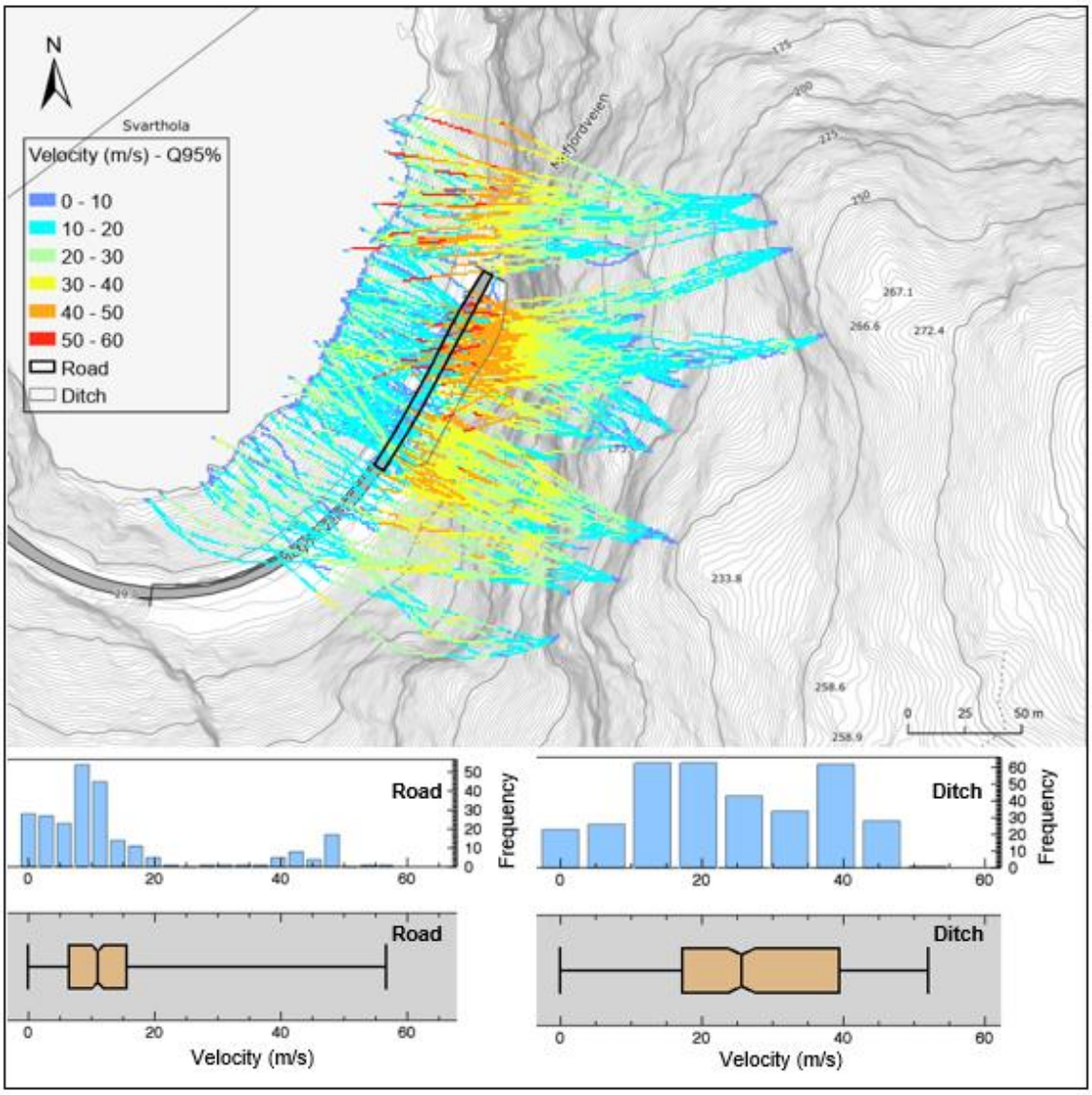

Figure 44. The 95th percentile velocities of 2 m^3 rockfalls for a 100-year return period are displayed. Note greater velocities in the northern part of the road (black rectangle). The maximum values range from 22 to 50 m/s. The frequency distribution and the box plots show that the ditch experiences more high velocity impacts with impact frequencies greatest between 20 and 40 m/s, reduced to 15 m/s at the road.

Figure 45 shows the jump height of the simulated rocks. The CDF curve indicates that 80% of the boulders got a jump height of less than 3 m and the median jump height is estimated to 1.2 m at the road. The box plots show that the ditch experiences higher frequency of greater jump heights than at the road.

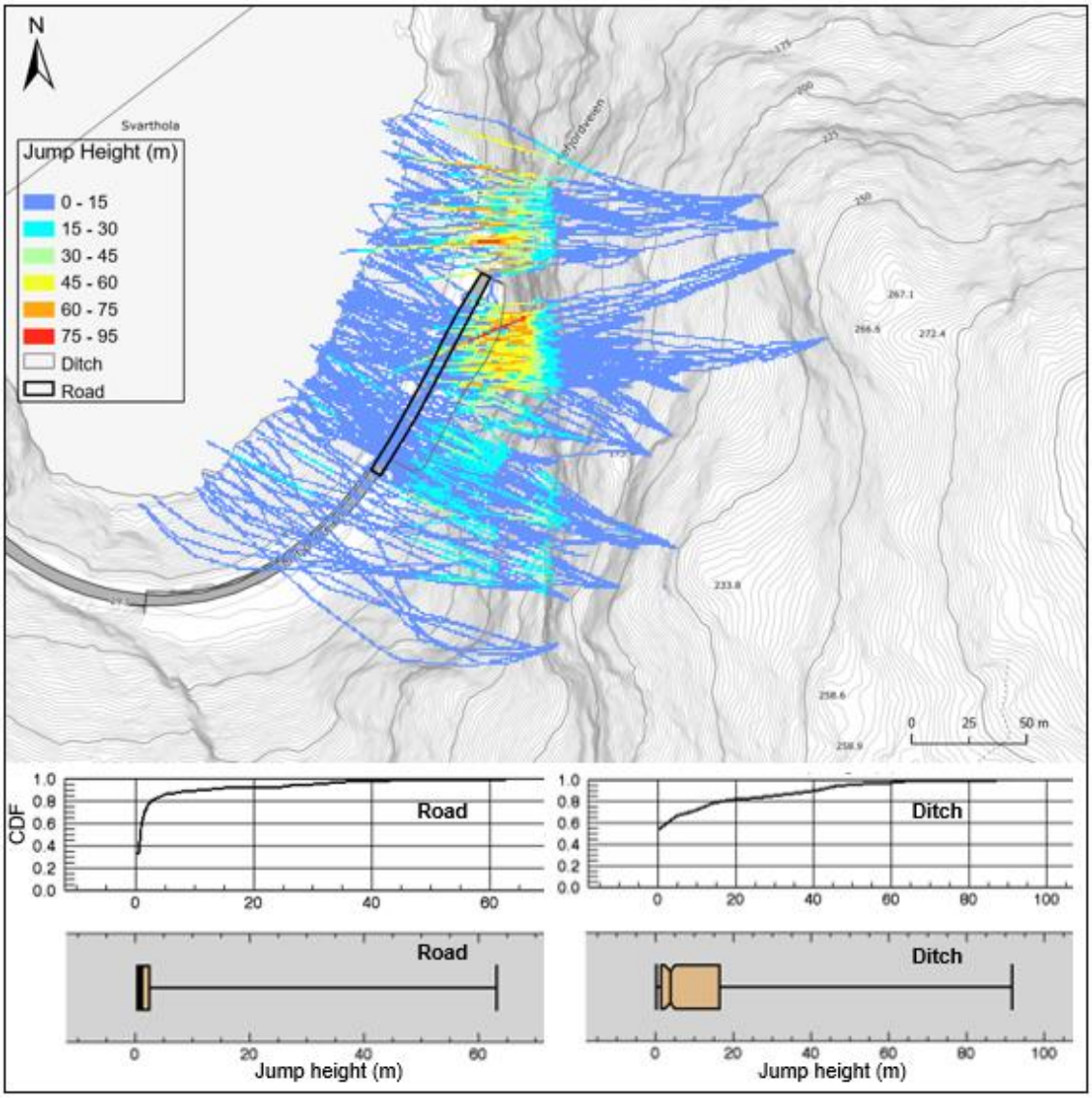

Figure 45. The 95th percentile jump heights of 2 m^3 rockfalls for a 100-year return period are displayed. Note higher jump heights in the northern part of the road (black polygon). The maximum values range from 1.2 to 3 m (CDF curve and median value). The box plots show that the ditch experiences higher frequency of greater jump heights than at the road.

Scenario 3b: 4 m^3 rock

Simulation results are presented in Figures 46-48. At the northern domain the maximum kinetic rock energy reach values of 13,995 kJ (Q99 = 16,209 kJ) at the road (corresponding to a 4 m^3 rock). At the southern domain, the same block hits the road with up to 7,203 kJ (Q99 = 11,473 kJ). The frequency distribution and box plots show that the ditch experiences more high energy impacts with impact frequencies greatest between 3,000 and 8,000 kJ, reduced to 4,000 kJ at the road.

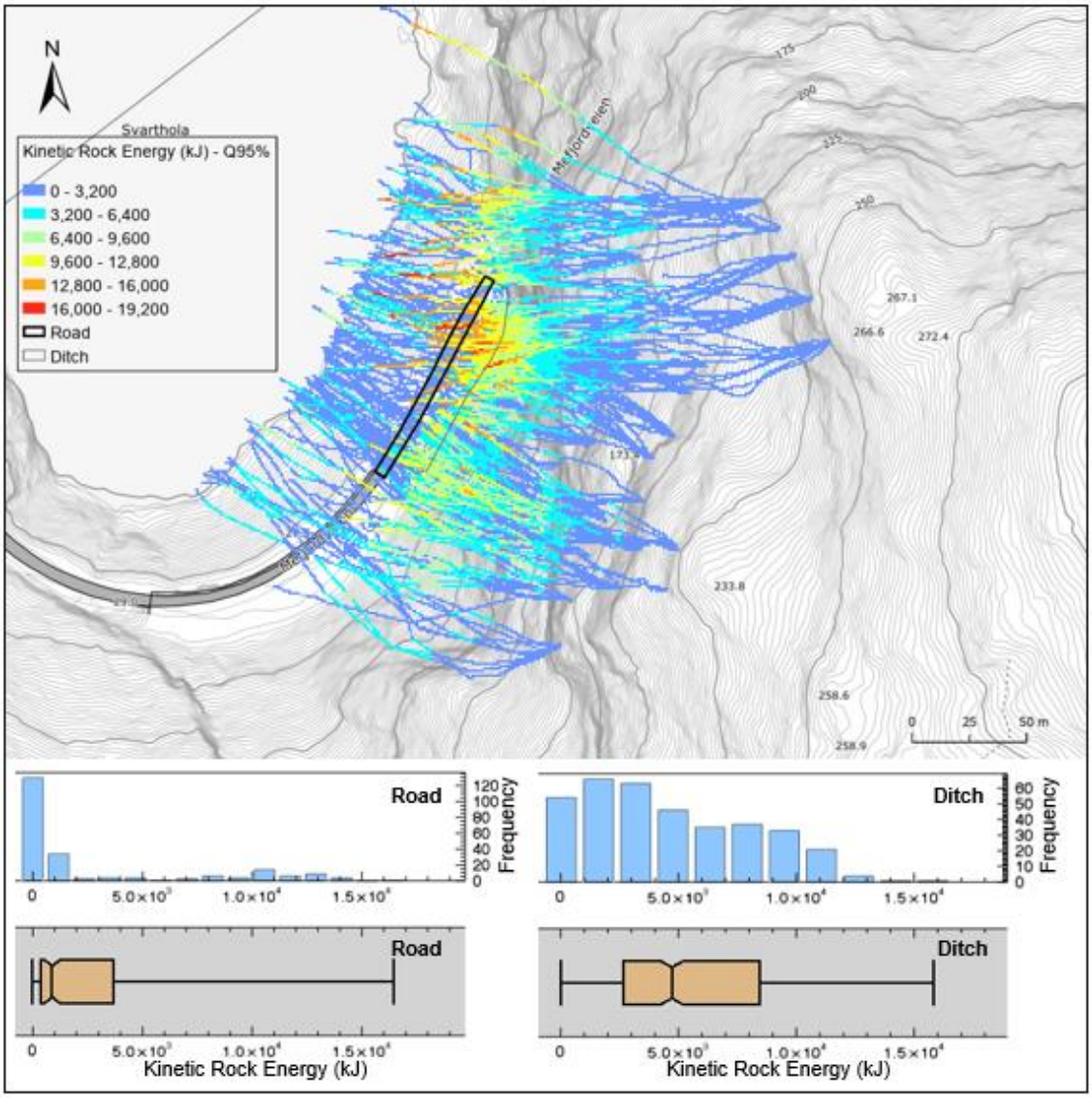

Figure 46. The 95th percentile kinetic energies of 4 m^3 rockfalls for a 100-year return period are displayed. Note higher energies in the northern part of the road (black polygon). The maximum values range from 7,203 to 13,995 kJ. The frequency distribution and the box plots show that the ditch experiences more high energy impacts with impact frequencies greatest between 3,000 and 8,000 kJ, reduced to 4,000 kJ at the road.

Figure 47 shows the velocity of the simulated rocks. At the northern domain the maximum velocity reach values of 50 m/s (Q99 = 56 m/s). At the southern domain, the same blocks hits the road with velocities of 33 m/s (Q99 =45 m/s). The frequency distribution and box plots show that the ditch experiences more high velocity impacts with impact frequencies greatest between 20 and 40 m/s, reduced to 25 m/s at the road.

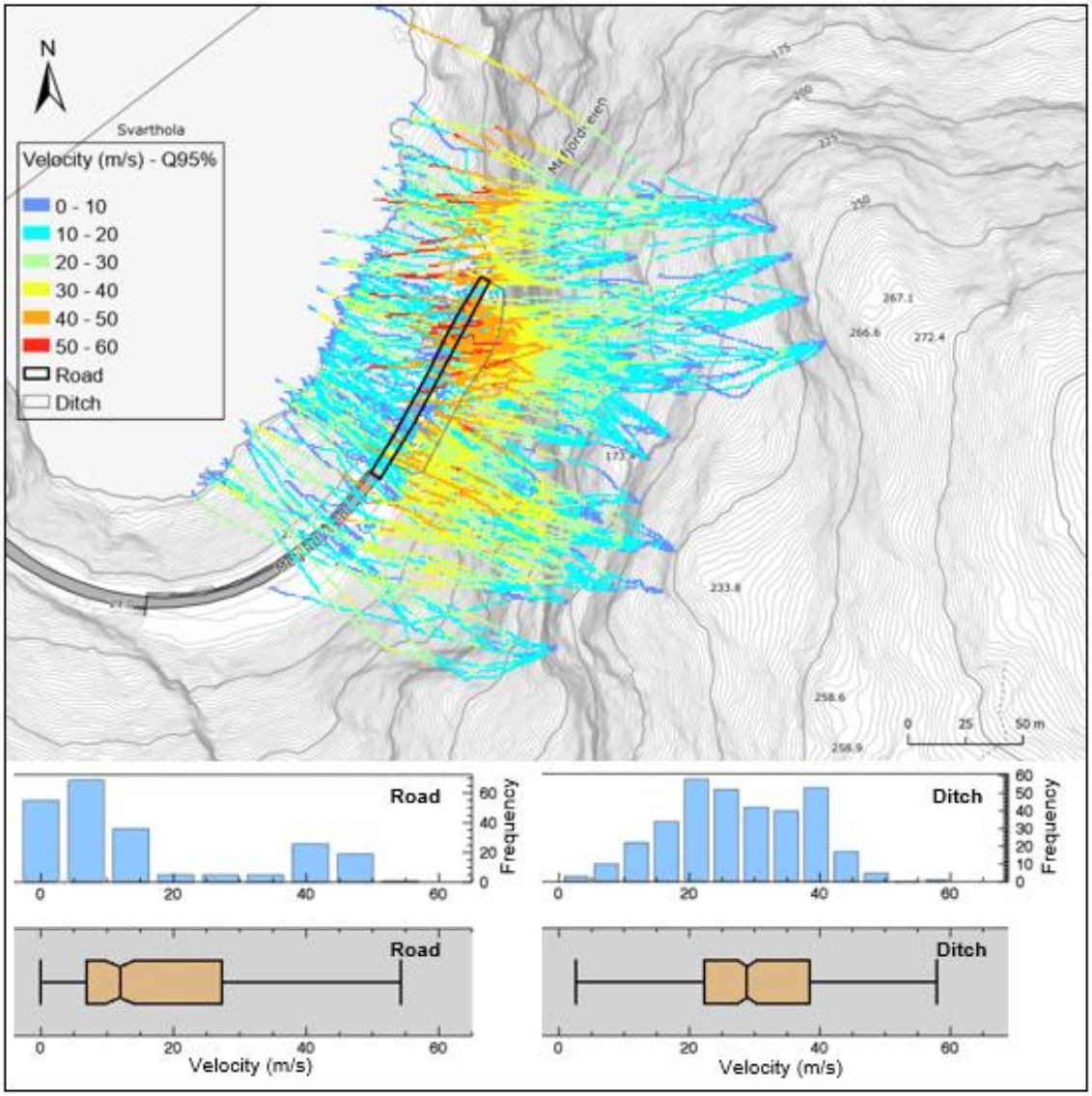

Figure 47. The 95th percentile velocities of 4 m^3 rockfalls for a 100-year return period are displayed. Note greater velocities in the northern part of the road (black rectangle). The maximum values range from 33 to 50 m/s. The frequency distribution and the box plots show that the ditch experiences more high velocity impacts with impact frequencies greatest between 20 and 40 m/s, reduced to 25 m/s at the road.

Figure 48 shows the jump height of the simulated rocks. The CDF curve indicates that 80% of the boulders got a jump height of less than 5 m and the median jump height is estimated to 1.8 m at the road. The box plots show that the ditch experiences higher frequency of greater jump heights than at the road.

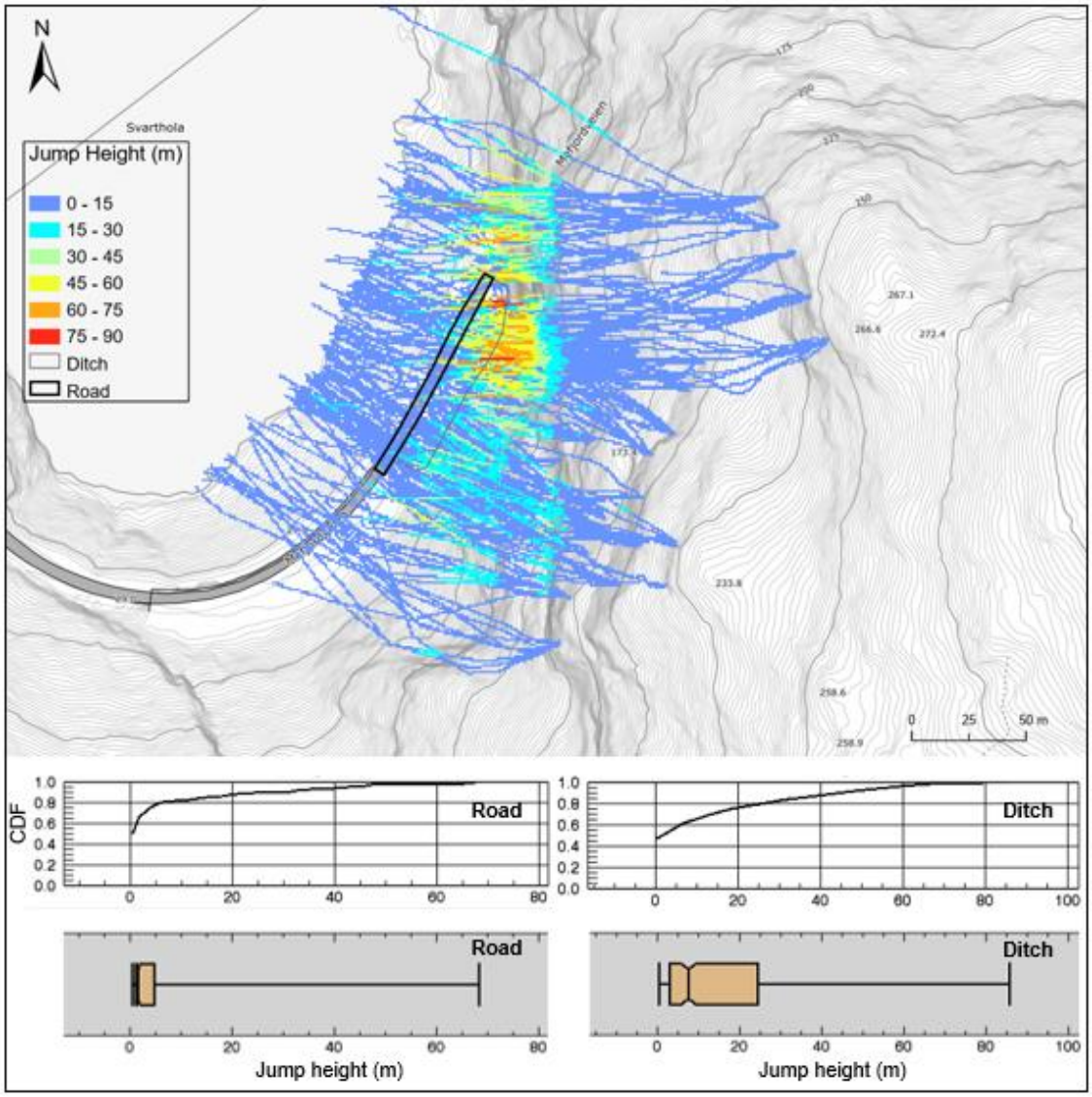

Figure 48. The 95th percentile jump heights of 4 m^3 rockfalls for a 100-year return period are displayed. Note higher jump heights in the northern part of the road (black polygon). The maximum values range from 1.8 to 5 m (CDF curve and median value). The box plots show that the ditch experiences higher frequency of greater jump heights than at the road.

5.3.4 Scenario 4: Worst-case

Simulation results are presented in Figures 49-51. At the northern domain the maximum kinetic rock energy reach values of 11,407 kJ (Q99 = 40,088 kJ) at the road (corresponding to rocks up to 12.5 m^3). At the southern domain, the same rocks hit the road with up to 2,783 kJ (Q99 = 12,635 kJ). The frequency distribution and box plots show that the ditch experiences more high energy impacts with impact frequencies greatest between 1,000 and 2,000 kJ, reduced to 1,000 kJ at the road.

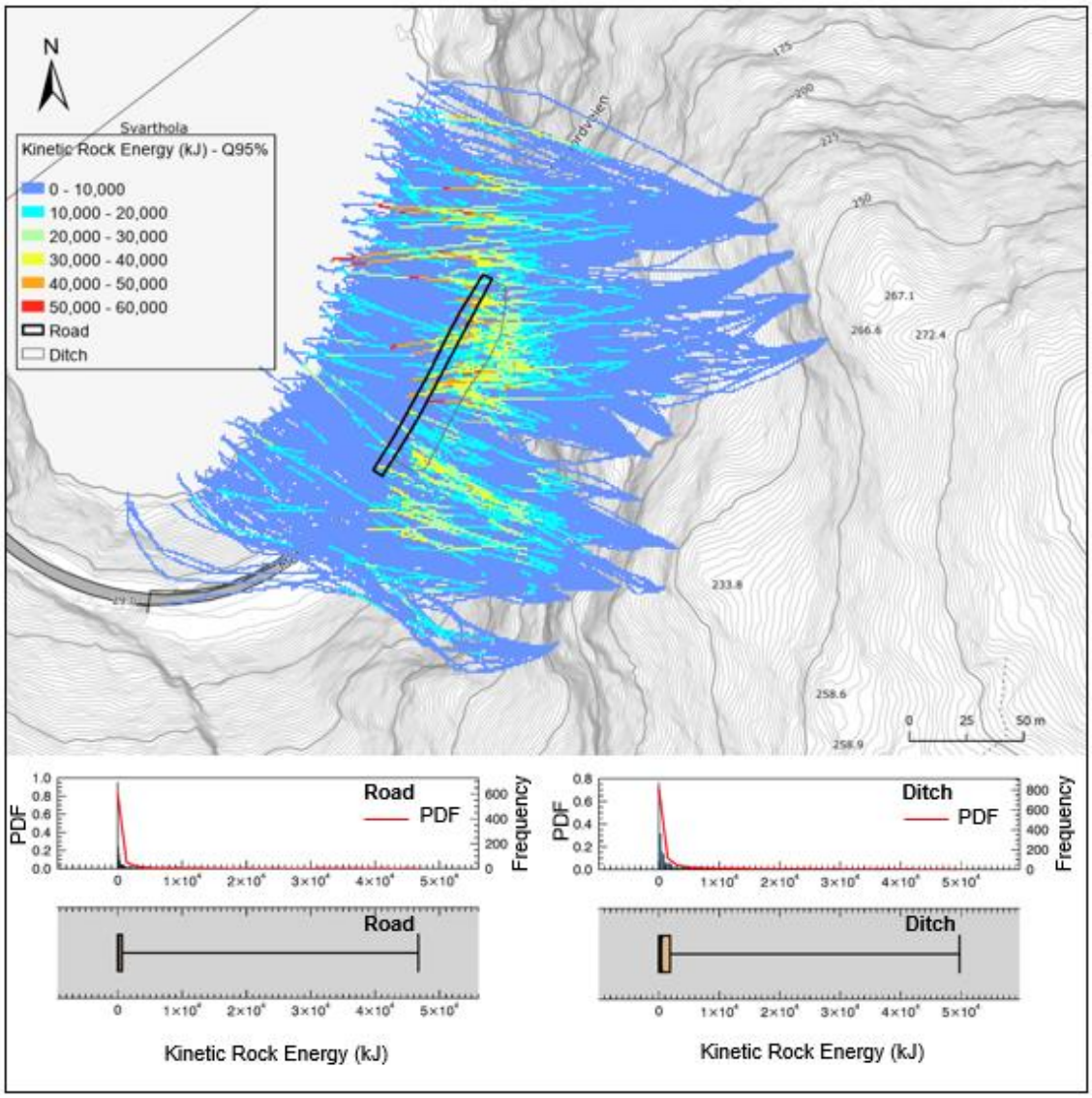

Figure 49. The 95th percentile kinetic energies of rockfalls for a worst-case scenario are displayed. Note higher energies in the northern part of the road (black polygon). The maximum values range from 2,783 to 11,407 kJ. The frequency distribution and the box plots show that the ditch experiences more high energy impacts with impact frequencies greatest between 1,000 and 2,000 kJ, reduced to 1,000 kJ at the road. Note that the PDF value (Probability Density Function) (red line) is added for better visualization of the big dataset. Also note that these values are multiplied by thousand.

Figure 50 shows the velocity of the simulated rocks. At the northern domain the maximum velocity reach values of 50 m/s (Q99 = 52 m/s). At the southern domain, the same blocks hits the road with velocities of 36 m/s (Q99 = 43 m/s). The frequency distribution and box plots show that the ditch experiences more high velocity impacts with impact frequencies greatest between 20 and 40 m/s, reduced to 20 m/s at the road

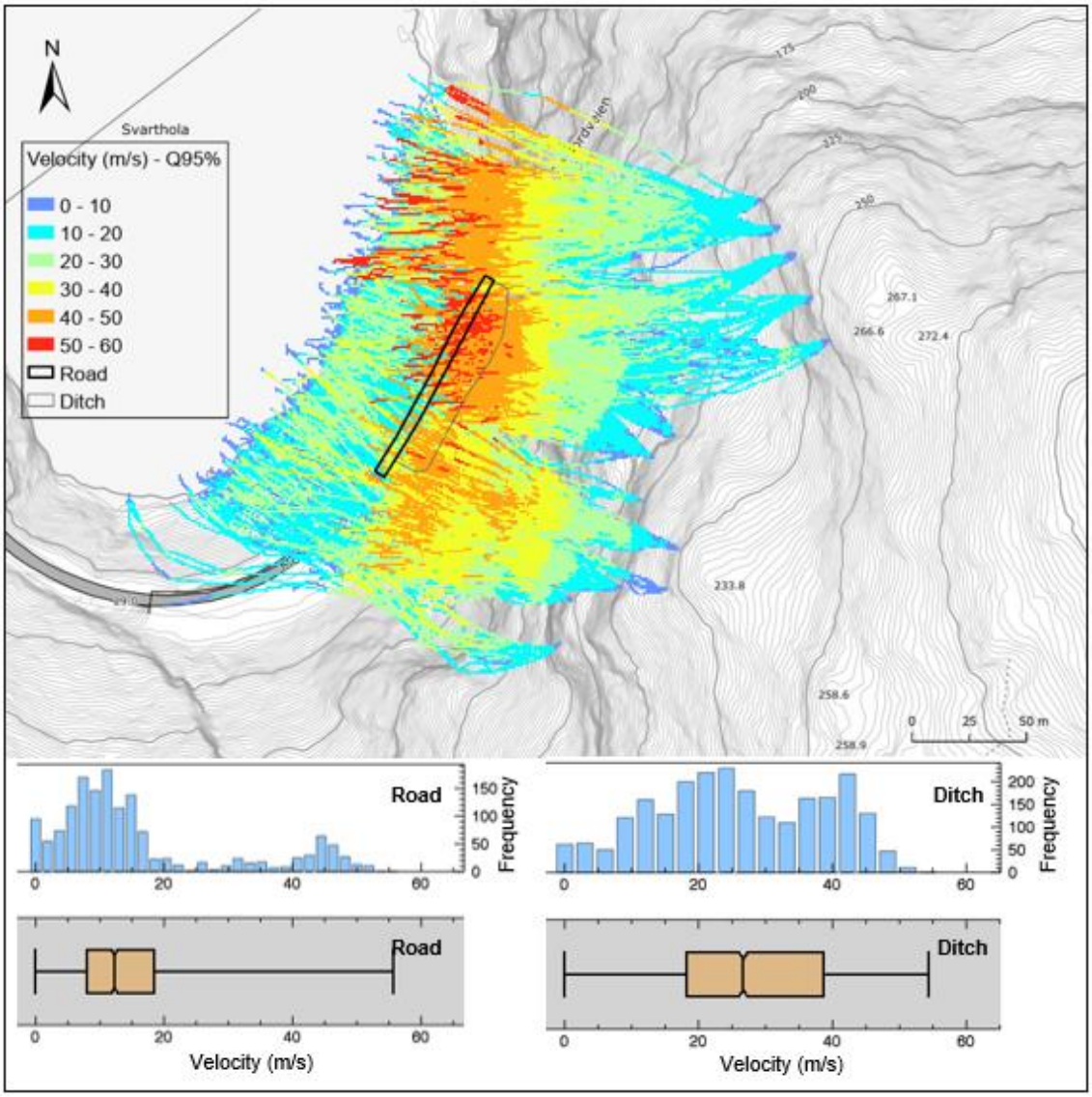

Figure 50. The 95th percentile velocities of rockfalls for a worst-case scenario are displayed. Note greater velocities in the northern part of the road (black polygon). The maximum values range from 36 to 50 m/s. The frequency distribution and the box plots show that the ditch experiences more high velocity impacts with impact frequencies greatest between 20 and 40 m/s, reduced to 20 m/s at the road.

Figure 51 shows the jump height of the simulated rocks. The CDF curve indicates that 80% of the boulders got a jump height of less than 4 m and the median jump height is estimated to 1.3 m at the road.

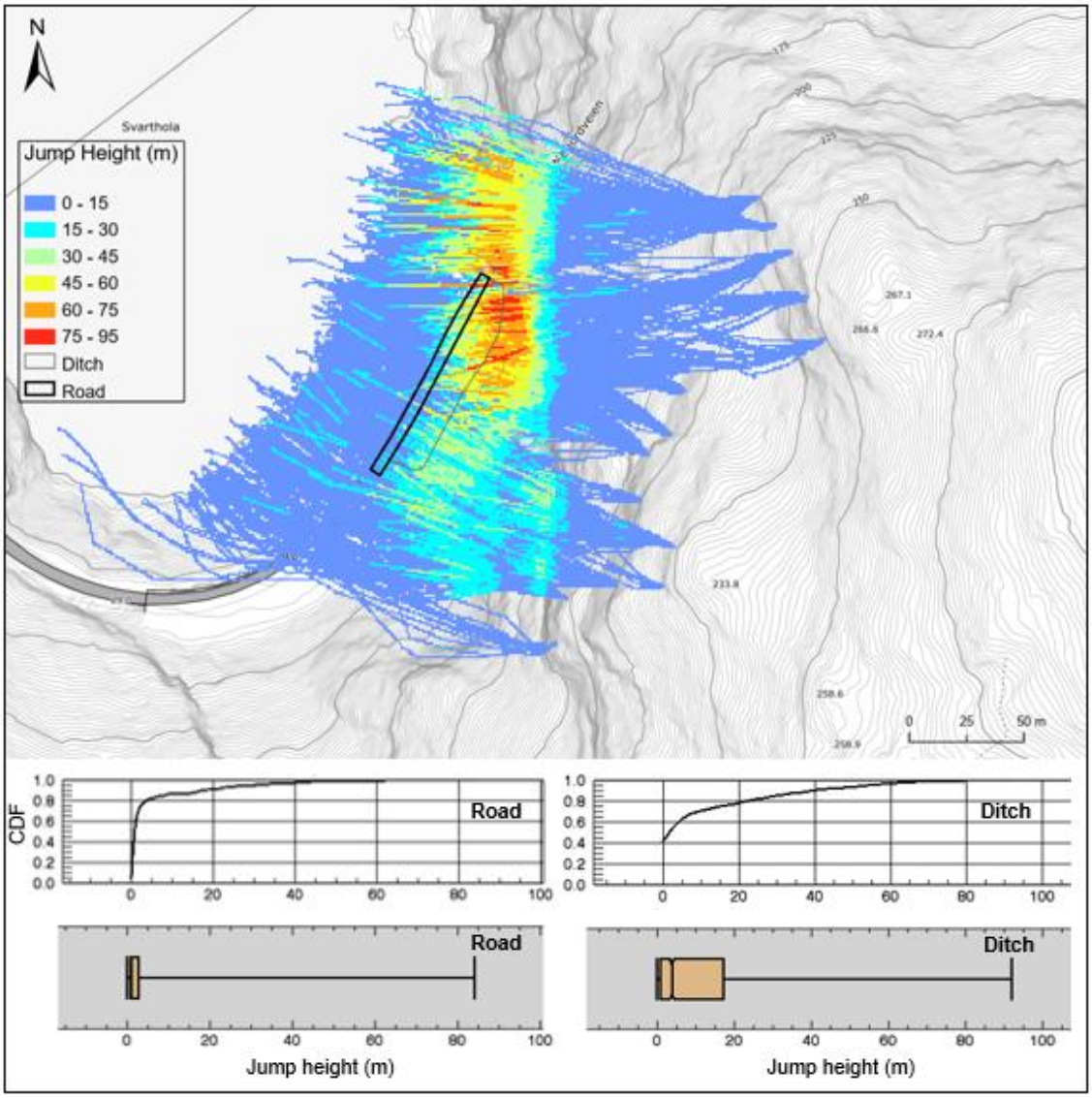

Figure 51. The 95th percentile jump heights of rockfalls for a worst-case scenario are displayed. Note higher jump heights in the northern part of the road (black polygon). The maximum values range from 1.3 to 4 m (CDF curve and median value). The box plots show that the ditch experiences higher frequency of greater jump heights than at the road.

5.4 Summary rockfall model outputs

Here we summaries rockfall modelling outputs (Table 10-12, Figure 52).

Table 10. Summary of the kinetic rock energy results obtained in RAMMS. Note that kinetic energy and velocity are presented in terms of the 95th percentile values, while the jump height is presented by the median value. Also note that observations of jump heights >20 m at the lower part of the cliff down to the fjord are not captured by the rockfall model.

Scenario	Rock volume (m^3)	Kinetic rock energy (kJ) Q95%	Rock velocity (m/s) Q95%	Median jump height (m)
1	0.5	1,734	50	0.9
2	1	3,560	49	1.0
3	2.0; 4.0	7,085; 13,995	50	1.2; 1.8
4	12.5	11,407	50	1.3

Model results for kinetic energy and velocity specifically were presented and discussed in terms of the 95th percentile values, but the 99th percentile values were included in order to investigate if they varied. The 99th percentile kinetic rocks energies are generally greater than the 95th percentile values. There is a significant difference for scenarios 3 and 4 where the simulations correspond to a greater rock volume. For scenario 3, corresponding to a 2 m^3 rock, the difference is between 1,864 and 4,069 kJ and for a 4 m^3 rock, the difference is between 2,214 and 4,270 kJ. Scenario 4 shows the greatest difference, up to 28,681 kJ (Table 11).

Table 11. Kinetic rock energies are displayed by the 95th and the 99th percentile for the different scenarios and road domains.

		Kinetic Rock Energy (kJ)			
		RAMMS Q95%	RAMMS Q99%	RAMMS Q95%	RAMMS Q99%
Scenario	Rock volume (m^3)	North domain	North domain	South domain	South domain
1	0.5	1,734	1,773	964	1,342
2	1	3,560	4,166	2,108	2,508
3	2.0; 4.0	7,085; 13,995	8,949; 16,209	1,783; 7,203	5,852; 11,473
4	12.5	11,407	40,088	2,783	12,635

The 99th percentile rock velocities are generally slightly greater than the 95th percentile values, especially for the south domain where the difference is greater. For the north domain the differences is between 0 and 6 m/s, and for the south domain it is between 7 and 12 m/s (Table 12).

Table 12. Rock velocities are displayed by the 95th and the 99th percentile for the different scenarios and road domains.

		Velocity (m/s)			
		RAMMS Q95%	RAMMS Q99%	RAMMS Q95%	RAMMS Q99%
Scenario	Rock volume (m^3)	North domain	North domain	South domain	South domain
1	0.5	50	50	37	44
2	1	49	54	40	43
3	2.0; 4.0	50; 50	56; 54	22; 33	44; 45
4	12.5	50	52	36	43

Design values

The 95th percentile energy values (Table 15) have been rounded to the nearest 100 kJ to provide design values for each relevant scenario, for use in rockfall protection design.

The design energies are between 1,700 and 7,100 kJ, and 1,000 and 1,800 kJ, for the north and south domain respectively (Figure 52). The impact velocity is between 22 and 50 m/s. The jump heights have little impact on the construction of the rock shed, but it might be relevant to consider the rocks with jump heights >20 m that hit the lower part of the cliff and get a horizontal jump down to the fjord.

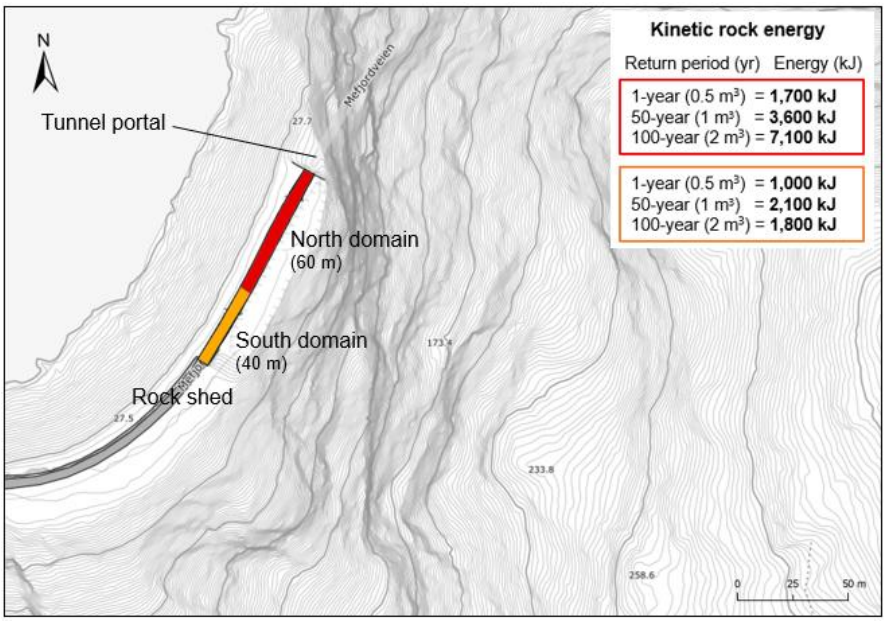

Figure 52. Topographic map with an overview of the impact energy of different rockfall scenarios for the return period of 1-100-year. The impact energies range between 1,700 and 7,100 kJ.

5.5 RAMMS::AVALANCHE input data

The snow avalanche results will be presented in two parts. The first part comprises the input data for the numerical modelling (5.5) and the second part covers the avalanche impact dynamic results (snow pressure, velocity and flow height) from the numerical model and the physical formulas (5.6). This workflow is followed for the three different methods: RAMMS, physical formulas and RAMMS and physical formulas.

Release area:

A release area mainly between 30 and 55° were found that were in agreement with the observations situated at 200-300 m a.s.l. with SW-NW aspect (Figure 53-43).

The physical formula methods were done with the same release area to the cliff point where parts of the avalanche masses might get airborne (Figure 53). A slope angle of 50° were used for the further calculations after a sensitivity analysis determined that the slope angle has little to no effect on the dynamic results.

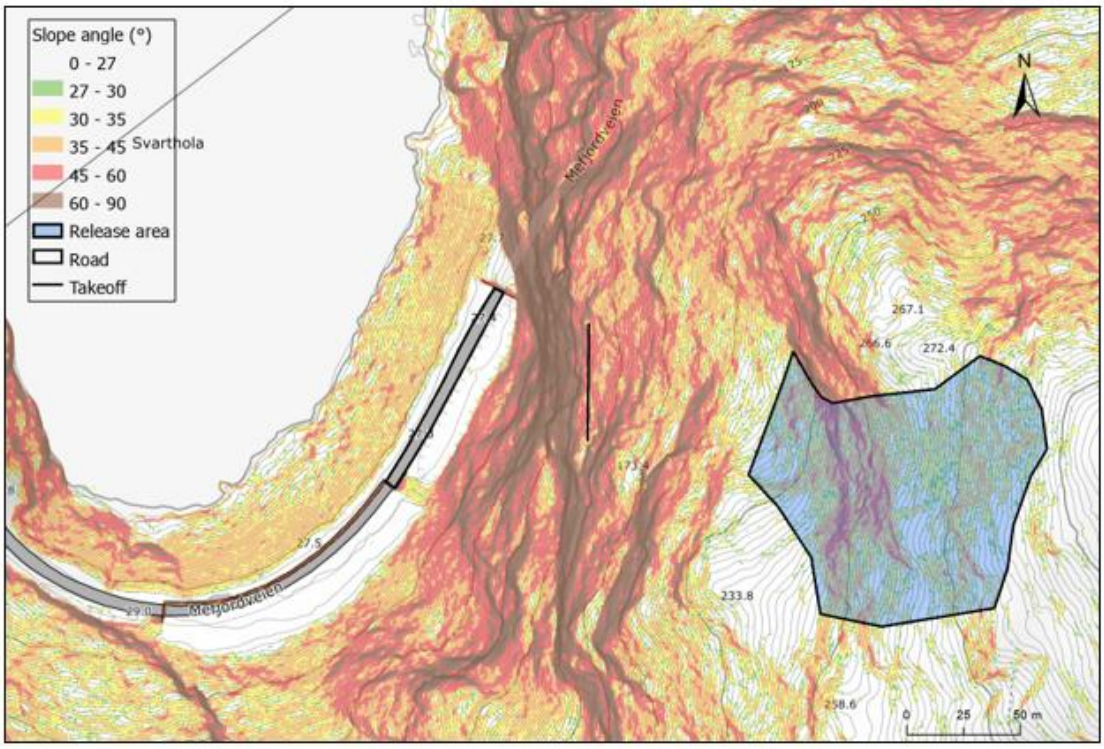

Figure 53. Topographic map with slope angle showing the release area (blue polygon) used for the RAMMS simulation. Note the black line (takeoff) which represents the area where parts of the snow masses might get airborne and fluidized. The mean slope angle at this point is 50°.

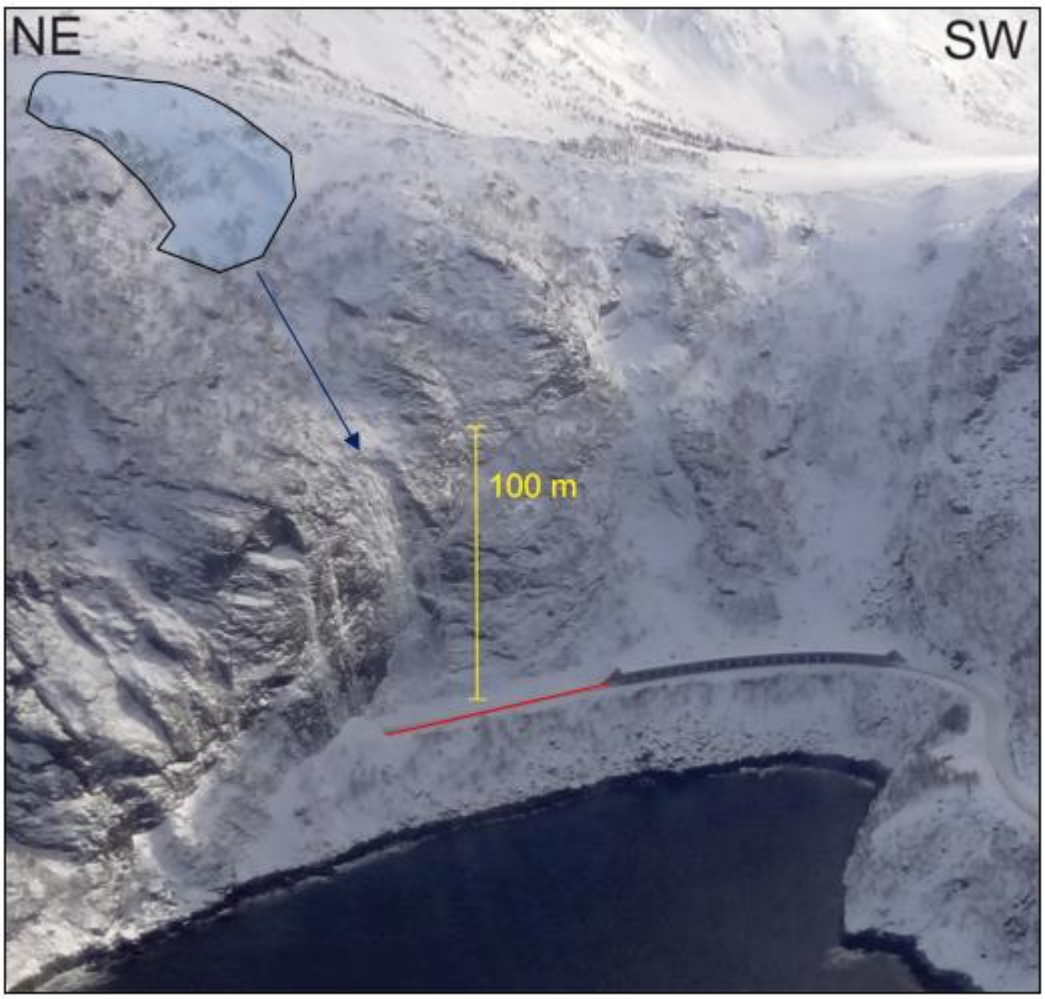

Figure 54. Photo that illustrates the release area (blue polygon) that are used for the RAMMS simulation (image is tilted which skews steepness perspective of avalanche path). Note the blue arrow which indicates the direction of the avalanche flow and the red line that shows the unprotected road. Photo: Andreas Persson, February 2018.

Release depth:

The release depth of the release area, based on the maximum 3-day precipitation for a 100-year return period (Table 13), were adjusted by the following points:

- +10 cm for the altitude difference of the weather stations and release area;
- +5 cm for the mean slope angle of 32°;
- +10 cm for snowdrift.

The snowdrift adjustment was estimated based on the wind data from the selected weather stations. Winds from NW normally lead to snowfall, and winds from W normally lead to the highest wind speeds. This implies that the release area, with SW-NW aspect, have less snow under normal conditions. However, there can be days when there is loose snow available for

transport (from Svartholavatnet) together with strong winds from S-SE-E that can load the release area with snow.

Table 13. Shows the expected 3-day maximum precipitation (mm) for the winter months (December-May) for a 100-return period. The chosen weather stations are located close to Svarthola. The estimated mean precipitation is used to calculate the snow release depth. The precipitation statistics were estimated by using a GUMBEL-distribution (NMI 2020).

Weather station	m a.s.l.	Distance (km)	3-day precipitation (100-year return period)
Gibostad	12	22 SE	102
Grunnfarnes	3	31 SW	102
Hekkingen Fyr	33	18 NNE	103
Leirkjosen	9	16 NE	112
3-day mean precipitation (mm)			**105**

A release depth of 1.3 m was used for the simulation of the release area. This resulted in a total starting volume of 16,900 m^3. This volume corresponds to an avalanche size of category 4 (volume <100 000 m^3), very large avalanche, according to the European avalanche warning services (based on the Canadian classification) (NVE, 2020a). In RAMMS it is classified as a small avalanche. A summary of the release area information and input parameters used in the model are presented in Table 14 (see Appendix B for all input settings):

Table 14. Summary of the release area information and the input data used for the RAMMS simulations.

	Release area
Mean slope angle (°)	32
Mean altitude (m)	260
Area (m^2)	13,000
Release depth (m)	1.3
Volume (m^3)	16,900
Volume category	Small
Density (kg/m^3)	300
Return period (yr)	100
Friction parameters	Default values (variable)
Altitude limit (m.a.s.l.)	500/0
Cohesion (Pa)	0
DTM (m)	5

5.6 RAMMS::AVALANCHE model- and physical formula results

Results for maximum snow impact pressure, velocity and flow height for the simulation and physical formulas (projectile motion and dynamic pressure) are presented in the following section. Model results are presented for both the road and the ditch, while the physical

formula results are presented to any impact point at the road or ditch. Model results are divided into two domains and presented for both the northern (60 m) and southern parts (40 m) of the road separately, to reduce the spatial bias. Statistics are presented across lines representing the ditch and the road location.

5.6.1 Method 1: RAMMS

Simulation results are presented in Figures 55-57. The maximum snow pressure reaches values of 130 kPa at the road. The pressure distribution shows that the ditch experiences higher snow pressures, up to 235 kPa compared to at the road.

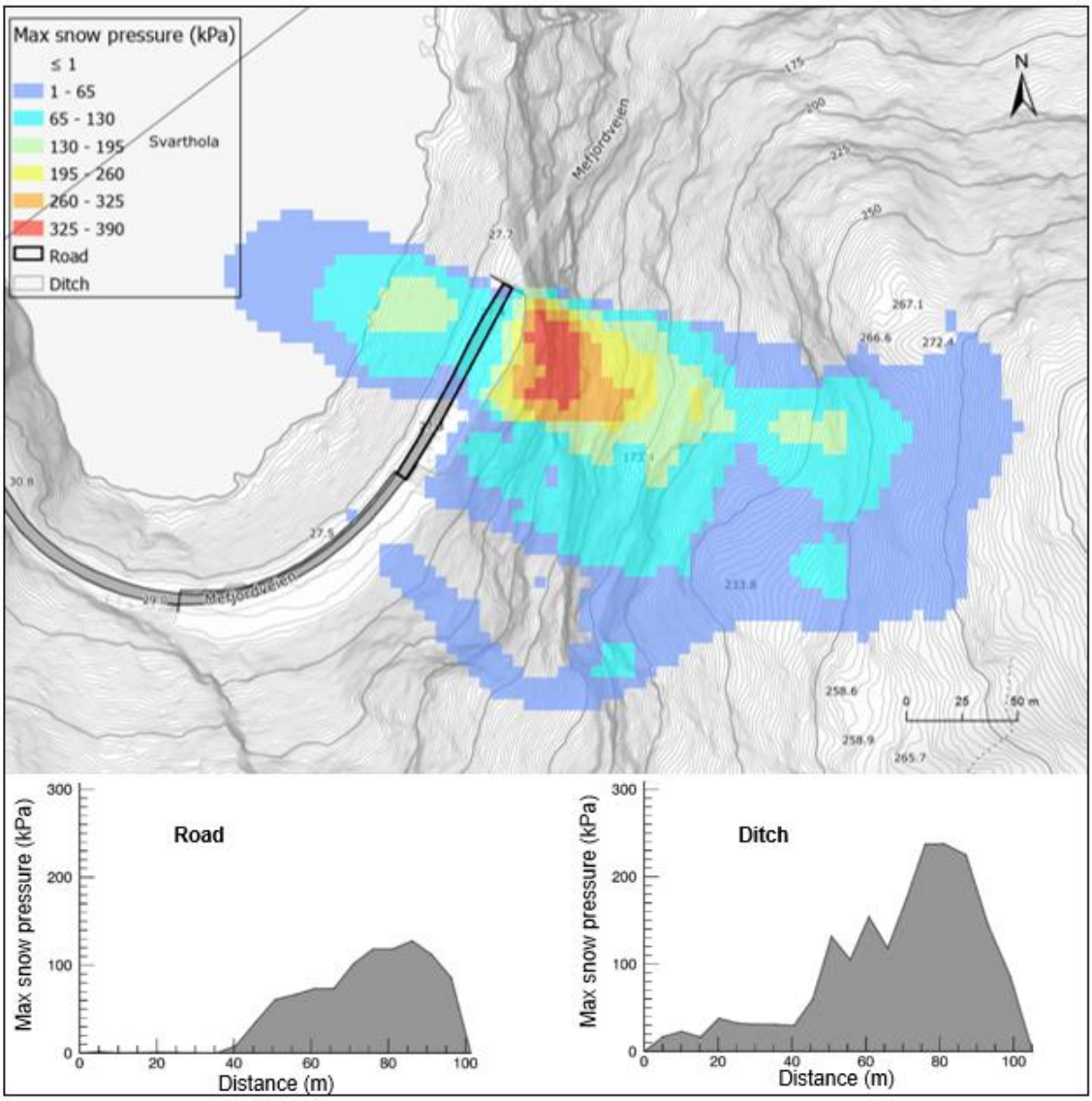

Figure 55. The maximum snow pressures of a dry-slab avalanche for a 100-year return period obtained by RAMMS are displayed. Note higher pressures in the northern part of the road (black polygon). The maximum snow pressure at the road is 130 kPa and 235 kPa in the ditch.

Figure 56 shows the velocity of the simulated snow avalanche. In the northern domain the maximum velocity reaches values of 20 m/s. The velocity distribution shows that the ditch experiences a higher velocity, up to 28 m/s. The velocity increases as the slope angle increases.

The velocity at the 'freefall' takeoff point varies between 25 and 35 m/s. A velocity of 30 m/s was specified to represent the average velocity at this point to be used for method 2 and 3.

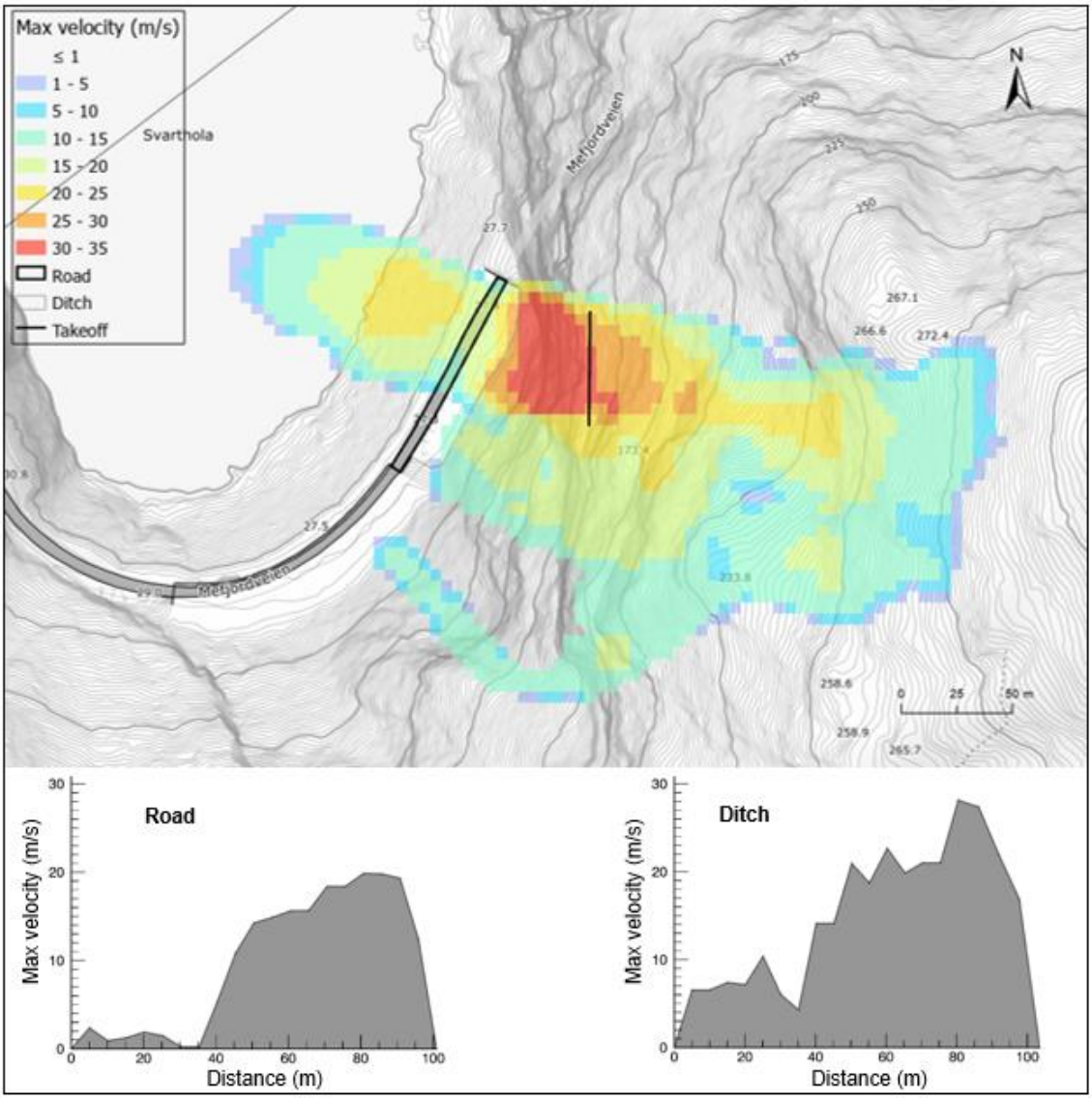

Figure 56. The maximum velocities of a dry-slab avalanche for a 100-year return period are displayed. Note higher velocities in the northern part of the road (black polygon). The maximum impact velocity at the road is 20 m/s and 28 m/s in the ditch. The average velocity at the 'freefall' takeoff point is 30 m/s (black line).

Figure 57 shows the flow height of the simulated snow avalanche. In the northern domain the maximum flow height reaches values of 3.7 m, reduced to 1.2 m and 3 m in the southern domain and the ditch respectively. The simulation indicates that the avalanche is channeled by the gully into the steep terrain shown by the deepest parts of the flow in this area.

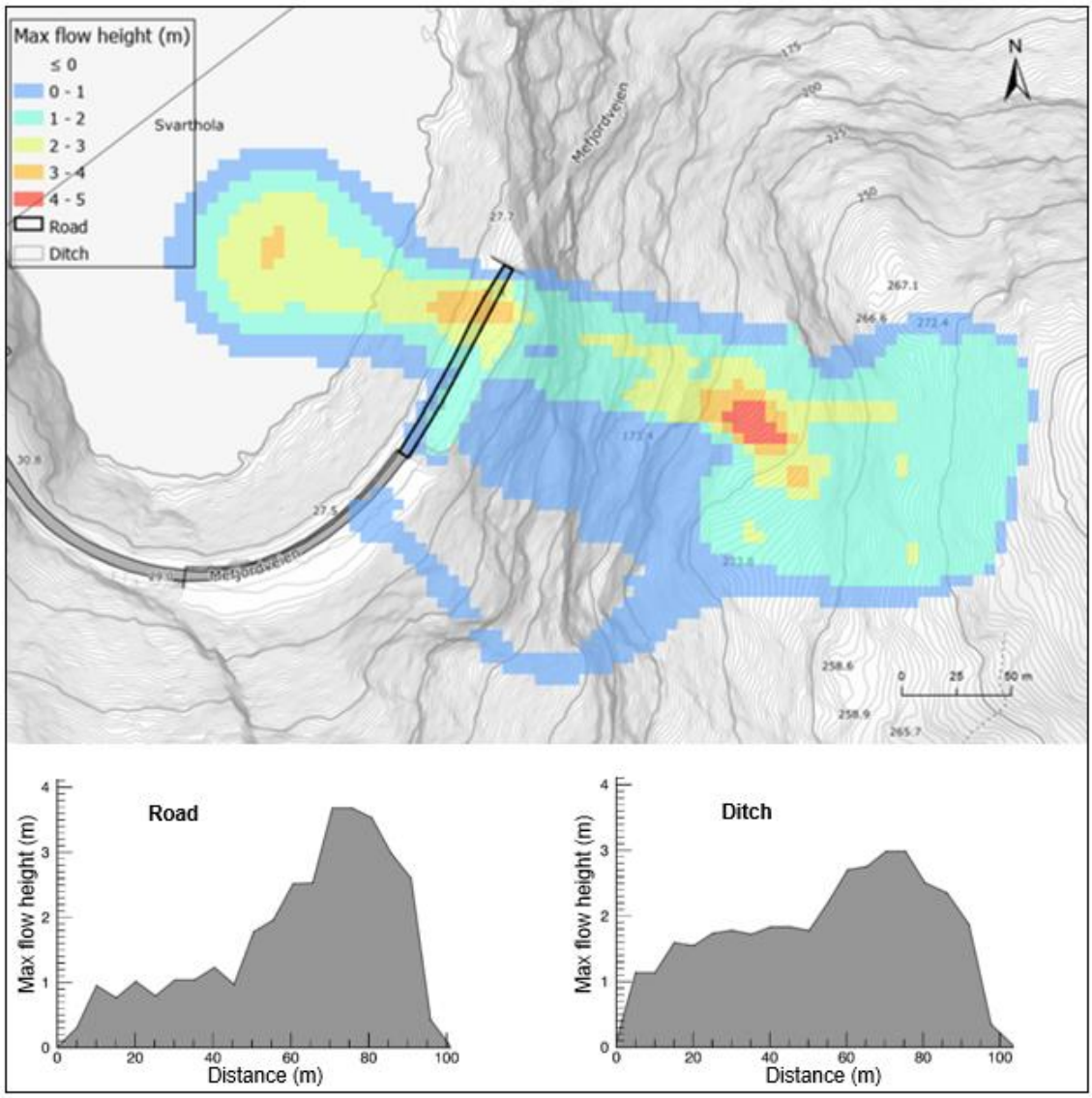

Figure 57. The maximum flow heights of a dry-slab avalanche for a 100-year return period are displayed. Note higher flow heights in the northern part of the road (black polygon). The maximum height at the road is 3.7 m, reduced to 1.2 m and 3 m at the southern part of the road and the ditch respectively.

5.6.2 Method 2: Physical formulas

Figure 58 shows the obtained results from the projectile motion formula and dynamic pressure formula. Note that the outgoing velocity (30 m/s) from the cliff is obtained from the avalanche model (see Figure 56) and the slope angle (50°) at this point from Figure 53. The impact velocity is 54 m/s and the impact pressure is 580 kPa (= 580 kN/m^2 = 58 t/m^2).

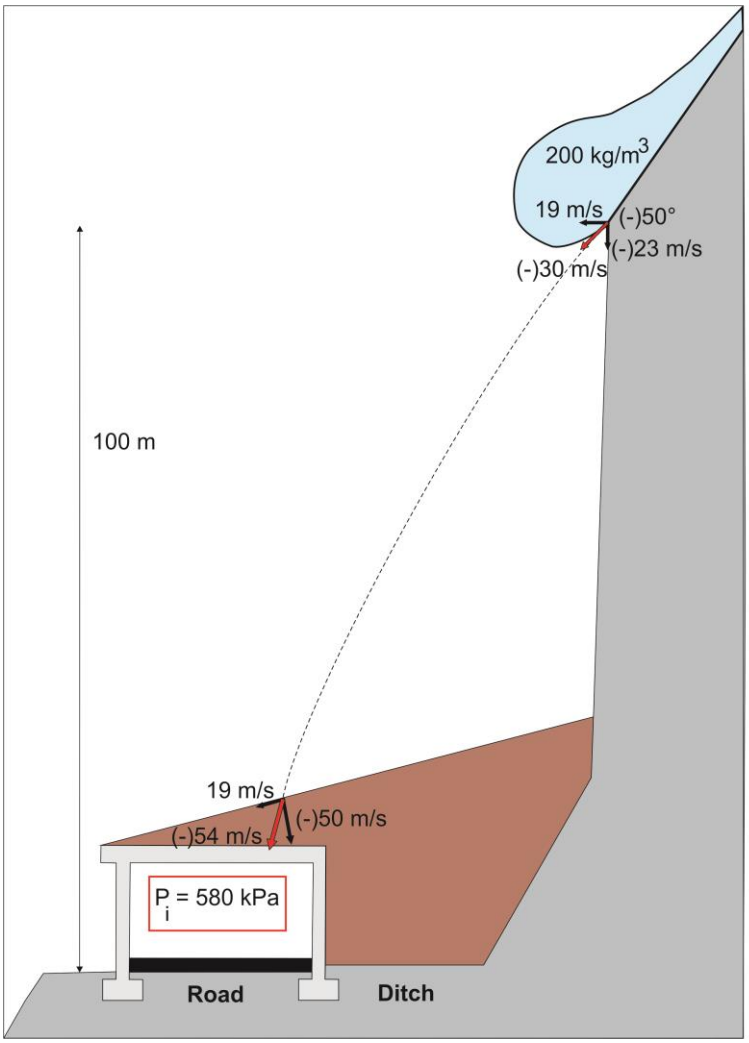

Figure 58. The snow avalanche impacts dynamics for a dry-slab avalanche with a 100-year return period by physical formulas are displayed. Note that a snow density of 200 kg/m^3 has been used. The maximum snow pressure at the road is calculated to 580 kPa. The vectors (arrows) show the horizontal and vertical velocities. The maximum impact velocity at the road is estimated to be 54 m/s.

5.6.3 Method 3: RAMMS and physical formulas

Figure 59 shows the obtained results from a combination of using RAMMS and the projectile motion formula and dynamic pressure formula. The impact velocity is 36 m/s obtained by the average velocity at impact. The impact pressure is 270 kPa (= 270 kN/m^2 = 27 t/m^2).

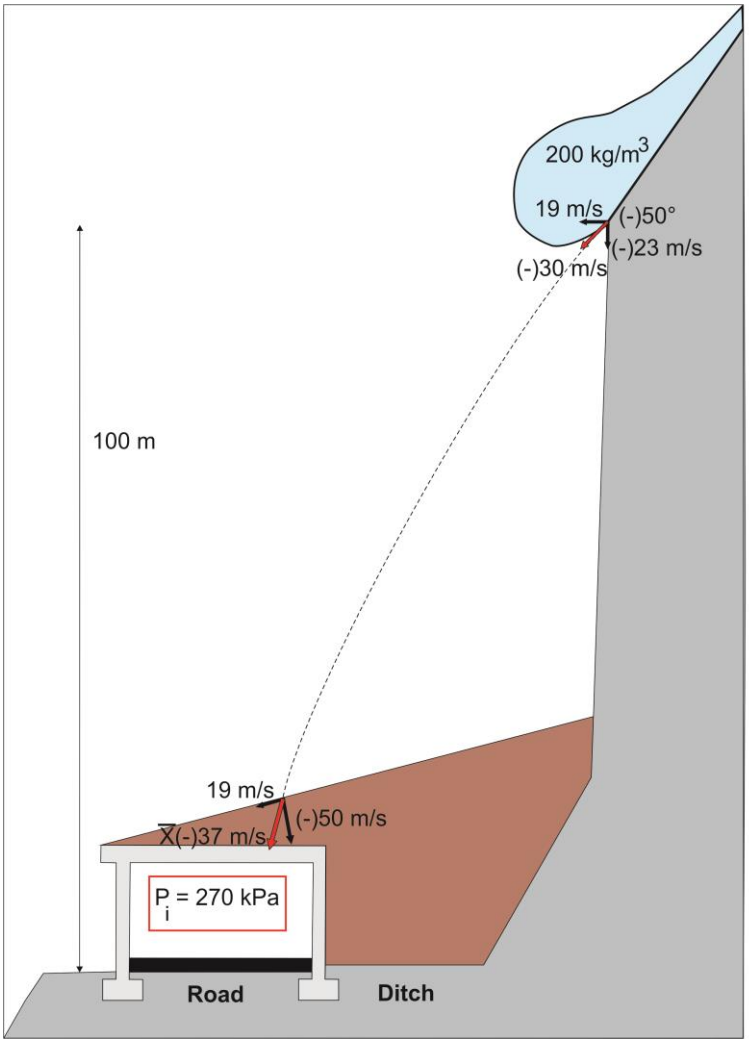

Figure 59. The snow avalanche impacts dynamics for a dry-slab avalanche with a 100-year return period by RAMMS and physical formulas are displayed. Note that a snow density of 200 kg/m^3 has been used. The maximum snow pressure at the road is calculated to 270 kPa. The vectors (arrows) show the horizontal and vertical velocities. The maximum impact velocity is estimated to be 37 m/s.

5.7 Summary snow avalanche results

Here we summarize the snow avalanche calculation outputs (Table 15, Figure 60).

Table 15. Summary of the snow avalanche dynamics at the road (velocity, snow pressure, flow height) for the different methods obtained by RAMMS and physical formulas.

Method	Volume (m^3)	Velocity (m/s)	Snow pressure (kPa)	Flow height (m)
1	16,900	20	130 (235 ditch)	1.2-3.7
2	16,900	54	580	-
3	16,900	37	270	-

Design values

The road impact pressures have been rounded to the nearest 10 kPa to provide design values for each method, for use in protection design (Figure 60).

The calculations of the snow pressure of the potential 100-year dry-slab avalanche are between 130 and 580 kPa. The velocity of the avalanche is estimated to be between 20 and 54 m/s. The flow height range from 2 to 3.7 m in the north domain and up to 1.2 m in the south domain.

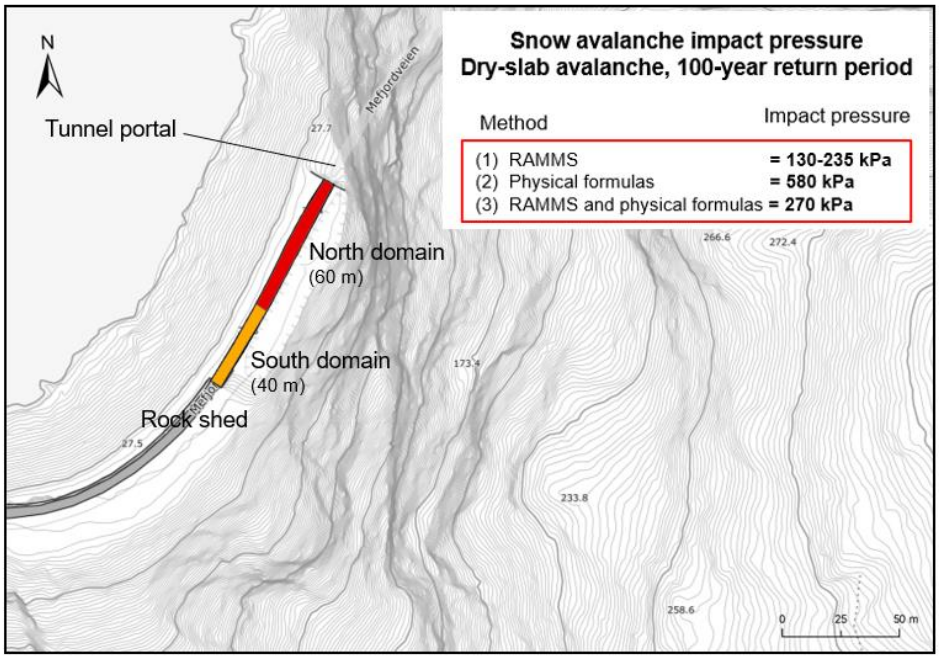

Figure 60. Topographic map with an overview of the impact pressure obtained by three different methods for a 100-year dry-slab avalanche. The maximum snow pressures range between 130 and 580 kPa.

5.8 Rockfall and avalanche history and weather

An analysis of the rockfall and avalanche event database was performed. These event observations are limited, with 13 rockfall events logged and eight snow avalanche events logged.

Table 16 shows the correlation between registered events and meteorological factors over a monthly period. The amount of precipitation is considered as a possible triggering factor in this study. The weather stations selected for this purpose were located no more than 31 km away (Grunnfarnes and Hekkingen fyr).

Table 16 shows that the fourth latest event had more than 35 mm of rain five days before the rockfall happened. For all events, the precipitation amount ranges from 15.9 to 62.9 mm (except from one event that had only 4.8 mm upon the release). All events had rain on the day the rockfall was released, except for two, where 50% of them had more than 10 mm of rain.

Table 16. Precipitation amount and temperature correlated to the registered rockfall database (NMI 2020).

	Total Precipitation (mm)				Temperature (°C)
Event	Month	5 days before	Event day	Daily average	Month
22.09.2020	233.4	61.4	26.4	7.8	9.5
18.08.2020	181.3	62.9	15.7	5.8	11.8
14.08.2020	181.3	43.2	11.2	5.8	11.8
01.06.2020	129.9	36.3	0.0	4.2	4.8
03.08.2017	52.8	17.0	0.6	1.7	11.1
15.12.2007	205.1	35.1	4.4	6.6	3.2
14.12.2007	205.1	19.1	18.9	6.6	3.2
13.12.2007	205.1	19.1	7.0	6.6	3.2
18.11.2007	157.5	15.9	10.7	2.2	5.3
01.07.2007	61.0	4.8	0.0	2.0	9.5
21.05.2007	93.3	23.7	10.3	3.0	6.4
06.05.2007	93.3	24.9	4.1	3.0	6.4

Table 17 presents the normal monthly precipitation and temperature. The daily average precipitation was calculated from the total monthly amount. Table 16-17 shed light on the following:

- a good correlation between higher monthly precipitation amount and rockfalls;
- a good correlation between higher daily average precipitation and rockfalls;
- a noticeable correlation between higher monthly temperature and rockfalls.

Table 17. Month normal precipitation and temperature over the 1961-1990 period. The daily average precipitation was calculated (NMI 2020).

	Precipitation (mm)		Temperature (°C)
	Month normal	Daily average	Month normal
Jan	104.0	3.4	-2.2
Feb	91	3.3	-2.1
Mar	85	2.7	-1.1
May	54.0	1.7	5.3
June	67.0	2.2	8.7
July	78.0	2.5	11.1
Aug	91.0	2.9	11.0
Sept	114.0	3.8	8.0
Nov	127.0	4.2	1.0
Dec	127.0	4.1	-1.1

An analysis of the 22nd September 2020 rockfall event shows that four days before the release the daily average precipitation was up to four times the historical normal. On the release day there was 26.4 mm of rain compared to 3.8 mm of the daily average for this month. The temperature trend goes down but sits above the normal during the whole month (Figure 61).

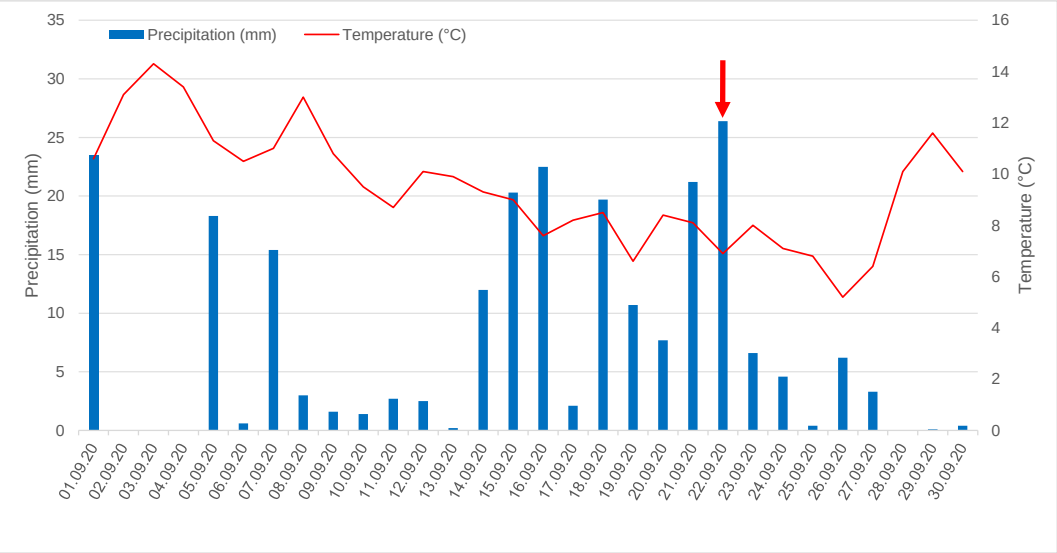

Figure 61. Daily precipitation and temperature for September 2020. The rockfall event happened on the 22nd (red arrow) (NMI 2020).

An analysis of the snow avalanche database was performed. Table 18 shows the correlation between registered events and meteorological factors over a monthly period. The amount of precipitation linked with the wind speed and direction are considered as possible triggering factors in this study. The weather stations selected for this purpose are the same as the

rockfall analysis, except for the event in 1986 where Leirkjosen (16 km NE) was selected as it was the closest station with available data at that time.

Table 18 shows that four out of five events have more than 12 cm of snow accumulated three days before the snow avalanche was released. For all events, the snow accumulation ranges from 13.0 to 31.6 cm (except for one event that had only 3.8 cm upon the release). Only two events had snowfall on the day the snow avalanche was released ranging between 15.1 and 35.2 cm. The wind speed on the event day ranged from 7.2 to 14.5 m/s from N-SW.

Tables 17-18 shed light on the following:

- a good correlation between higher monthly precipitation amounts and snow avalanches;
- a good correlation between higher daily average precipitation and snow avalanches;
- no noticeable correlation between temperature and snow avalanches.
- no noticeable correlation between the wind speed and direction before the event and the snow avalanche release.
- a noticeable correlation between wind speed and direction on the event day and snow avalanches;

Table 18. Precipitation amount, temperature and wind speed and direction correlated to the registered snow avalanche database (NMI 2020).

	Total Precipitation (mm)				Temperature (°C)	Wind Speed (m/s) and Direction	
Event	Month	3 days before	Event day	Daily average	Month	5 days before	Event day
22.05.2020	129.9	3.8	0.0	4.2	4.8	4.0 N-E	7.4 SE-S
06.02.2016	95.0	17.1	0.0	3.3	-0.4	6.0 N-SE	14.5 SE
31.03.2013	173.8	31.6	35.2	5.6	-2.6	5.2 SE-S	7.2 N-NE-S
13.01.1997	205.4	13.0	0.0	7.1	-1.6	16.0 SE-NW	10.3 SE-SW
12.02.1986	67.5	14.7	15.1	2.3	-2.3	6.9 SE-SW	12.3 SE-SW

5.9 Climate change

Climate projections of the Troms region and northern Senja were obtained in order to investigate the possible implications on the avalanche frequency.

Figure 62 shows the expected increase in precipitation for the Troms region according to a high emission scenario (RCP8.5). These climate predictions are based on assumptions about emission scenarios concerning greenhouse gasses of global and regional climate models. The RCP8.5 scenario refers to an ongoing increase in the greenhouse gas emissions following an observation period. According to this scenario, the Troms region will experience an increase in the annual precipitation of 15% whereas northern Senja is

expected to get an annual increase of 12.5-17.5%. The precipitation change for the winter season is estimated to increase by 10% and by 30% and 20% for the summer- and autumn seasons respectively (Metereological Institute et al., 2021).

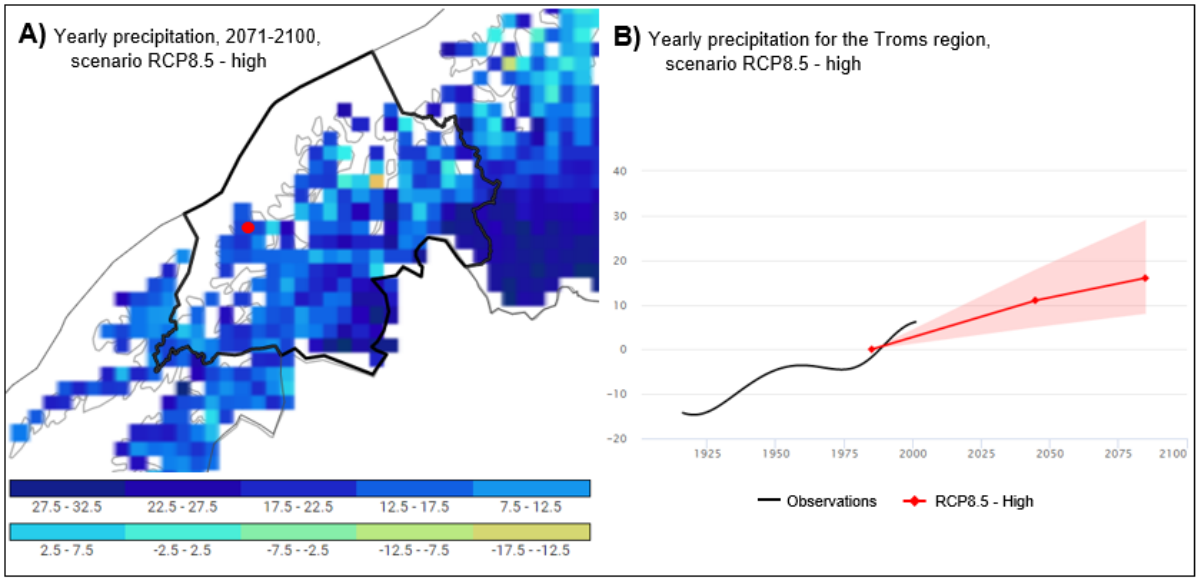

Figure 62. A) Predicted change in annual precipitation (%) from the period 1971-2000 to 2071-2100 for the Troms region according to a high emission scenario (RCP8.5). At the location of Svarthola (red point), the expected increase is about 15%. B) Development of the yearly precipitation for the Troms region, expressed as percentage deviation for the time period of 1971-2000; the black curve shows the measured variations whereas the red curve shows the median values from several climate model predictions. The shaded area shows the spread between low and high climate prediction scenarios (10 and 90 percentiles). Modified after Meteorological Institute et al. (2021).

The intensity and the frequency of short periods with heavy precipitation is also expected to rise in the future, for all seasons. The precipitation intensity for a 24-hour period is thought to be increased by about 25% and there are indications of even higher percentage increases for shorter periods. In Figure 63 estimated IVF values (intensity-duration-frequency value) of maximum precipitations are plotted for one to 24-hours (1440 minutes) for an interval between two to 200 years (Metereological Institute et al., 2021). The IVF values are calculated by using a Bayeasian hierarchical modelling, based on measuring stations from across Norway. There are large uncertainties connected to ITF-statistics and increases at areas with few measuring stations (like northern Norway) and for a longer time interval. Bodø measuring station is the closest station to the study area, situated along the coast and the recommended procedure by MET has been used to check that these values are similar to projections at Senja. These projections indicate that is possible with maximum precipitation events with more than 80 mm in 24-hours at Svarthola in the next 200 years (Figure 63).

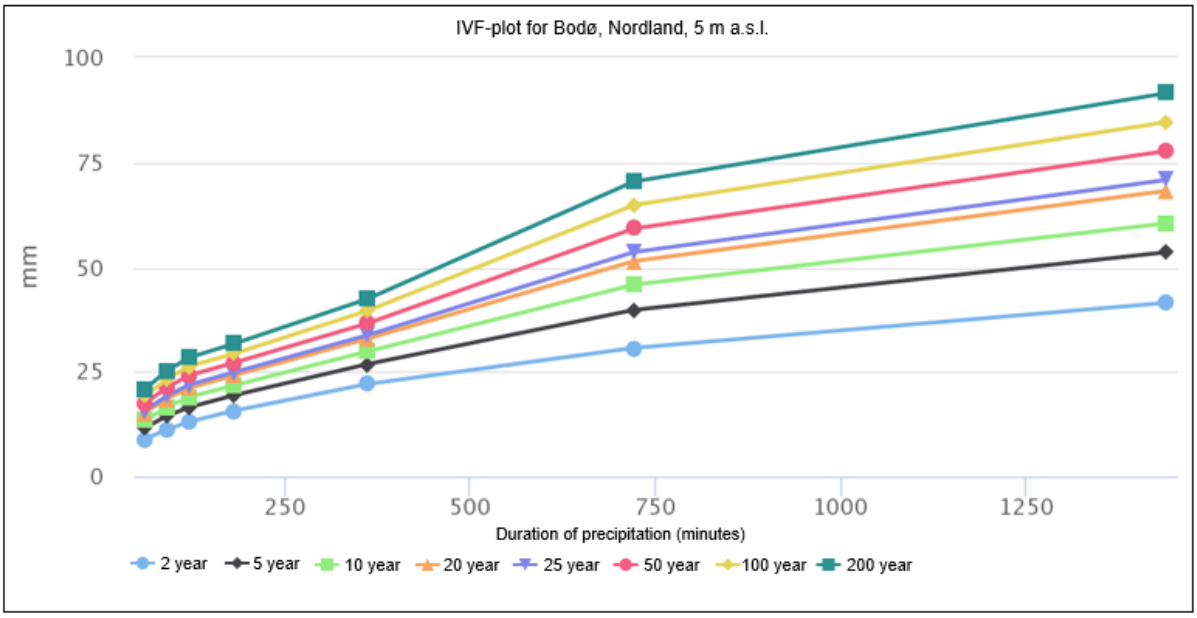

Figure 63. IVF-plot of the maximum expected precipitations at Bodø, Nordland. The study area can be expected to experience similar values. The mm of precipitation is plotted for durations of one to 24 hours (1440 minutes). The IVF-statistics were estimated by using a GUMBEL-distribution (GEV type I). The plot indicates that in 200 years it can be possible with more than 80 mm in 24 hours. Modified after Meteorological Institute et al. (2021).

Figure 64 displays the expected change in temperature for the winter season for the Troms area according to a high emission scenario (RCP8.5) (Metereological Institute et al., 2021). According to this scenario, the Troms region will experience an increase of 6°C whereas northern Senja is expected to get an increase of 4-5°C.

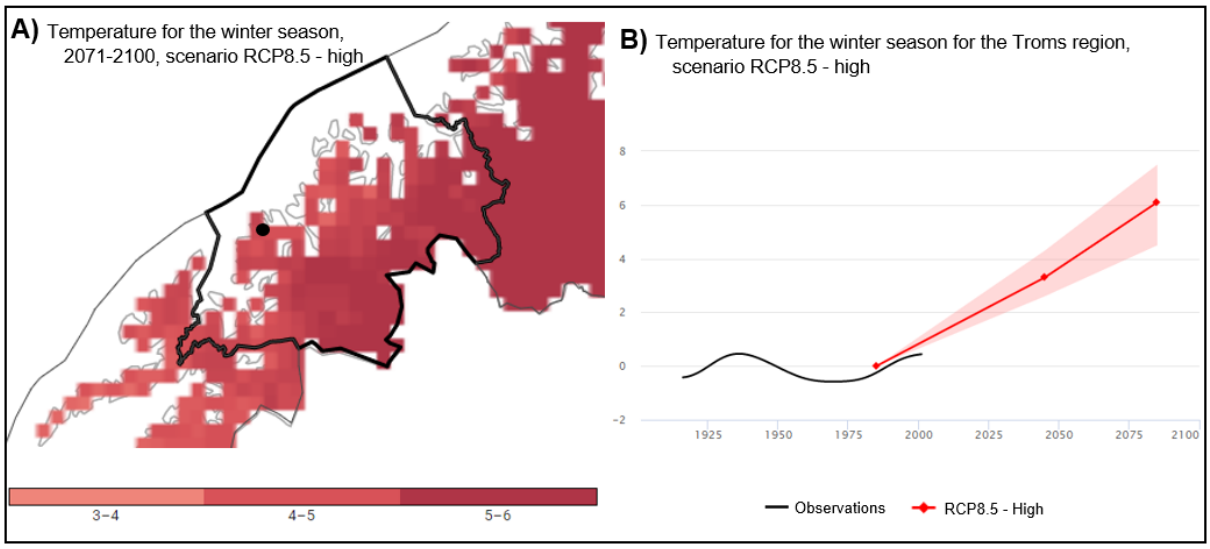

Figure 64. A) Predicted change in temperature (°C) from the period 1971-2000 to 2071-2100 for the winter season in the Troms region according to a high emission scenario (RCP8.5). At the location of Svarthola (black point), the expected increase is about 5%. B) Development of the temperature for the winter season for the Troms region, expressed as percentage deviation for the time period of 1971-2000; the black curve shows the measured variations whereas the red curve shows the median values from several climate model predictions. The shaded area shows the spread between low and high prediction scenarios (10 and 90 percentiles). Modified after Meteorological Institute et al. (2021).

The increase in temperature during the winter season will have an impact in the snow cover, which is expected to decrease significantly as well as the number of days with snow cover per year. A RCP8.5 scenario predicts that the winter season will be reduced to three to four months in duration, compared with the current season which is six months.

6 Discussion

The main aim of this study has been to determine the impact dynamics on the 100 m stretch of road on Fv 862, Svarthola, Senja, relevant for protection design. The study has also included impacts significant for academic purpose. This chapter is divided into three parts, starting with discussing the rockfall findings in context to rock dynamics and the reliability of model results and their implications (6.1). In the second part, the snow avalanche results and the different methods that were applied will be discussed (6.2). Finally, climate change and its implications for the site are explored (6.3).

6.1 Rockfall

6.1.1 Results summary

The rockfall design scenarios indicate an impact energy from 1,700 kJ to 7,100 kJ, corresponding to a 0.5-2 m^3 block size and a return period of 1-, 50- and 100-year. The impact velocity is 50 m/s and the jump height is up to 3 m at the road.

6.1.2 Input data for numerical modelling

Block size

One of the most important input for rockfall protection design is the selection of the rock block size (volume). A very large design block could result in an unnecessary expensive, over-engineered structure. If the design block is too small, the structure could be damaged if impacted by a larger rock block. Selection of design blocks for the protection structure is therefore crucial and should be based on information collected from the fieldwork, preferably from measurements of block size made both at the rockfall source and from fallen blocks located in the runout zone (Green, 2016). This can allow to evaluate the tendency of block fragmentation, which is quite common and can affect runout properties and impact dynamics (Ruiz-Carulla et al., 2015).

The measurements of the size of the forty randomly chosen blocks in the runout zone provide a sufficient basis for the selection of block sizes used in the scenarios. The frequency distribution of rockfall sizes showed a majority of small blocks, where almost 80% were up to 0.5 m^3, 7.5% were up to 1 m^3 and the other three size groups stood for 5% each of the total mapped blocks (Figure 27). The highest frequency of rockfalls of 0.5 m^3 is supported by the experience from the contractors (B. A. Reilertsen, personal communication, October 18, 2020). It cannot be excluded that few of the rocks mapped below the road can have been placed there when the road was built, as filling. The database of historic rockfalls

at the site contain sparse information about the block size and with the first event registration only 18 years ago is difficult to compare these events with the mapped boulders (Table 5). This implies that the frequency (return period) of the bigger blocks are difficult to determine from the site assessment and they are somewhat based on subjective judgement. This is a common limitation for engineers in the framework for hazard mapping due to lack of information for events with high return period.

Location of fresh scars in the source areas were identified, but the steep terrain made it difficult to measure these (Figure 25). The size of the fallen blocks in the runout zone could therefore not be compared with the block sizes at the source. Block fragmentation was observed by the scaling team (H. L. Haukenes, personal communication, November 10, 2020), but it is not believed to affect the impact dynamics significantly because of the occurrence of blocks in free-fall motion for 100 m before they hit the road and whereby the block's mass become more crucial for the results.

Block shape

The boulder shapes are based on the dimensions from the measured blocks in the runout zone. The block shape can have an effect on the rockfall energy, and especially on the rotational kinetic energy. The removal of the tabular/long blocks from the design scenarios are not believed to have a significant effect on the results since the spherical/equant blocks are often able to maintain the angular momentum better and should normally give higher impacts (Wylie Mah, 2004). From a practical standpoint, it was often difficult to make accurate definition of the block shapes and there is naturally some uncertainty connected to these results.

The measured block shapes can be compared with the identified joint sets (J1-4) where J1 is most likely giving the form of the platy blocks, and J2 together with J3 and/or J4 result in the spherical and/or tabular blocks (Table 7, Figure 29).

Release areas

The localization of the release areas has a strong impact on the results (Bartelt et al., 2016), and therefore it is important that this parameter was specified as accurate as possible. There are several fresh scars that could easily be included in the study and in order to cover all potential areas the outcropping rock over 60° were selected as well. The specification of the uppermost parts of the cliff were used to give the highest possible impact energies. By varying the rock shapes and the rock release orientations the range of possible trajectory fall lines have been incorporated into the rockfall event and ensured the natural variability at

every ground contact. However, it is still a simplification of reality since it difficult to include every potential release area, but the main and most important areas were specified.

Terrain types

Another important input for rockfall protection design is the delineation of the terrain materials. It has a considerable influence on the model output (Bartelt et al., 2016), where a rock can lose up to 86% of the energy on the first ground contact (Dorren, 2003; Evans Hungr, 1993) which means that the different terrain types determines how much kinetic energy is lost when the block collides with ground.

The selection of the terrain materials were made on the basis of the field observations and drone images, in addition to model calibration. The terrain above the road is assigned as hard to medium hard, which means that less kinetic energy is lost compared to in softer materials, and accordingly this result in higher impact energy. The ditch was delineated as soft terrain, which replicates the present ground conditions and this will naturally change when the protection structure is built. The ability of the energy absorption of the cushion layer on the structure roof is important for the design capacity (further discussed in 6.1.4). Another uncertainty is connected to the season variations, which can affect the moisture content of the terrain and its properties (Vick et al., 2019).

6.1.3 Scenarios

In order to give a technical overview of the rockfall situation at Svarthola different scenarios were presented. This is a common practice by engineers during the design process, where the scenarios are proposed with different year recurrence intervals and each with a different design block size (Green, 2016). The scenarios cover the lifespan of the construction and the magnitude and frequency of the impact dynamics determines what the construction should withstand.

Scenario comparison

The simulated scenarios show consistency in higher dynamic impacts at the road and in the ditch with bigger block size (Figure 65). The maximum kinetic energy is doubled for each scenario as the block size is doubled, and this corresponds well to the physical understanding of kinetic energy, being a function of mass, it is greater for bigger blocks when they have similar velocities (Vick, 2015).

The rockfall model outputs show a clear pattern of higher energy impacts in the northern domain compared to the south domain and with higher frequency impacts in the ditch. This

can be explained by the steeper terrain that sits in the north, which can give blocks longer fall heights and higher velocities, thereby increasing the kinetic energy at impact. All scenarios show that the majority of the rockfall impacts are lower than the maximum impact energy, which can be interpreted that blocks giving higher impacts happen more seldom. However, this has no meaning for the construction design.

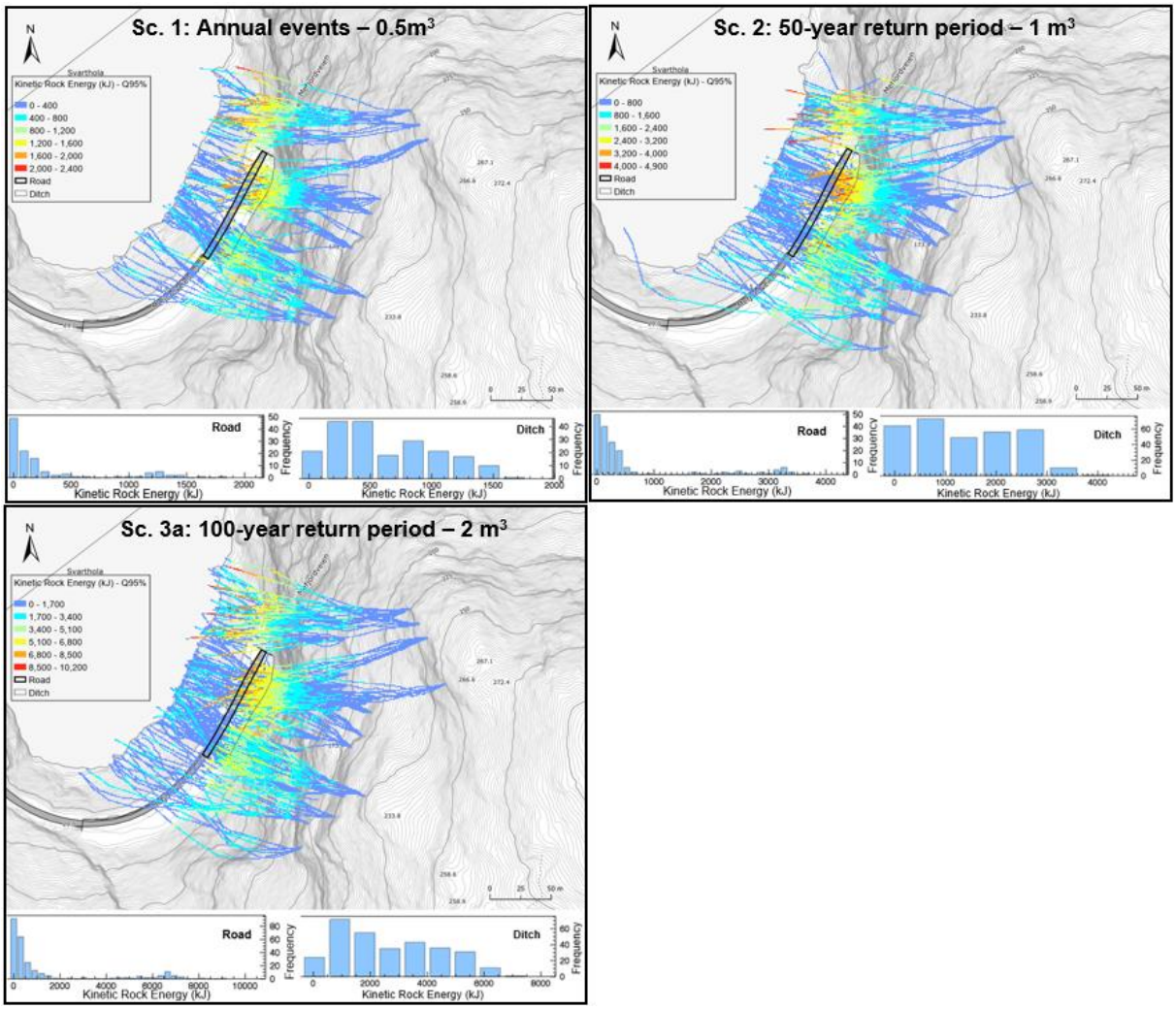

Figure 65. Design scenarios show consistency in higher dynamic impacts at the road and in the ditch with bigger block size accordingly to the kinetic energy formula. Note that the kinetic rock energy scale is different for the scenarios and is increasing with block size.

The rock velocity and the jump height varies little across the different scenarios. These findings suggest that there is no strong correlation between block size and velocity or jump height. This can be due to the steep cliff situated above the road, which means that most blocks move in free-fall and the weight of the blocks have little effect on the velocity and jump height. This is supported by the acceleration (from 20 to 50 m/s) of the detached block at the point where the slope angle is more than 70°, which corresponds well to movement of the block through the air by a period of free-fall before it hits the ground.

At the terrain above the cliff, the initial impact for a detached block happens close to the source area, which implies that less potential energy is generated. Nevertheless, the slope angle and ground conditions (medium hard) make most of these rocks run out from the slope and they will very likely reach the road or the ditch. The low velocity and bounce height in the upper terrain is assumed to be caused by the fact that the boulders have not yet have time to build up momentum, but more momentum is built up the further they travel from the source area.

Implications of design block and return period for scenarios

For design purposes, a so-called design block derived from the block size distribution and event frequency was used to assess the rockfall hazard. This approach was chosen because it follows the general guideline for dimensioning a rockfall protection structure (Green, 2016; Vagnon et al., 2020). The database of historic events covers the period from 1980 and therefore the volumes of the annual events are quite certain, as they are registered often. The 50-year events are more statistically uncertain because the first registration is 18 years ago. The 100-year event is the most uncertain since there is no clear statistical data for these events. This means that the simulation with the entire block size distribution (worst-case) gives the most realistic distribution of the dynamic impacts and trajectories since the maximum block sizes are not disregarded prior to the modelling. It is therefore important to acknowledge that it may be possible for a larger block to fall, but it is uncertain when or if this will ever happen. These events can be included in the residual risk acceptance and/or it may be possible to identify and secure large unstable blocks at the source to minimize this risk.

6.1.4 Protection structure design

The rockfall analysis shows that stretch of road can be hit by rock blocks with high impact dynamics and by which it is important to reduce these impacts against the construction as much as possible. A common practice is to divert the fallen block over the roof to reduce the impact dynamics. Another important factor to avoid the risk of impact failure is the selection of the cushion layer. This layer absorbs energy and limit the impact energy that is transmitted into the structure (Volkwein et al., 2011).The magnitude of the impact reduction depends on the thickness and properties of the material, as well as the flexibility of the structure. There have been several test studies of the efficiency of different cushion materials and new suggestions keep arising to optimize the protection design (Yoshida et al., 2007).

6.1.5 Q95 and Q99 percentiles

Q95 and Q99 percentiles for kinetic rock energies show unexpected great differences for the scenarios with greater rock volume and greater data sets, e.g. the worst-case scenario (4)

has a difference of almost 30,000 kJ between these percentiles. The discrepancy is thought to be caused by a statistical function. With bigger dataset, you are more likely to remove extreme values when you perform the normalization. These values are not included because they are defined as outliners. Based on this, we suggest that the user should be aware of this before they get their results. For this study, the design values are not affected by this inconsistency. However, special consideration of these values are required for the design on a site-specific basis.

6.1.6 Design values conclusion

Several scenarios have been presented with the purpose to outline the potential year recurrence (1-, 50-, 100-year) of different design block sizes. The relevant design scenarios, corresponding to a 0.5 m^3, 1 m^3 and 2 m^3 block, result in maximum impact energies of 1,700 kJ, 3,600 kJ and 7,100 kJ respectively. The maximum impact velocity of the rock block is estimated to range between 20 and 50 m/s. The rockfall modelling shows a clear pattern that one can expect higher and more energy impacts (and naturally higher impact velocity) at the north domain and in the ditch compared to the south domain. The fall height can be up to 100 m and the median jump heights are between 0.9 and 1.2 m. Some blocks can jump significantly longer (>20 m) if they hit the lower part of the cliff wall and down to the fjord. This can cause a horizontal force on the future construction, depending on the design.

6.1.7 Limitations

This study provides valuable insight into the rockfall impact dynamics at the site, but there are few limitations, some have already been mentioned in this chapter and in the method chapter. They concern the following:

- The field mapping is limited to the fallen blocks in the runout zone and no comparison is made to the size of blocks at the source. Therefore, no evaluation of the block fragmentation tendency is included in the investigation.
- The terrain types are mainly delineated from drone images due to the steep and inaccessible terrain and seasonal variations are neglected, and there are naturally some uncertainty connected to this input data.
- The rockfall design scenarios follow general guidelines to assess the rockfall hazard, however this process disregard the largest blocks and the selection of the design blocks are based on subjective judgement.

6.2 Snow avalanche

6.2.1 Results summary

The snow avalanche analysis indicates a maximum impact pressure from 130 kPa to 580 kPa based on three different methods, corresponding to a dry-slab avalanche of 16,900 m^3 with a 100-year return period. The impact velocity at the road is between 20 and 54 m/s and the flow height is between 1.2 and 3.7 m.

6.2.2 Input data for numerical modelling

One of the most important inputs for avalanche protection design is the selection of the release area and depth. This determines the size of the avalanche and has great impact on the dynamic outputs (Bartelt et al., 2017).

The selection of these parameters for the design were challenging due to the sparse information of the historical events. They were limit to few observations of small avalanches that had been artificially released (A. Persson, personal communication, October 29, 2020). There is no documentation (e.g. videos, photos) of the deposits, except from one event in the 1986, or on the avalanche motion at the 100 m high cliff.

The design avalanche is limit to one scenario (an extreme event), but in reality there will be a natural variability, mainly because of the highly variable, layered character of the snowpack and the complex interaction between terrain, snowpack, and meteorological conditions leading to avalanche release (Schweizer et al., 2003).

Release area

The location of the release area was identified by information from TFFK, based on the slope angle and from observations of avalanches that were artificially released. However, the extent of the area is unknown and therefore the potential area was enlarged to a maximum extent in order to represent the 100-year event. This potential area was delineated with attention paid to the steepness and terrain form to reflect a realistic scenario. Based on this, the specified release area can with high confidence be regarded as the largest possible event. Despite this, it is still uncertain if an avalanche of this size would ever occur.

Release depth

There is no information on the release depth of the naturally or artificially released avalanches. This input parameter was determined by a well-used approach (Swiss guidelines) (NVE, 2020b; Salm et al., 1990), with site-specific adjustments (height difference,

slope angle, snow drift). The adjustments are subjective, i.e. the snowdrift accumulation was determined from the possibility of snow transportation from the Svartholavatnet, with wind directions from S-SE. The specified release depth (1.3 m) is in the range of observed release depths of avalanches with a 100-1000 year return period (100-200 cm; (Gauer Kristensen, 2016)). However, this empirical data comes from southern Norway, at high altitudes (1,500 m a.s.l.) where the mountains accumulate more snow. The specified release depth is greater compared to the snow depth NGI used for a 300-1000 year event in their avalanche hazard mapping more locally, on Senja (Langeland et al., 2019). This implies that the methods used to determine the release depth functions more accurately for high altitude areas with a greater snow accumulation. The release depth determined by NGI also employs the Swiss method, however several adjustments are subjective and somewhat based on user preference and chosen weather station. The release depth determined here is therefore likely larger than is necessary, but is also defensible, as it was determined through a commonly employed method with subjective adjustments.

6.2.3 Methods

The lower 100 m of the avalanche path has a slope gradient ranging between 45-90°, with most of the slope being 75-80°. As a result the avalanche dynamics become complicated as the snow mass can become an airborne flow in parts before it reaches the road (S. Margreth, personal communication, January 18, 2020; (Haukenes L, 2021)). As RAMMS does not replicate this process, it was necessary to investigate a range of different methods to get the impact dynamics so that the results could be compared and by this process propose reasonable design values for the protection design.

It is important to also note that the terrain in the runout zone will be modified when they build the protection structure because of the backfilling of materials and the angle of the roof towards the cliff, and consequently this will affect the impact dynamics. Engineers should take this into account during design (see 6.2.4).

Method comparison

Method 1 (RAMMS) does not include masses that might become an airborne flow (powder part) in reality since it is calibrated for avalanches that flow along the terrain (Figure 66). This can explain why the application of this method gives the lowest impact dynamics at road (130 kPa, 20 m/s), because it replicates a situation where the frictional resistance is larger than the other two methods. Both the 100 m high cliff and the 6-12 m wide ditch reduce the avalanche impact, which is supported by the higher impact dynamics in the ditch (235 kPa, 28 m/s) compared to the road. The avalanche model seem to replicate the nature of the

avalanche flow well, since the flow it deepest in the gully and being channeled here towards the north, resulting in deeper flow heights at the northern part of the road. This is the only method that give any indications of the lateral distribution at impact, and for this study it is seems that the model visualize this process at best. The impact pressure and velocity may be an underestimation of the simulated event if the avalanche motion appear to be airborne due to the frictional resistance that is included. Nevertheless, the avalanche size used in the model may be an exaggeration and it can be discussed if this exceeds the effect of the possible airborne masses on the impact dynamics and its implication of the design.

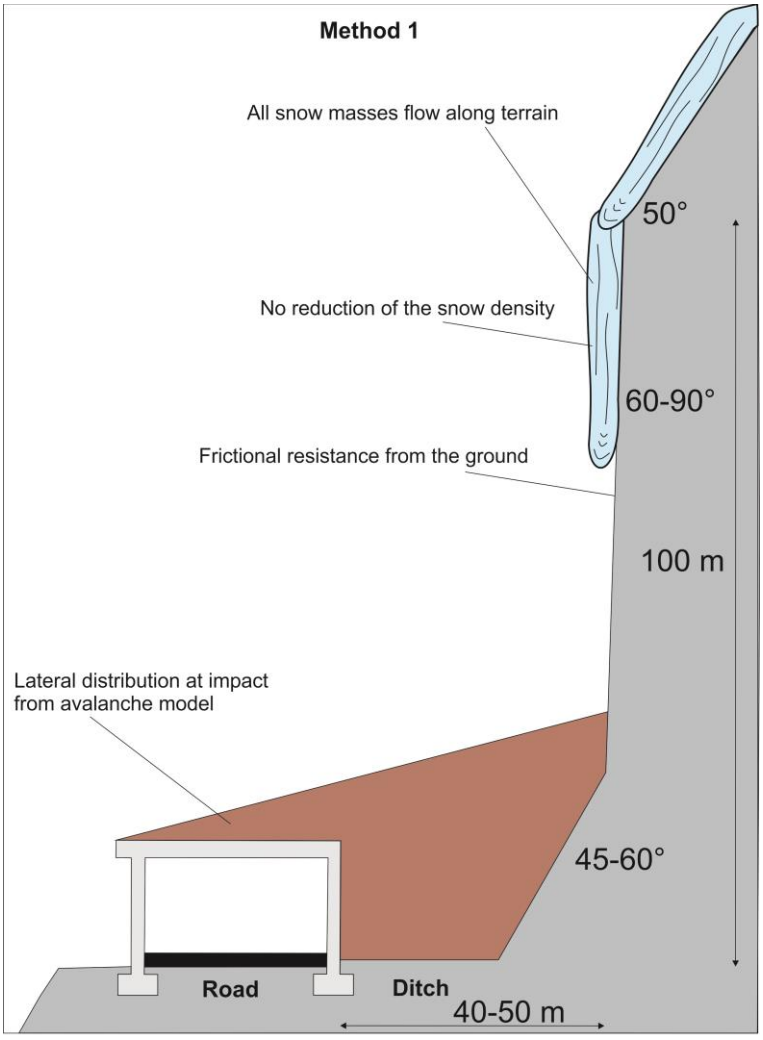

Figure 66. Schematic sketch of motion of the snow avalanche at the steep cliff above the road by applying method 1 (RAMMS). All snow masses are estimated to flow along the terrain and this implies that there is no reduction of the snow density at this steep terrain. Frictional resistance against the ground is included in the calculations resulting in reduced impacts. The lateral distribution at impact can be derived from the avalanche model.

Method 2 (physical formulas) is dependent on the calculated velocity from RAMMS and a realistic estimate of the snow density (Figure 67). This approach implies that the snow avalanche shoots over the cliff and become airborne. This can explain why the general

agreement between these results and the other are very poor, because there is no frictional resistance included in the calculations. This gives a very high impact velocity and hence high impact pressure. These impacts are more than doubled compared to method 1 (580 kPa against 130 kPa, and 54 m/s against 20 m/s). The cliff part closer to the road is less steep than the upper part and it is 40-50 m from the 'takeoff' point to the road (horizontal distance), which means that it is likely that parts of the parts of the snow masses flow/splashes along the cliff and/or flow over the ditch before it reaches the road. This suggests that the employed method may give an overestimation of impact velocity, and hence impact pressure.

This is also supported by the artificially released avalanche on the 11th of April 2021 at the test site in southern Norway, Ryggfonn, where the maximum avalanche velocity was recorded to 50 m/s. The size of the avalanche was between 10,000-20,000 m^3 (similar to this study), but with a vertical drop of 900 m and an avalanche path of 2,100 m, which is significantly larger than the path at Svarthola. The impact pressures based on four decades of observations from this avalanche test size are typically of the order of 100 kPa, but may reach several hundred kPa (Langeland Gauer, 2021). These measurements are from the beginning of the runout area and all methods are within these values, but it seems unrealistic that the design avalanche in this study would give the same impacts as the one at Ryggfonn based on the terrain conditions.

Furthermore, this approach is dependent on a realistic estimate for the snow density, which is challenging due to the complex nature of the avalanche dynamics and it is also problematic with snow/ice balls within the snow masses that will not change weight during the fall (S. Margreth, personal communication, January 22, 2021).

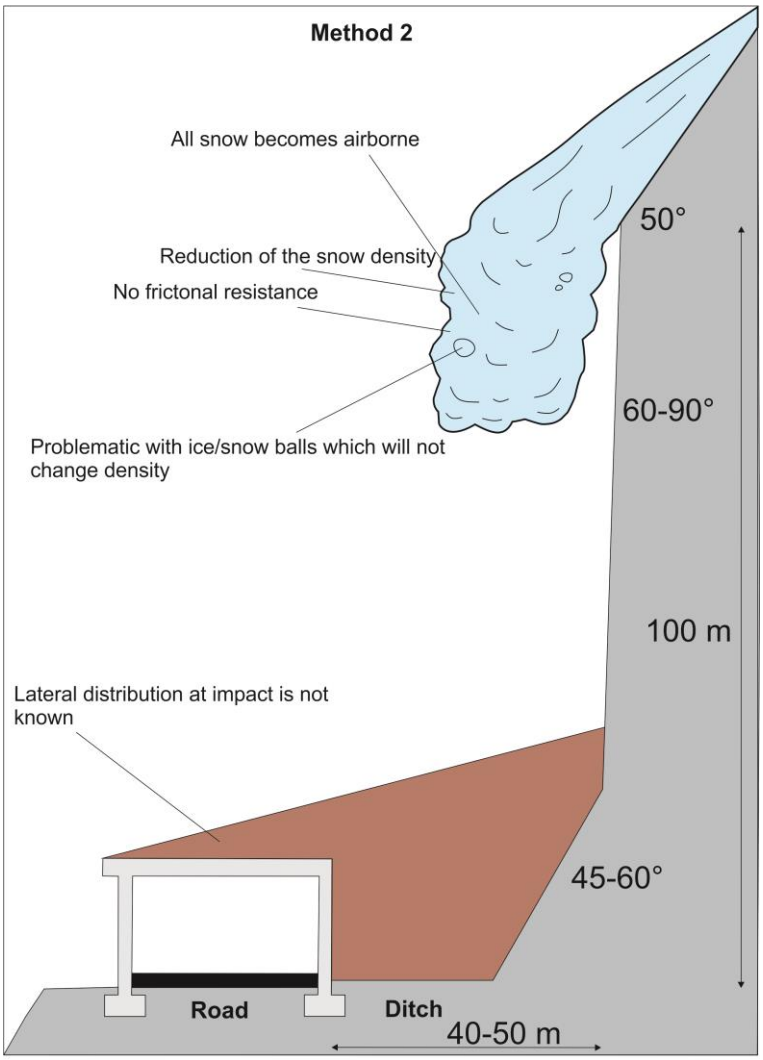

Figure 67. Schematic sketch of motion of the snow avalanche at the steep cliff above the road by applying method 2 (physical formulas). All snow masses are estimated to get airborne and this implies that there the snow density is reduced at this steep terrain. Frictional resistance is not included in the calculations resulting in amplified impacts. The lateral distribution at impact cannot be derived with this method.

Method 3 (RAMMS and physical formulas) give naturally results in-between the other two methods. This approach might replicate the impact velocity (37 m/s) best if parts of the snow masses become airborne since it includes some frictional resistance (Figure 68). The impact pressure (270 kPa) is close the snow pressure obtained in the ditch by method 1, which can indicate that this is a reasonable result for this case. The drawback of this approach is to be able to specify a suitable estimate of the snow density as for method 2.

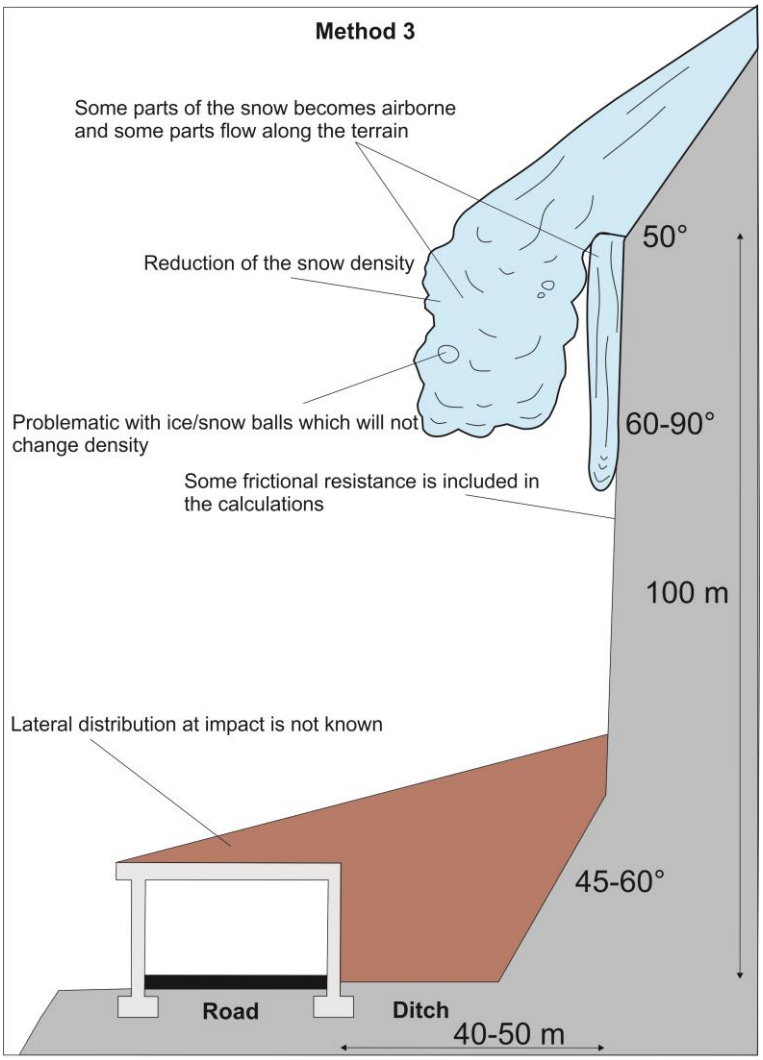

Figure 68. Schematic sketch of motion of the snow avalanche at the steep cliff above the road by applying method 3 (combination of RAMMS and physical formulas). Parts of the snow masses are estimated to get airborne and parts are flowing along the terrain. This implies that the snow density is reduced to a certain extent. Frictional resistance is included to some extent in the calculations. The lateral distribution at impact can not be derived with this method.

Implications of snow avalanche dynamics for the methods

One of the big challenges at Svarthola is that it requires deep knowledge of the avalanche dynamics in order to understand what effect this have on the results. The selection of a representative method would have been easier if the movement of the avalanche along the cliff were known (both for dry- and wet-avalanches of a certain size).

Based on this, it was valuable for this site-specific case to not only trust in the numerical model in order to achieve higher confidence in the results. It made the advantages with the usage of an avalanche model even more obvious because you can easily derive information (i.e. impact pressure, velocity, flow height) at any point along the path, the initial conditions (avalanche size) are taken into account and the lateral width of the avalanche distribution in

the runout zone are displayed. In comparison with method 2 and 3 that do not account for the avalanche size, interaction of the snow particles or frictional forces since it is a 2D point-mass model and it is therefore not possible to derive any details about the avalanche impacts.

6.2.4 Protection structure design

The snow avalanche analysis shows clearly that road is exposed for potential high impact dynamics and the design of the construction will determine how much these impacts are reduced. They are normally designed to carry the snow over the roof shed to minimalize the impacts. Additional to the actions from the avalanches (friction, normal loads and deviation loads) there is also the earth load and increased earth pressures (from snowpack or deposited avalanche snow) to be taken into account during the design (Norem, 2014; Rudolf-Miklau et al., 2015). These loads will be dependent on the distribution of the backfill, cushion layer on the roof and the gradient change between the terrain and shed.

6.2.5 Design values conclusion

An impact pressure from 130 to 270 kPa and an impact velocity between 20 and 37 m/s are considered realistic according to avalanche size and its vertical drop height and the horizontal runout distance. The flow height is estimated to be between 1.2 and 3.7 m. The design impacts and the reduction of these are depended on external factors, such as the residual risk acceptance, cushion layer/backfilling material and project budget.

6.2.6 Limitations

This study provides valuable insight into the snow avalanche impact dynamics at the site, but there are few limitations, some have already been mentioned in this chapter and in the method chapter. They concern the following:

- There is little to no documentation of the avalanche history at the road. As the analyses are mainly based on theory and the largest potential avalanche, this may affect the outputs from the avalanche dynamic model.
- The wet-avalanche hazard is not considered in this study. It can be assumed that the velocity is lower at the cliff above the road, but the snow density reduction is probably smaller if the flow gets airborne and this could give higher impact dynamics than for the dry-snow avalanche.
- The behavior (movement) of the avalanche flow from the top of the cliff wall and down to the road is not fully understood. There are naturally some uncertainties connected

to the results due to the limitations in our understanding of the complex nature of the snow avalanche flow.

6.3 Climate change

This analysis is somewhat limited do the few registrations in the mass movement event database. It is based on 13 rockfall events and eight snow avalanche events.

6.3.1 Rain

The findings displayed a good correlation between higher precipitation and the frequencies of rockfalls. This means that Svarthola will most likely experience more rockfall events in the nearest 50-100 years based on the climate projections that show an increase up to 50% of rain during the months with highest frequencies of rockfalls, and more days with intense rainfall, up to 80 mm.

6.3.2 Snow

The results showed a good correlation between higher precipitation and the release of snow avalanches. It also showed a noticeable correlation between southerly wind directions and the release of avalanches. Climate projections indicate a slight increase of precipitation during the winter months, but more importantly, the temperature during the winter is expected to increase with 4-5°C which will result in a mean temperature of 2.8-10.3°C. The implication of this is that most of the precipitation will come as rain instead of snow. This will naturally affect the snow cover, and it will very likely reduce the avalanche size (release area extent and release depth), and hence the impacts. If the snow at these low altitudes and coastal areas disappear completely, there will be no snow avalanches in the future. However, the warmer temperatures could potentially increase the occurrences of wet-snow avalanches, and if 80 mm of snow falls during a short-time period there could still be days with high avalanche danger. Nevertheless, the reduced risk of snow avalanches at the site in the future is also supported by Dyrrdal et. al. (2019) where they conclude that the snow cover in Senjahopen and Mefjordvær (10 km NW of Svarthola) may be a rarity by 2100. Their study also indicates that events of heavy rain during winter are likely to increase and the likelihood of wet-snow avalanches and slushflows will happen more frequently in a wetter climate. There are still uncertainties in the development of snow avalanches from climate change climate change due to the complexity of avalanche release (Dyrrdal et al., 2020).

6.3.3 Implications of climate change for avalanches at Svarthola

As Svarthola is close to sea level on a coastal island with an open slope to the fjord, it receives a low amount of snow. Given the potential for less snow, the avalanche risk to the

road will be reduced over time. This means the protection structure may be ‘over-designed’ with reference to snow at some point in the future of the design life of the structure (100 years). However, this is irrelevant given the likelihood of increased rockfall frequency.

7 Conclusions

The main objective of this study was to determine the impact dynamics of rockfalls and snow avalanches at the 100 m stretch of road at Fv 862 Svarthola, Senja, for protection design. Another objective was to investigate the mass movement impact history in relationship with meteorological factors and the implications of climate change. The main findings can be summarized by the following points:

- The maximum kinetic rock energy are expected to be (acknowledging that it may be possible for a larger block to fall):
    - 1,700 kJ for annual events, corresponding to a 0.5 m^3 block.
    - 3,600 kJ for a 50-year event, corresponding to a 1 m^3 block.
    - 7,100 kJ for a 100-year event, corresponding to a 2 m^3.
- The maximum impact velocity of the rock block is estimated to range between 22 and 50 m/s.
- The northern part of the road and the ditch are more likely to get impacts from rockfalls.
- The median jump heights are 0.9-1.2 m, where some blocks can jump >20 m if they hit the lower part of the cliff and get a horizontal throw down to the fjord.
- The fall height of a rock block can be up to 100 m.
- The maximum snow pressure of a 100-year dry-slab avalanche event with a volume of 16,900 m^3 is expected to be 130-270 kPa (acknowledging that the direction of the avalanche flow is not determined in this study).
- The maximum impact velocity of the avalanche is estimated to range between 20 and 37 m/s.
- The maximum flow height of the avalanche is 2-3.7 m in the northern part of the road and up to 1.2 m in the southern part.
- The northern part of the road and the ditch are more likely to get higher impacts from a snow avalanche.
- There is a good correlation between higher precipitation and the frequencies of rockfalls and snow avalanches.
- Climate projections show an increase of rain and days with heavy rain during the months with highest frequencies of rockfalls, this will expect to increase the number of rockfall events in the future.
- Climate projections show a reduction of snow during the winter months due to warmer temperatures, this will expect to reduce the number of dry-snow avalanche events and possible remove the hazard completely due to rarity of snow cover at this

altitude. However, the frequency of wet-snow avalanches and slushflows might increase due to a wetter climate.

These findings presents rockfall and snow avalanche impact dynamics and climate data that can be valuable in terms of risk management, for example, for optimizing the design of the rock/snow shed and forecast days when the hazard risk will be high. This study is does not estimate impacts of wet avalanches, and additional calculations of the load distribution from rockfalls and snow avalanches should be made during the design.

Based on the experiences from this study, there are several topics that have been raised that need further considerations and future work is suggested to include:

- The implications of rock fragmentation and block collision on a rockfall event.
- Back-calculation of known snow avalanche events with similar terrain. This could help to consider the accuracy of the numerical model and get a better understanding of the limitations.
- Improved understanding of the avalanche dynamics in steep terrain in order to replicate this process better. The snow module could also be compared with another model, i.e. SAMOS-AT that provides tools for dense and power snow avalanches, in order to validate the results.
- An improved workflow to map and specify impacts for rare avalanche events to obtain more confidence in the results.

References

Azzoni, A., & De Freitas, M. H. (1995). Experimentally Gained Parameters, Decisive for Rock Fall Analysis. *Rock mechanics and rock engineering, 28*(2), 111-124.

Ballantyne, C. K. (2002). Paraglacial geomorphology. *Quaternary Science Reviews, 21*(18-19), 1935-2017. doi:10.1016/S0277-3791(02)00005-7

Barbolini, M., Domaas, U., Faug, T., Gauer, P., Hákonardóttir, K., Harbitz, C., . . . Naaim, M. (2009). *The design of avalanche protection dams: recent practical and theoretical developments*: European Commission. European Research Area

Bartelt, P., Bieler, C., Bühler, Y., Christen, M., Christen, M., Dreier, L., . . . Glocker, C. (2016). RAMMS rapid mass movements simulation. A numerical model for rockfall in research practice. User Manual v.1.6 - Rockfall. *WSL-Institute for Snow and Avalanche Research SLF*, 102.

Bartelt, P., Bühler, Y., Christen, M., Deubelbeiss, Y., Salz, M., Schneider, M., & Schumacher, L. (2017). RAMMS rapid mass movements simulation. A numerical model for snow avalanches in research and practice. User Manual v1.7.0 - AVALANCHE. *WSL Institute for Snow and Avalanche Research SLF*, 104.

Bergh, S. G., Kullerud, K., Armitage, P. E., Bouke Zwaan, K., Corfu, F., Ravna, E. J., & Inge Myhre, P. (2010). Neoarchaean to Svecofennian tectono-magmatic evolution of the West Troms Basement Complex, North Norway. *Norwegian Journal of Geology, 90*, 21-48.

Bozzolo, D., & Pamini, R. (1986). Simulation of rock falls down a valley side. *Acta Mechanica, 63*(1-4), 113-130. doi:10.1007/BF01182543

Braathen, A., Blikra, L. H., Berg, S. S., & Karlsen, F. (2004). Rock-slope failures in Norway; type, geometry, deformation mechanisms and stability. *Norwegian Journal of Geology, 84*(1), 67-88.

Bühler, Y., Kumar, S., Veitinger, J., Christen, M., Stoffel, A., & Snehmani, S. (2013). Automated identification of potential snow avalanche release areas based on digital elevation models. *Nat. Hazards Earth Syst. Sci., 13*(5), 1321-1335. doi:10.5194/nhess-13-1321-2013

Christen, M., Bühler, Y., Bartelt, P., Leine, R., Glover, J., Schweizer, A., . . . Deubelbeiss, Y. (2012). *Integral hazard management using a unified software environment. Numerical simulation tool "RAMMS" for gravitational natural hazards.* Paper presented at the 12th Congress Interpraevent, Grenoble / France

Christen, M., Kowalski, J., & Bartelt, P. (2010). RAMMS: Numerical simulation of dense snow avalanches in three-dimensional terrain. *Cold Regions Science and Technology, 63*(1-2), 1-14. doi:10.1016/j.coldregions.2010.04.005

Crosta, G., & Agliardi, F. (2004). Parametric evaluation of 3D dispersion of rockfall trajectories. *Nat. Hazards Earth Syst. Sci.*(4), 583-589. doi:10.5194/nhess-4-583-2004

Delonca, A., Gunzburger, Y., & Verdel, T. (2014). Statistical correlation between meteorological and rockfall databases. *Nat. Hazards Earth Syst. Sci.*(14), 1953-1964. doi:10.5194/nhess-14-1953-2014

Dorren, L. K. (2003). A review of rockfall mechanics and modelling approaches. *Progress in Physical Geography, 27*(1), 69-87. doi:10.1191/0309133303pp359ra

Dyrrdal, A. V., Isaksen, K., Jacobsen, J. K. S., & Nilsen, I. B. (2020). Present and future changes in winter climate indices relevant for access disruptions in Troms, northern Norway. *Nat. Hazards Earth Syst. Sci., 20*(6), 1847-1865. doi:10.5194/nhess-20-1847-2020

Eckerstorfer, M. (2013). *Snow avalanches in central Svalbard: a field study of meteorological and topographical triggering factors and geomorphological significance.* (Ph.D. Thesis). Arctic Geology Department, The University Centre in Svalbard, Norway. Department of Geosciences, Faculty of Mathematics and Natural Sciences, University of Oslo, Norway,

Evans, S., & Hungr, O. (1993). The assessment of rockfall hazard at the base of talus slopes. *Canadian geotechnical journal, 30*(4), 620-636. doi:10.1139/t93-054

Fernandez-Hernández, M., Paredes, C., Castedo, R., Llorente, M., & de la Vega-Panizo, R. (2012). Rockfall detachment susceptibility map in El Hierro Island, Canary Islands, Spain. *Natural Hazards, 64*(2), 1247-1271. doi:10.1007/s11069-012-0295-1

Fredin, O., Bergstrøm, B., Eilertsen, R., Hansen, L., Longva, O., Nesje, A., & Sveian, H. (2013). Glacial landforms and Quaternary landscape development in Norway. *Quaternary Geology of Norway, Geological Survey of Norway Special Publication, 13*, 5-25.

Gauer, P., & Kristensen, K. (2016). Four decades of observations from NGI's full-scale avalanche test site Ryggfonn—Summary of experimental results. *Cold Regions Science and Technology, 125*, 162-176. doi:10.1016/j.coldregions.2016.02.009

Glover, J. M. H. (2015). *Rock-shape and its role in rockfall dynamics.* (Ph.D. Thesis). Durham University,

Green, R. (2016). *Rockfall: Design considerations for passive protection structures*: New Zealand Geotechnical Society (NZGS) Guidelines

Hákonardóttir, K. M., Hogg, A. J., Batey, J., & Woods, A. W. (2003). Flying avalanches. *Geophysical Research Letters, 30*(23). doi:10.1029/2003GL018172

Hanssen-Bauer, I., Drange, H., Førland, E. J., Hisdal, H., Lawrence, D., Nesje, A., . . . Ådlandsvik, B. (2017). *Climate in Norway 2100 - a knowledge base for climate adaption*: The Norwegian Centre for Climate Services (NCCS)

Haukenes L, H. (2021). *Skredoverbygg Svarthollatunnelen vest (Report No. 2165008) [unpublished]* Troms og Finnmark fylkeskommune

Hestnes, E., & Lied, K. (1980). Natural-Hazard Maps for Land-Use Planning in Norway. *Journal of Glaciology, 26*(94), 331-343. doi:10.3189/S002214300001087X

Håland, G., Orset, K. I., Frekhaug, M. H., & Norem, H. (2015). *Sammenligning av modelleringsverktøy for norske snøskred*. NIFS (Naturfare - Infrastruktur - Flom - Skred) The Norwegian Water Resources and Energy Directorate - NVE.

Jaedicke, C., Solheim, A., Blikra, L., Stalsberg, K., Sorteberg, A., Aaheim, A., . . . Sletten, K. (2008). Spatial and temporal variations of Norwegian geohazards in a changing climate, the GeoExtreme Project. *Nat. Hazards Earth Syst. Sci., 8*(4), 893-904. doi:10.5194/nhess-8-893-2008

Kvalvågens, J., Rasmussen, E., Nilsen, T. J., Haukenes L, H., Skoglund, R., Shi, J., . . . Helgaas, O. A. (2019). *Skredsikringsbehov langs riks og fylkesveg. Nordland - Troms - Finnmark.* : Statens vegvesen.

Langeland, H., & Gauer, P. (2021, 13.04.2021). Snøskred, Ryggfonn. The Norwegian Geotechnical Institute. Retrieved from https://www.ngi.no/Tjenester/Fagekspertise/Snoeskred/Ryggfonn

Langeland, H., Ragulina, G., Gauer, P., Høydal, Ø., Sverdrup-Thygeson, K., & Sandersen, F. (2019). *Faresonekartlegging på Senja. Faresonekartlegging skredfare i bratt terreng (NGI)* (54). Retrieved from The Norwegian Water Resources and Energy Directorate (NVE): www.nve.no

Lied, K., & Kristensen, K. (2003). *Snøskred, Håndbok om snøskred.* : Vett og Viten

McClung, D., & Schaerer, P. (2006). *The avalanche handbook* (3 ed.): The Mountaineers Books.

Metereological Institute, Norwegian water resources and energy directorate (NVE), Norwegian Research Center AS (NORCE), & Bjerknes Center for Climate Research. (2021). Norwegian Centre for Climate Services (NCCS). Retrieved from https://klimaservicesenter.no/climateprojections

NGU. (2020). Map and Data. [Accessed 01 Oct 2020]. Retrieved from www.ngu.no/en/topic/maps-and-data.

NMA. (2020a). Norwegian Mapping Authority. DTM 1 (UTM33).[Accessed 10 Sept 2020]. Retrieved from https://kartkatalog.geonorge.no/

NMA. (2020b). Norwegian Mapping Authority. Norge i bilder. [Accessed 18 Aug 2020]. Retrieved from www.norgeibilder.no.

NMA. (2020c). Norwegian Mapping Authority. Topografisk Norgeskart gråtone WMS-tjeneste. [Accessed 24 Aug 2020]. Retrieved from www.kartkatalog.geonorge.no.

NMI. (2020). Norwegian Meteorological Institute. [Accessed 15 Sept 2020]. Retrieved from www.eklima.met.no.

Norem, H. (2014). *Håndbok V138 Veger og snøskred*. Håndbøker i Statens vegvesen: Statens vegvesen.

NVE. (2020a). Snøskredskolen. Snøskredstørrelser. Norwegian Water Resources and Energy Directorate Retrieved from www.varsom.no/snøskredskolen

NVE. (2020b). Veileder for utredning av sikkerhet mot skred i bratt terreng. Prosedyre snøskred Retrieved from https://www.nve.no/veileder-skredfareutredning-bratt-terreng

NVE. (2020c). Veileder for utredning av sikkerhet mot skred i bratt terreng. Prosedyre steinsprang. Retrieved from https://www.nve.no/veileder-skredfareutredning-bratt-terreng

Palma, B., Parise, M., Reichenbach, P., & Guzzetti, F. (2012). Rockfall hazard assessment along a road in the Sorrento Peninsula, Campania, southern Italy. *Natural Hazards, 61*(1), 187-201.

Perla, R. I., & Martinelli, M. (1976). *Avalanche handbook*: U.S. Department of Agriculture, Forest Service.

Pudasaini, S. P., & Hutter, K. (2007). *Avalanche Dynamics: Dynamics of Rapid Flows of Dense Granular Avalanches*: Springer

Ramberg, I. B., Bryhni, I., & Nøttvedt, A. (2013). *Landet blir til: Norges geologi (2nd ed.)*: Trondheim: Norsk geologisk forening.

Rasmussen, E. (2019). Naturfarer i 1903 Senja. Byggherrens beredskapsplan for håndtering av naturfarer., 74.

Rudolf-Miklau, F., Sauermoser, S., & Mears, A. I. (2015). *The technical avalanche protection handbook*: Ernst & Sohn, A Wiley Brand

Ruiz-Carulla, R., Corominas, J., & Mavrouli, O. (2015). A methodology to obtain the block size distribution of fragmental rockfall deposits. *Landslides, 12*, 815-825. doi:10.1007/s10346-015-0600-7

Salm, B., Burkhard, A., & Gubler, H. (1990). *Berechnung von Fliesslawinen: eine Anleitung für Praktiker mit Beispielen*: Eidgen. Inst. für Schnee-und Lawinenforschung, Weissfluhjoch/Davos.

Scheck, F. (2010). *Mechanics: From Newton's Laws to Deterministic Chaos* (5 ed.): Springer

Schweizer, J., Jamieson, J. B., & Schneebeli, M. (2003). Snow avalanche formation. *Reviews of Geophysics, 41*(4). doi:10.1029/2002RG000123

Smithson, S. B. (1971). Densities of metamorphic rocks. *Geophysics, 36*(4), 650-787. doi:10.1190/1.1440205

Solheim, A., Bhasin, R., De Blasio, F. V., Blikra, L. H., Boyle, S., Braathen, A., . . . Glimsdal, S. (2005). International Centre for Geohazards (ICG): Assessment, prevention and mitigation of geohazards. *Norwegian Journal of Geology*, 18. Retrieved from https://foreninger.uio.no/ngf/ngt/pdfs/NJG_85_N1&2_45-62.pdf

Statens vegvesen. (2015). *Håndbok N400 Bruprosjektering, Prosjektering av bruer, ferjekaier og andre bærende konstruksjoner.* . Staens vegvesen

SVV. (2020). Vegkart. [Accessed 25 Oct 2020]. Retrieved from www.vegkart.no

Troms og Finnmark fylkeskommune. (2020). Fylkestinget vedtok torsdag et helhetlig skredsikringsprogram for fylkesvegene i Troms og Finnmark. Forebyggende skredkontroll skal nå vurderes for alle rasutsatte strekninger. Retrieved from https://www.tffk.no/aktuelt/vedtok-helhetlig-skredsikringsprogram.22429.aspx

Vagnon, F., Bonetto, S., Ferrero, A. M., Harrison, J. P., & Umili, G. (2020). Eurocode 7 and Rock Engineering Design: The Case of Rockfall Protection Barriers. *Geosciences, 10*(8), 305.

Varnes, D. J. (1978). Slope Movement Types and Processes. *Special report, 176*, 11-33.

Vick, L. (2015). *Evaluation of field data and 3D modelling for rockfall hazard assessment.* (Ph.D). University of Canterbury.,

Vick, L., Zimmer, V., White, C., Massey, C., & Davies, T. (2019). Significance of substrate soil moisture content for rockfall hazard assessment. *Nat. Hazards Earth Syst. Sci., 19*(5), 1105-1117. Retrieved from https://nhess.copernicus.org/articles/19/1105/2019/

Volkwein, A., Schellenberg, K., Labiouse, V., Agliardi, F., Berger, F., Bourrier, F., . . . Jaboyedoff, M. (2011). Rockfall characterisation and structural protection–a review. *Nat. Hazards Earth Syst. Sci., 11*(9), 2617-2651. doi:10.5194/nhess-11-2617-2011

Walder, J., & Hallet, B. (1985). A theoretical model of the fracture of rock during freezing. *Geological Society of America Bulletin, 96*(3), 336-346.

Winiger, M., Gumpert, M., & Yamout, H. (2005). Karakorum–Hindukush–western Himalaya: assessing high‐altitude water resources. *Hydrological Processes, 19*(12), 2329-2338. doi:10.1002/hyp.5887

Wylie, D. C., & Mah, C. W. (2004). *Rock Slope Engineering.* (4 ed.): CRC Press.

Yoshida, H., Nomura, T., Wyllie, D. C., & Morris, A. J. (2007). *Rock fall sheds - application of Japanese designs in North America*. Paper presented at the North American landslide conference; Landslides and society

Zwaan, K. B. (1995). Geology of the West Troms Basement Complex, northern Norway, with emphasis on the Senja Shear Belt: a preliminary account. *Norges geologiske undersøkelse Bulletin*(427), 33-36.

Appendices

Appendix A: RAMMS::ROCKFALL input settings

Calibration:

Simulation Settings:	Input Settings:	Input Settings:
Nr_Source_Points: 5	General:	Rock:
Nr_Simulated_Rocks: 9	Time Step (s): 0.010	Rock Density (kg/m3): 2700.00
Nr_Random_Orientations: 5	Dump Step (s): 0.020	Block Volumes (m3):
Nr_Z-Offset_Iterations: 1 (Nr_Simulations_Per_Source_Point: 45)	DEM Resolution (m): 1.00	- Min = 0.10 - Mean = 0.30
Total_Nr_Simulations: 225	Friction:	- Max = 0.49
	Overall Type: Medium Hard	Rock Forms:
	Additional Friction Areas:	Real_Equant_0.1m3.pts
	Hard	Real_Equant_0.3m3.pts
	Medium Hard	Real_Equant_0.5m3.pts
	Soft	Real_Flat_0.1m3.pts
	Forest/Moor:	Real_Flat_0.3m3.pts
	Medium Forest (35 m2/ha)	Real_Flat_0.5m3.pts
	Lake	Real_Long_0.1m3.pts
		Real_Long_0.3m3.pts
	Release:	Real_Long_0.5m3.pts
	Type: MultiPoint Automatic Z-Offset(s): 0.50 - 0.95 m	

Scenario 1: Annual events

Simulation Settings:	Input Settings:	Input Settings:
Nr_Source_Points: 51	General:	Rock:
Nr_Simulated_Rocks: 2	Time Step (s): 0.010	Rock Density (kg/m3): 2700.00
Nr_Random_Orientations: 5	Dump Step (s): 0.020	Block Volumes (m3):
Nr_Z-Offset_Iterations: 1 (Nr_Simulations_Per_Source_Point: 10)	DEM Resolution (m): 1.00	- Min = 0.48 - Mean = 0.50
Total_Nr_Simulations: 510	Friction:	- Max = 0.51
Real_Nr_Simulations: 495	Overall Type: Medium Hard	Rock Forms:
	Additional Friction Areas:	Real_Equant_1.08.1.04.0.89_0.5m3.pts
	Hard	Real_Flat_1.3.1.1.0.8_0.5m3.pts
	Medium Hard	
	Soft	
	Forest/Moor:	
	Medium Forest (35 m2/ha)	
	Lake	
	Release:	
	Type: Line	

	Automatic Z-Offset(s): 0.87 - 0.92 m	

Scenario 2: 50-year return period

Simulation Settings:	Input Settings:	Input Settings:
Nr_Source_Points: 51	General:	Rock:
Nr_Simulated_Rocks: 2	Time Step (s): 0.010	Rock Density (kg/m3): 2700.00
Nr_Random_Orientations: 5	Dump Step (s): 0.020	Block Volumes (m3):
Nr_Z-Offset_Iterations: 1 (Nr_Simulations_Per_Source_Point: 10)	DEM Resolution (m): 1.00	- Min = 1.00 - Mean = 1.01
Total_Nr_Simulations: 510	Friction:	- Max = 1.02
Real_Nr_Simulations: 500	Overall Type: Medium Hard	Rock Forms:
	Additional Friction Areas:	Real_Equant_1.4.1.3.1.1_1.0m3.pts
	Hard	Real_Flat_1.6.1.3.1.0_1.0m3.pts
	Medium Hard	
	Soft	
	Forest/Moor: Medium Forest (35 m2/ha)	
	Lake	
	Release:	
	Type: Line Automatic Z-Offset(s): 1.12 - 1.16 m	

Scenario 3a: 100-year return period

Simulation Settings:	Input Settings:	
Nr_Source_Points: 51	General:	Rock:
Nr_Simulated_Rocks: 2	Time Step (s): 0.010	Rock Density (kg/m3): 2700.00
Nr_Random_Orientations: 5	Dump Step (s): 0.020	Block Volumes (m3):
Nr_Z-Offset_Iterations: 1 (Nr_Simulations_Per_Source_Point: 10)	DEM Resolution (m): 1.00	- Min = 2.01 - Mean = 2.01
Total_Nr_Simulations: 510	Friction:	- Max = 2.02
	Overall Type: Medium Hard	Rock Forms:
	Additional Friction Areas:	Real_Equant_1.7_1_7_1.6_2.0m3.pts
	Hard	Real_Flat_1.7_2.1_1.2_2.0m3.pts
	Medium Hard	
	Soft	
	Forest/Moor:	

	Medium Forest (35 m2/ha) Lake Release: Type: Line Automatic Z-Offset(s): 1.40 - 1.46 m	

Scenario 3b: 100-year return period

Simulation Settings:	Input Settings:	
Nr_Source_Points: 51	General:	Rock:
Nr_Simulated_Rocks: 2	Time Step (s): 0.010	Rock Density (kg/m3): 2700.00
Nr_Random_Orientations: 5	Dump Step (s): 0.020	Block Volumes (m3):
Nr_Z-Offset_Iterations: 1 (Nr_Simulations_Per_Source_Point: 10)	DEM Resolution (m): 1.00	- Min = 4.01 - Mean = 4.03
Total_Nr_Simulations: 510	Friction:	- Max = 4.04
	Overall Type: Medium Hard Additional Friction Areas: Hard Medium Hard Soft	Rock Forms: Real_Equant_2.3_2_1.6_4.0m3.pts Real_Flat_2.9_2.4_1.2_4.0m3.pts
	Forest/Moor: Medium Forest (35 m2/ha) Lake Release: Type: Line Automatic Z-Offset(s): 1.72 - 1.99 m	

Scenario 4: Worst-case

Simulation Settings:	Input Settings:	Input Settings:
Nr_Source_Points: 51	General:	Rock:
Nr_Simulated_Rocks: 40	Time Step (s): 0.010	Rock Density (kg/m3): 2700.00
Nr_Random_Orientations: 5	Dump Step (s): 0.020	Block Volumes (m3):
Nr_Z-Offset_Iterations: 1 (Nr_Simulations_Per_Source_Point: 200)	DEM Resolution (m): 1.00	- Min = 0.10 - Mean = 0.88
Total_Nr_Simulations: 10200	Friction:	- Max = 12.54
Real_Nr_Simulations: 4870	Overall Type: Medium Hard	Rock Forms:
	Additional Friction Areas:	Real_Equant_0.63_0.61.0.52_0.1m3.pts
	Hard	Real_Equant_0.63_0.61.0.52_0.1m3.pts
	Medium Hard	Real_Equant_0.63_0.61.0.52_0.1m3.pts
	Soft	Real_Equant_0.63_0.61.0.52_0.1m3.pts
	Forest/Moor:	Real_Equant_0.63_0.61.0.52_0.1m3.pts
	Medium Forest (35 m2/ha)	Real_Equant_0.63_0.61.0.52_0.1m3.pts
	Lake	Real_Equant_0.63_0.61.0.52_0.1m3.pts
		Real_Equant_0.63_0.61_0.52_0.1m3.pts
	Release:	Real_Equant_0.63_0.61_0.52_0.1m3.pts
	Type: Line	Real_Equant_0.63_0.61_0.52_0.1m3.pts
	Automatic Z-Offset(s): 0.51 - 2.69 m	Real_Equant_1.17_1.25_1_0.7m3.pts
		Real_Equant_1.66_1.44_1.17_1.5m3.pts
		Real_Equant_2.47_2.14_1.74_5m3.pts
		Real_Flat_0.74_0.61_0.47_0.1m3.pts
		Real_Flat_0.74_0.61_0.47_0.1m3.pts
		Real_Flat_0.74_0.61_0.47_0.1m3.pts
		Real_Flat_0.74_0.61_0.47_0.1m3.pts
		Real_Flat_0.74_0.61_0.47_0.1m3.pts
		Real_Flat_0.74_0.61_0.47_0.1m3.pts
		Real_Flat_0.74_0.61_0.47_0.1m3.pts
		Real_Flat_0.92_0.76_0.58_0.2m3.pts
		Real_Flat_0.93_0.77_0.58_0.2m3.pts
		Real_Flat_1.08_0.89_0.67_0.3m3.pts

	Real_Flat_1.08_0.89_0.67_0.3m3.pts
	Real_Flat_1.10_0.91_0.69_0.33m3.pts
	Real_Flat_1.14_0.94_0.72_0.36m3.pts
	Real_Flat_1.2_1_0.8_0.4m3.pts
	Real_Flat_1.35_1.12_0.85_0.6m3.pts
	Real_Flat_1.3_1.1_0.8_0.5m3.pts
	Real_Flat_1.82_1.52_1.15_1.5m3.pts
	Real_Flat_2.4_2_1.5_3.5m3.pts
	Real_Flat_3.7_3.1_2.4_12.5m3.pts
	Real_Long_0.57_0.69_0.58_0.1m3.pts
	Real_Long_0.57_0.69_0.58_0.1m3.pts
	Real_Long_0.57_0.69_0.58_0.1m3.pts
	Real_Long_0.57_0.69_0.58_0.1m3.pts
	Real_Long_0.57_0.69_0.58_0.1m3.pts
	Real_Long_0.57_0.69_0.58_0.1m3.pts
	Real_Long_1.1_1.4_1.2_0.8m3.pts
	Real_Long_2_2.4_2_4.0m3.pts

Appendix B: RAMMS::AVALANCHE input settings

General Simulation Parameters:	Input settings:
DEM resolution (m): 5.00	Release:
Simulation time (s): 300.000	Depth: 1.30 m
Dump interval (s): 2.00	Vol: 16899.7 m3
Stopping criteria (momentum threshold) (%): 5	Delay: 0.00 s
Constant density (kg/m3): 300	
	Friction MUXI:
Return Period (y): 100	Altitude_limit_1: 500 m a.s.l
Volume category: Small	Altitude_limit_2: 0 m a.s.l
Cohesion:	
No Cohesion specified.	Open slope parameters:
	Mu: 0.275 - 0.260 - 0.245
Numerics:	Xi: 1500 - 1750 - 2000
Numerical scheme: SecondOrder	Channelled parameters:
H Cutoff (m): 0.000001	Mu: 0.320 - 0.310 - 0.290
Curvature effects are ON!	Xi: 1200 - 1350 - 1500
	Gully parameters:
	Mu: 0.410 - 0.390 - 0.380
	Xi: 1000 - 1100 - 1200
	Flat parameters:
	Mu: 0.255 - 0.240 - 0.225
	Xi: 2000 - 2250 - 2500
	Forest parameters:
	Mu (delta): 0.020 - 0.020 - 0.020
	Xi: 400 - 400 - 400